Aus dem Fachbereich Biologie
der Justus-Liebig-Universität
Gießen

betreut am
Max-Planck-Institut für Herz- und Lungenforschung
durch Prof. Dr. med. Stefan Offermanns

The Amyloid Precursor Protein Family and its Functional Role in Endothelium

Dissertation
zur Erlangung des Doktorgrades der Naturwissenschaften
des Fachbereichs Biologie
der Justus-Liebig-Universität Gießen

vorgelegt von
Sabrina Kurz

2024

MAX-PLANCK-INSTITUT
FÜR HERZ- UND LUNGENFORSCHUNG

JUSTUS-LIEBIG-
UNIVERSITÄT
GIESSEN

Vom Fachbereich Biologie und Chemie der
Justus-Liebig-Universität Gießen als Dissertation angenommen.

Dekan:	Prof. Dr. Thomas Wilke
Gutachter:	Prof. Dr. Ivan Manzini
	Prof. Dr. Stefan Offermanns

Datum der Disputation: 28.08.2024

„It is impossible to live without failing at something
unless you live so cautiously, that you might
as well not have lived at all,
in which case you have failed by default."

J.K. Rowling

Table of Contents

1 List of Tables

2 List of Figures

3 Abstract

Amyloid Precursor Protein (APP), Amyloid Precursor-like Protein 1 (APLP1) and APLP2, are part of the APP protein family. They are characterized as type 1 single-pass transmembrane proteins. APP and APLP2 are ubiquitously expressed, whereas APLP1 is restricted to neuronal tissue. Consequently, I decided to focus solely on APP and APLP2 in my studies. The strong conservation of APP and APLP2 from invertebrates to humans implies they have fundamental roles in cellular function. They show high structural similarities. However, the amyloid β (Aβ) sequence, which is known to play a critical role in the development of Alzheimer's disease, is not expressed in APLP2. Several studies have suggested that APP and APLP2 might act like cell surface receptor-like proteins or ligands. The suggested functions range from playing a role in transcriptional regulation to synaptic functions or involvement in cell adhesion. In contrast to the single *App* or *Aplp2* knockout mice, gene deficiency for both genes is perinatal lethal. Therefore, it is assumed that both genes have, at least in part, overlapping functions during development. Apart from its involvement in Alzheimer's disease, the function of APP and APLP2 remain poorly understood.

According to our RNA sequencing data, *APP* and *APLP2* are among the most highly expressed genes in endothelial cells. Therefore, I hypothesized that they have a critical, yet unknown role in either the development or functionality of blood vessels. The aim of this study was to unravel the function of APP and APLP2 within the endothelium. APP and APLP2 can potentially affect a wide array of endothelial cell-related processes, such as inflammation, vessel remodeling and regulation of blood homeostasis and vascular permeability. To identify the most suitable mouse model for *App* and/or *Aplp2* endothelial-specific knockout (KO) mice, I initiated a series of *in vitro* experiments. The particular focus on the role of APP and/or APLP2 in angiogenesis stemmed from my intriguing observation of compromised tube formation in HUVECs subsequent to the double knockdown (KD) of both *APP* and *APLP2* in an *in vitro* matrigel assay. As a next step, I used different *in vivo* models to investigate a potential role of the protein family in angiogenesis *in vivo*. Hereby, I observed fewer muscle fibers, less proliferation and a dilated vessel perimeter in double KO mice 28 days after femoral artery ligation. However, no significant differences directly related to the KO of *App* and *Aplp2* in the endothelium were detected.

Overall, these results describe an important role of APP in angiogenesis *in vitro* that could not be compensated by APLP2. However, the underlying mechanisms *in vivo* appear to be much more complex and could potentially be compensated by as-yet-unkown backup mechanisms. Future studies in other tissues and other species would certainly help to unravel the physiological role of App and Aplp2 within the endothelium.

4 Zusammenfassung

Amyloid Precursor Protein (APP), Amyloid Precursor-like Protein 1 (APLP1) und APLP2, gehören zur APP-Proteinfamilie. Sie sind als Typ 1 Single-Pass-Transmembranproteine charakterisiert. APP und APLP2 werden ubiquitär exprimiert, während APLP1 auf neuronales Gewebe beschränkt ist. Daher beschloss ich, mich in meinen Studien auf APP und APLP2 zu konzentrieren. Die Konservierung von APP und APLP2 von Wirbellosen bis zum Menschen deutet auf ihre grundlegende Rolle bei der Zellfunktion hin, da sie große strukturelle Ähnlichkeiten aufweisen. Die Amyloid β (Aβ) -Sequenz, von der bekannt ist, dass sie eine entscheidende Rolle bei der Entwicklung der Alzheimer-Krankheit spielt, wird jedoch in APLP2 nicht exprimiert. Mehrere Studien haben nahegelegt, dass APP und APLP2 wie rezeptorähnliche Proteine oder Liganden auf der Zelloberfläche wirken könnten. Die vorgeschlagenen Funktionen reichen von einer Rolle bei der Transkriptionsregulierung über synaptische Funktionen bis hin zur Beteiligung an der Zelladhäsion. Im Gegensatz zu Mäusen, bei denen nur ein Gen ausgeschaltet ist, sind Mäuse mit einem Genmangel für beide Gene perinatal letal. Es wird daher angenommen, dass beide Gene zumindest teilweise überlappende Funktionen während der Entwicklung haben. Abgesehen von ihrer Beteiligung an der Alzheimer-Krankheit, ist noch wenig über die Funktion von APP und APLP2 bekannt. Unseren RNA-Sequenzierungsdaten zufolge gehören APP und APLP2 zu den am stärksten exprimierten Genen in Endothelzellen, und ich stelle daher die Hypothese auf, dass sie eine entscheidende, bisher unbekannte Rolle bei der Entwicklung oder Funktionalität der Blutgefäße spielen. Ziel dieser Studie war es, die Funktion von APP und APLP2 innerhalb des Endothels zu entschlüsseln. APP und APLP2 können möglicherweise eine Vielzahl von Prozessen beeinflussen, die mit Endothelzellen zusammenhängen, wie Entzündungen, Gefäßumbau und die Regulierung der Bluthomöostase und der Gefäßpermeabilität. Um das am besten geeignete Mausmodell für App- und/oder Aplp2-Endothel-spezifische Knockout-Mäuse (KO-Mäuse) zu identifizieren, habe ich eine Reihe von *In-vitro*-Experimenten durchgeführt. Ich begann, mich auf die Rolle von APP und/oder APLP2 bei der Angiogenese zu konzentrieren. Dieser besondere Fokus ergab sich aus meiner faszinierenden Beobachtung einer beeinträchtigten Röhrenbildung in HUVECs nach dem doppelten Knockdown (KD) von APP und APLP2 in einem *in vitro* Matrigel-Assay. In einem nächsten Schritt habe ich verschiedene *In-vivo*-Modelle verwendet, um eine mögliche Rolle der Proteinfamilie bei der Angiogenese *in vivo* zu untersuchen. Dabei beobachtete ich weniger Muskelfasern, eine geringere Proliferation und einen erweiterten Gefäßumfang bei Mäusen mit doppeltem Gendefizit 28 Tage nach Ligatur der Oberschenkelarterie. Es wurden jedoch keine signifikanten Unterschiede mit unmittelbarem Bezug auf die Gendefizite von *App* und *Aplp2* im Endothel festgestellt. Insgesamt beschreiben diese Ergebnisse eine wichtige Rolle von APP bei der Angiogenese *in vitro*, die nicht durch APLP2 kompensiert werden konnte. Die zugrundeliegenden Mechanismen *in vivo* scheinen jedoch viel komplexer zu sein und könnten möglicherweise durch noch unbekannte Ersatzmechanismen kompensiert werden. Zukünftige Studien in anderen Geweben und bei anderen Spezies könnten dazu beitragen, die physiologische Rolle von App und Aplp2 im Endothel weiter zu entschlüsseln.

5 Abbreviations

Table 1
Overview of Abbreviations

Abbreviation	Meaning
°C	Degree celcius
AB	Antibody
ADAM	A disintegrin and metalloproteinase
AICD	APP intracellular domain
APLP	Amyloid Precursor-like Protein
APP	Amyloid precursor protein
CD	Cluster of differentiation
cDNA	Complementary deoxyribonucleic acid
CTF	C terminal fragment
DAPI	Diamidino-2-phenylindole
DMEM	Dulbecco’s modified eagle’s medium
DPBS	Dulbecco’s phosphate buffer saline
EC	Endothelial cells
ECM	Extracellular matrix
EDTA	Ethylenediaminetetraacetic
EdU	5-Ethynyl-2’-desoxyuridine
EGM	Endothelial growth medium
eNOS	Endothelial nitric oxide synthase
ERG	Avian v-ets erythroblastosis virus E26 oncogene homolog
FACS	Fluorescence-activated cell sorting
FAL	Femoral artery ligation
FBS	Fetal bovine serum
FGF	Fibroblast growth factor
FMO	Fluorophores minus one
GAPDH	Glycerinaldehyd-3-phosphat-dehydrogenase
HIF	Hypoxia inducible factor
HUVEC	Human umbilical vein endothelial cells
IB4	Isolectin-B4
IF	Immunofluorescence
KD	Knockdown
KO	Knockout
L	Ligated hind limb
LDPI	Laser doppler perfusion imaging
LLC1	Lewis lung carcinoma cell line 1
loxP	Locus of X-over P1
M1	Classically activated macrophages
M2	Alternatively activated macrophages
n-L	Non-ligated hindlimb
PBS	Phosphate buffered saline
PDGF	Platelet-derived growth factor
PFA	Paraformaldehyde

qPCR	Quantitative polymerase chain reaction
RT	Room temperature
SCR	Scramble
SD	Standard Deviation
VEGF	Vascular endothelial growth factor

6 Introduction

6.1 APP family

6.1.1 Structure and processing

Amyloid precursor protein (APP), amyloid precursor-like protein 1 (APLP1), as well as APLP2, are part of the APP protein family. They are all type 1 single-pass transmembrane proteins (Deyts et al., 2016; D'Uscio et al., 2017). As shown in Figure 1, the three members share structural similarities (Jacobsen & Iverfeldt, 2009).

Figure 1
Schematic Illustration of the domain organization of the APP family members

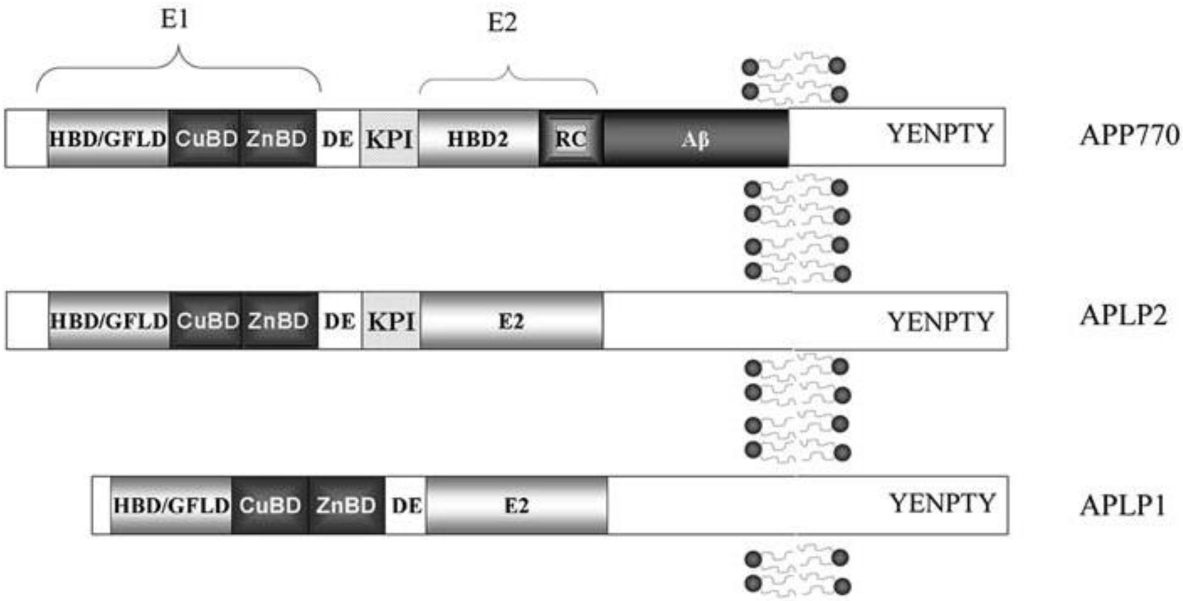

Note. All members of the APP family contain heparin-binding/growthfactor-like domains (HBD/GFLD), copper and zinc binding domains (CuBD and ZnBD), an acidic domain (DE), and a protein interaction motif (YENPTY) in the C-terminal (Source: Jacobsen & Iverfeldt (2009), p.2300).

They all have a large extracellular N-terminal domain and a short cytoplasmic C-terminal tail. In addition, they share the cysteine-rich E1 region, region E2 and the protein interaction motif YENPTY. APP is clearly distinguished from APLP2 and ALPL1 by the presence of the Aβ region, which exists solely in APP (Jacobsen & Iverfeldt, 2009; Müller et al., 2017; Wasco et al., 1993). It is known that a single gene encodes human APP, located on chromosome 21. It consists of 18 exons and there are three main isoforms, APP_{695}, APP_{751} and APP_{770}, that originate from alternative splicing of exons 7 and 8, however, many other isoforms are present in different cell types (Dunot et al., 2023). The gene for APLP2, on the other hand, is assigned to chromosome 11 in humans (von der Kammer et al., 1994). APP and APLP2 are ubiquitously expressed, whereas APLP1 is restricted to neuronal tissue (Müller et al., 2017; Sandbrink et al., 1994).

There are two major processing pathways that are mutually exclusive, the non-amyloidogenic and the amyloidogenic pathway. Under physiological conditions, APP is first cleaved by an α-secretase, this is known as the non-amyloidogenic pathway. Here APP is cut at the 17^{th} amino acid within the Aβ peptide sequence, resulting in APPsα and the C-terminal fragment (CTF) α. Subsequent processing of a γ-secretase releases p3 and the APP intracellular domain (AICD), both of which are rapidly degraded (Deyts et al., 2016; Zhang et al., 2012). Since it was discovered that APP is always cleaved at the α-site to produce APPsα, three “a disintegrin and metalloproteinase” (ADAM) enzymes, namely ADAM-10, ADAM-17, and ADAM-9, have been suggested to act as the α-secretase (Buxbaum et al., 1998; Esch et al., 1990; Koike et al., 1999; Lammich et al., 1999). However, ADAMs do not solely cleave APP, as they can also cleave Notch, tumor necrosis factor-α, epidermal growth factor family members and other proteins (Black et al., 1997; Hartmann et al., 2002; Liu et al., 2009; Peschon et al., 1998). In contrast, the amyloidogenic pathway describes β-secretase cleaving initially at the 1^{st} or the 11^{th} residue of the Aβ peptide, resulting in APPsβ and CTFβ, a membrane associated CTF which consists of 99 amino acids (Cole & Vassar, 2007; Zhang et al., 2012). Subsequently, β-amyloid peptide (Aβ) as well as AICD are released after γ-secretase cleavage (Müller et al., 2017; Puig & Combs, 2013) (Figure 2).

Figure 2
Overview of canonical processing of APP

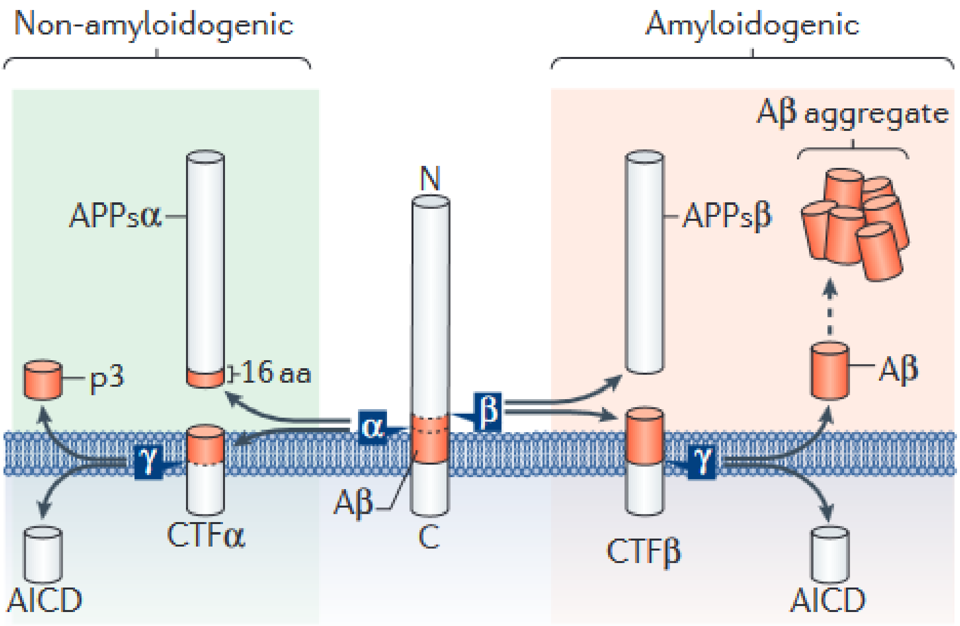

Note: The schematic shows the canonical amyloid precursor protein (APP) processing pathways. Processing by α-secretase along the non-amyloidogenic pathway (green background) occurs in the amyloid-β (Aβ) region (shown in red), liberates APPsα (α-secretase-generated APP ectodomain fragment) and generates p3. By contrast, processing along the amyloidogenic pathway (red background) generates Aβ (through β-secretase and γ-secretase cleavage) and liberates APPsβ. An intracellular fragment (APP intracellular domain (AICD)) is released in both pathways. The positions of cleavage sites are indicated.(Source: Müller et al. (2017), p.284)

Even though, APPsα is only 16 amino acids longer, the structure of APPsα differs significantly from that of APPsβ. This possibly explains the different physiological properties of these two secreted fragments (Gralle et al., 2006; Müller et al., 2017; Peters-Libeu et al., 2015). Additionally, AICD, which is produced in both non-amyloidogenic and amyloidogenic pathways and has the same peptide sequence in each pathway, appears to be functionally distinct. In contrast, AICD coming from the non-amyloidogenic pathway is rapidly degraded in the cytosol by an enzyme called insulin-degrading enzyme. AICD resulting from the amyloidogenic pathway, however, is transported to the nucleus to bind the neprilysin promotor, showing again the complexity of the whole APP family (Andrew et al., 2016; Belyaev et al., 2010).

More recently, novel APP processing pathways have been discovered (Norstrom, 2017; Willem et al., 2015). An overview of all processing pathways is shown in Table 2 and is visualized in Figure 3. Within the δ-processing pathway, APP is first cleaved by δ-secretase, releasing $sAPP_{1–585}$, $sAPP_{1–373}$, and $sAPP_{374–585}$ as well as CTFδ. Afterwards, Aβ and AICD are released after β- and γ-secretase cleaving. In the η-secretase pathway, sAPPη and CTFη results from η-secretase cleavage. Further processing of CTFη by either α- or β-secretase releases Aη-α or Aη-β and additional processing by γ-secretase releases p3 and AICD or Aβ and AICD, respectively. In the meprin-β pathway, meprin β acts as a β-secretase to produce a fragment similar to sAPPβ as well as $sAPP_{1–380/3}$ and $sAPP_{1–124}$. Further processing by β-secretase releases $Aβ_{2-X}$ and AICD (Andrew et al., 2016).

Table 2

Proteolytic pathways of the APP metabolism

Pathway	Activity	Products	Activity	Products	Activity	Products
1) Non-amylodoigenic			α-secretase	sAPPα, **CTFα**	γ-secretase	P3, AICD
2) Amylodoigenic			β-secretase	sAPPβ, **CTFβ**	γ-secretase	Aβ AICD
3) η-secretase followed by pathway 1 or 2	η-secretase	sAPPη, **CTFη**	α-secretase	Aη-α, **CTFα**	γ-secretase	P3, AICD
			β-secretase	Aη-β, **CTFβ**		Aβ, AICD
4) δ-secretase followed by pathway 1 or 2	δ-secretase	$sAPPδ_{373}$ $sAPPδ_{585}$ $sAPPδ_{374-585}$ $CTFδ_{586}$ $CTFδ_{374}$	α-secretase		γ-secretase	P3, AICD
			β-secretase			Aβ, AICD
5) θ-secretase followed by γ-secretase			θ-secretase	sAPPθ **CTFθ**	γ-secretase	P3-like, AICD
6) Meprin β cleavage followed by γ-secretase			Meprin β cleavage	$sAPP_{18-124}$ $sAPP_{18-305/308}$ $sAPPβ_2$ **CTFβ2**	γ-secretase	$Aβ_{2-x}$, AICD

Note. The APP metabolism begins with full-length APP (leftmost column "Pathway") and proceeds to the right. Products in bold are substrates for the subsequent proteolytic activity (adapted from Norstrom (2017), p.273).

Figure 3
Overview of the so far known APP processing pathways

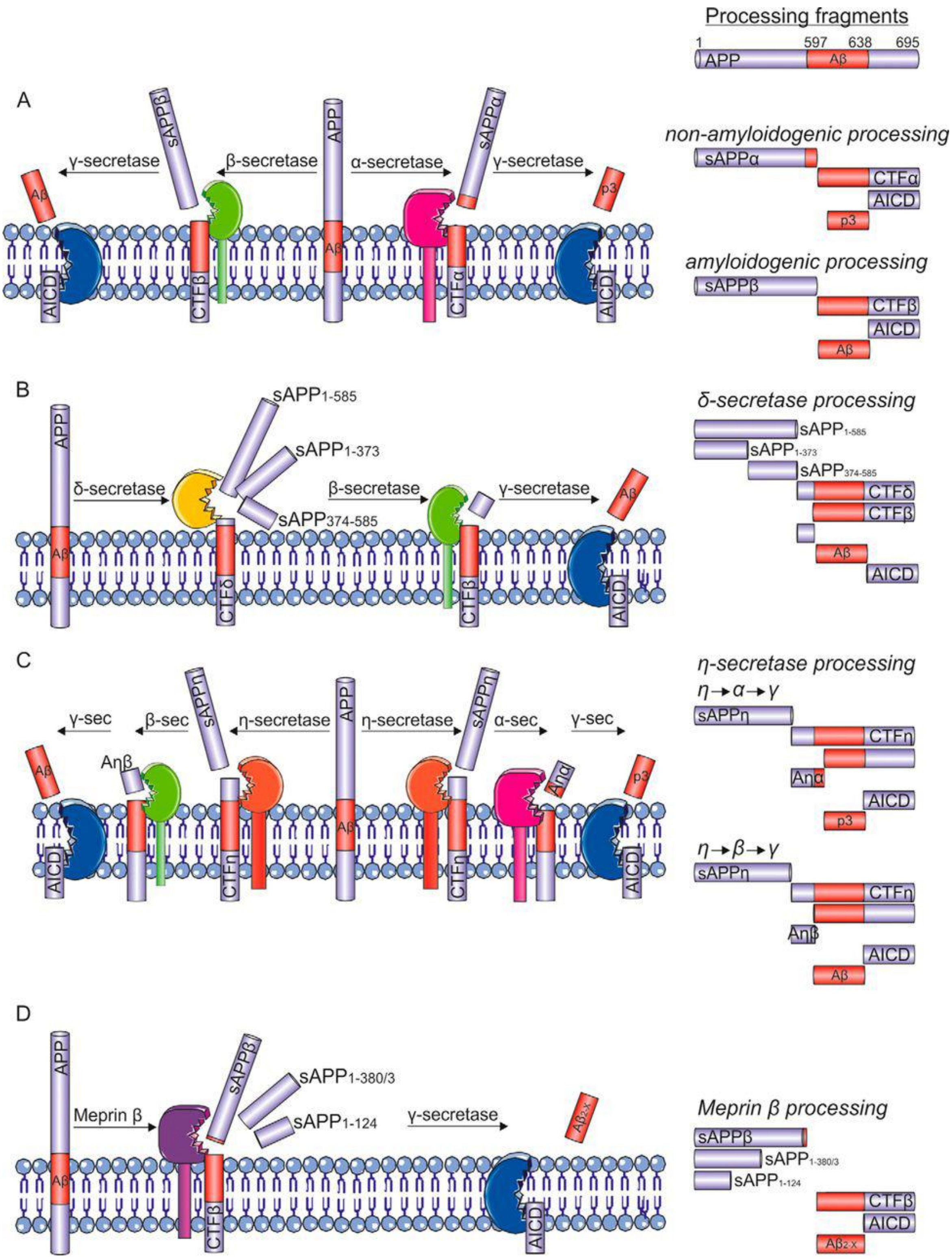

Note. (A) the traditional model of APP proteolysis involves APP processing either in the non-amyloidogenic pathway, where sequential cleavage by α-secretase (ADAM10; pink) and the γ-secretase multisubunit complex (here shown for simplicity as a single entity; blue) liberates sAPPα and p3, or in the amyloidogenic pathway, where sequential cleavage by β-secretase (BACE1 or possibly cathepsin B; green) and γ-secretase liberates sAPPβ and Aβ. Both pathways produce AICD, which can be proteolytically degraded or translocated to the nucleus, where it is involved in transcriptional regulation. (B) APP processing by the δ-secretase (AEP; yellow) causes the release

of three soluble fragments of APP ($sAPP_{1–585}$, $sAPP_{1–373}$, and $sAPP_{374–585}$). The remaining CTFδ is then further processed by β- and γ-secretases to release Aβ and AICD. (C) η-secretase (suggested to be MT5-MMP; orange) releases the soluble sAPPη fragment and leaves the membrane-bound CTFη. CTFη can be further processed by α- or β-secretase to release Aη-α or Aη-β, respectively. Following α- or β-cleavage, the remaining CTF can be cleaved by γ-secretase to release p3 and AICD, or Aβ and AICD, respectively.
sec, secretase. (D) meprin β (purple) acts as a β-secretase producing a fragment similar to sAPPβ as well as two shorter, soluble fragments ($sAPP_{1–380/3}$ and $sAPP_{1–124}$). The remaining CTF can then be processed by β-secretase to release $Aβ_{2-X}$ and AICD (Source: Andrew et al. (2016), p. 192363),

Regarding the processing of APP, it is crucial to acknowledge its dynamic and complex nature, which consistently influences the generation of various bioactive fragments. This process is constitutive, which may be the main reason why the half-life of full length APP is less than one hour (Dunot et al., 2023; Weidemann et al., 1989). These peptides can be rapidly produced and exert their effects on specific targets within small cellular regions. Addressing such fast-scale dynamics is very challenging, and only limited information is available. For instance, controlling the cleavage of APP at precise locations, such as the synapse, within a short timeframe (e.g., seconds to minutes) and without affecting other protease targets, remains a significant challenge (Dunot et al., 2023).

As all APP-cleaving enzymes are transmembrane proteins, the processing of APP is influenced by cholesterol and sphingolipids. In this context, it is already known that cholesterol depletion favors non-amyloidogenic APP processing (Müller et al., 2012).

6.1.2 Expression and conservation of APP family members in different tissues and species

Due to the high degree of homology of the APP family members, it was suspected that individual functions of APP could be compensated by the APLPs. To investigate this hypothesis, combined knockout (KO) mouse lines have been created. The combinations of APP/APLP2, as well as APLP1/APLP2 gene deficiencies were found to be perinatal lethal (Anliker & Müller, 2006; Heber et al., 2000). However, double KO mice of APP and APLP1 survive and appear normal. Surprisingly, no upregulation of APLP2 expression for compensatory effects was found (Heber et al., 2000). Taken together, mice deficient in APLP2 in combination with APP, APLP1 or both, proved to be perinatal lethal. This suggests some kind of redundancy between APLP2 and the other family members, emphasizing APLP2's key role. Additionally, different KO combinations resulted in varying phenotypes. Despite lethality in some mutants, no obvious organ abnormalities were observed, nor was there any change in neuronal survival rates (Heber et al., 2000). Early postnatal lethality of APP/APLP2 mutants was also assessed by (Von Koch et al., 1997), showing slightly different results. Here, 26% of double mutants survived well into adulthood. Since the same line of APLP2$^{-/-}$ was used to generate double mutants, the observed differences are likely attributed to the APP KO strain. Both APP KO strains differ in the composition of their genetic background alleles, as well as the targeted deletion introduced into the APP locus (Heber et al., 2000; Von Koch et al., 1997). Due to the similar phenotypes observed in both single KO lines of APP, variations in genetic backgrounds likely influenced the degree of expression (Müller, 1999).

Complete loss of APP expression, as well as APP-deficiency induced by the deletion of exon 2, leads to viable and fertile mice. However, both APP KO mouse lines show a loss in body weight, reduction in forelimb strength, and decreased locomotor activity compared to wild-type controls of the same age and sex. This suggests that, the lack of APP results in impaired muscular and/ or moto neuronal function (Senechal et al., 2006). The interpretation that compensatory up-regulation of the other APP family members leads to the viable phenotype of *App* KO mice is not supported by expression studies of *Aplp1* and *Aplp2*. No compensatory upregulation of *Aplp1* and *Aplp2* could be observed in these mice (Zheng et al., 1995). The question remains whether the more severe phenotypes in double mutant mice are because of the complete loss of a redundant function or the disruption of multiple independent pathways that coincidently lead to similar phenotypes (Shariati & De Strooper, 2013).

Another aspect is the conservation of the APP family in different species. It has already been demonstrated by Northern blot analysis of RNA that a similarly sized messenger RNA and equivalent amount of APP RNA is present in eight mammalian species as well as in chicken. Consequently, the conservation of both size and abundance of APP mRNA is suggested (Goldgaber et al., 1987; Johnstone et al., 1991; Manning et al., 1988). Studies have found a 90% homology between human and mouse or rat complementary deoxyribonucleic acid (cDNA) and discovered that mainly three amino acid substitutions within the β/A4 region seem responsible for the differences between human, mouse, and rat sequences (Shivers et al., 1988; Yamada et al., 1987). Figure 4 shows the evolution of the APP family. Ensemble comparative genomic tools revealed five nodes of duplications in the phylogenetic tree of the APP family. The paradoxical pattern of both expansion and contraction within the APP family hints at the intricate interplay of selective evolutionary pressures acting upon the duplicated encoding genes. Ultimately, the intricate journey of the APP protein family's evolution culminates in the three most extensively studied members in mammals: APP, APLP1, and APLP2 (Shariati & De Strooper, 2013).

Figure 4
Evolution of the APP family

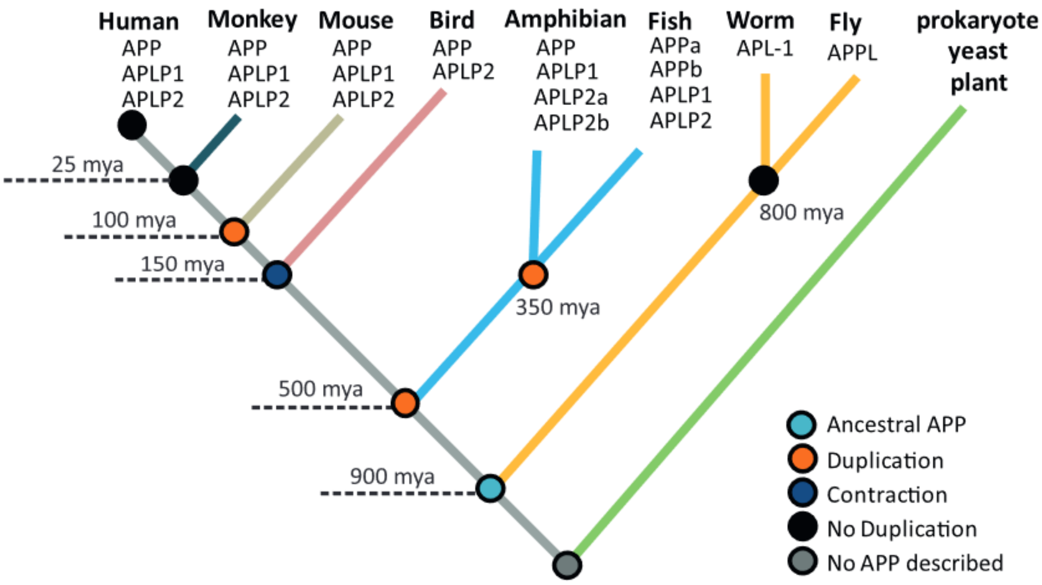

Note. A simplified dendrogram based on the APP protein family tree from Ensemble illustrates the important events in the evolution of the APP gene family. The duplication and contraction nodes are color coded. The lengths of the lines are not proportional to the evolutionary distance of species. Mya: million years ago.(Source: Shariati & De Strooper, 2013, p. 2037).

Different studies have shown that mRNA as well as protein of APP are expressed in tissues throughout the body, like adipose tissue, brain, heart, intestine, kidney, liver, lung, muscle, spleen, and thymus (Akaaboune et al., 2000; Galloway et al., 2007; Y. H. Lee et al., 2008; Sandbrink et al., 1994; Selkoe et al., 1988; Yamada et al., 1989).

6.1.3 Functions of APP and interacting partners

While the role of Aβ in Alzheimer's disease and the mechanisms generating Aβ have been of intensive studies, the physiological role and function of APP and its cleaving products are still mostly unknown. The potentially compensatory functional redundancy and the functional diversity, resulting from different APP processing pathways, complicate the analysis of APP functions *in vivo* (Ring et al., 2007).

Over the last decades, it has been shown that APP family members are multimodal proteins. They can regulate biological processes, act as cell-surface receptor-like proteins, or ligands and thereby can contribute to cell adhesion and cell-cell interactions (Puig & Combs, 2013). Several Studies have reported promotion of cancer cell proliferation and metastasis, as well as adverse effects on prognosis in pancreatic and colorectal cancer by APP (Krause et al., 2008; Takayama et al., 2009). Soluble APP-α, the N-terminal fragment, is known to be neuroprotective, facilitate learning and memory, regulate cell adhesion and promote neurite outgrowth, synaptogenesis, and act as growth factor. Soluble APP-β in contrast, can promote neuronal cell death and axonal pruning (Puig & Combs, 2013). It is also known that AICD can control cell death, alter calcium and ATP homeostasis, as well as behave as a transcription factor (Puig & Combs, 2013). In the endothelium, APP modulates the expression and function of endothelial nitric oxide synthase (eNOS) (d'Uscio et al., 2018). Furthermore, loss of APP results in decreased eNOS protein expression and additionally in an elevated level of oxidative stress *in vitro* and *in vivo* ((d'Uscio et al., 2018; D'Uscio & Katusic, 2019). In aged mice, APP expression in the aorta increased, proposing an adaptive response to protect and preserve eNOS expression and function (d'Uscio & Katusic, 2021).

Most of the studies, however, did not take into account that different isoforms of APP might have different physiological functions *in vivo*. For instance, APP_{770} incorporate exon 7 and 8, APP_{751} in contrast does not contain exon 8, and APP_{695} lacks both of them. It should be considered that these different ways of splicing must hold a physiological meaning, of which so far nobody is aware (Dunot et al., 2023). Another important point, which may influence various physiological functions of APP, is the intracellular positioning, particularly by regulating its cleavage. For instance, the enzymatic action of β-secretases is more pronounced in acidic cellular compartments, such as late endosomes or multi-vesicular bodies, compared to neutral pH environments. This acidic environment favors the cleavage of APP along the β-amyloid pathway (Kimura & Yanagisawa, 2018). Additionally, there is evidence suggesting that both APP and its fragments can be detected in exosomes

(Dunot et al., 2023; Zhao et al., 2023). This implies that even when attempting to dissect the function of this protein based on cell type or substructure, it is essential to consider its ability to signal over long distances (Dunot et al., 2023).

More than 200 potential interactors of the APP family have already been identified. These interactions with intra- and extracellular binding partners could mediate the regulatory role of APP (Müller et al., 2017; van der Kant & Goldstein, 2015). Additionally, the interaction with itself and the other family members by generation of cis- and trans-dimers through the E1 and E2 domains can modulate APP's signaling (Hoefgen et al., 2014). Some examples for extracellular binding partners are Reelin, F-spondin, Lingo-1, Tag1, Pancortins and Netrin, while JIP, Fe65, JNK, Dab1, and Mint1/X11 were found to be intracellular binding partners to APP (Reinhard et al., 2005; Rice et al., 2012; Zheng & Koo, 2011).

However, in many studies, the interactions with binding partners have only been studied *in vitro* (Müller et al., 2017).

6.2 Blood vessels, endothelial cell characteristics and physiological functions

Within the context of blood vessels, there exist three major types: 1) Arteries are responsible for transport of blood from heart to periphery, 2) veins in contrast return the blood from periphery to the heart, and 3) capillaries regulate exchange of water and chemicals between blood and tissues by surrounding all body tissues and cells. Whereas capillaries consist of only a single layer of endothelium and connective tissue, arteries and veins are composed of three tissue layers. The inner layer is the endothelium, the middle layer is comprised of elastic fibers and smooth muscle cells and the outer layer, tunica externa, consists of connective tissue (Aird, 2007; Carmeliet, 2003). Blood vessels deliver oxygen and nutrients while serving as pathways for immune surveillance. Additionally, tumor cells use blood vessels to metastasize (Potente et al., 2011).

Endothelial cells (EC) line the inside of blood vessels and lymphatic system. A monolayer of ECs, known as the endothelium, is in direct contact with the blood, lymph and all circulating cells. Since Wilhelm His used the term “endothelium” in 1865 for the first time, there has been a significant gain in knowledge. Initially, the endothelium was believed to only prevent the blood cells accessing the underlying vascular matrix and act as a passive barrier. However, several decades later, it is known to play a role in controlling the blood fluidity, vascular tone and platelet aggregation. As well as regulating inflammation, immunology, and angiogenesis. In healthy adults, the main portion of ECs is kept in a quiescent state. But if necessary, EC can switch between quiescent and active states. Upon stimulation with growth factors or hypoxia, EC can rapidly turn to active growth during angiogenesis (Félétou, 2011; Triggle et al., 2012).

6.3 Angiogenesis

Angiogenesis is defined by the growth of new blood vessels from the existing vasculature. It occurs throughout life, beginning in utero and continuing until death. A schematic overview of the different steps including involved key growth factors is shown in Figure 5. Briefly, low oxygen concentrations lead to the inhibition of the intracellular degradation of hypoxia inducible factor (HIF)-1α. This causes accumulation of the latter and allows binding to HIF-1β and activation of hypoxia-responsive elements within target genes. Thereby, different angiogenic factors, such as vascular endothelial growth factor (VEGF), are produced which can diffuse into the nearby tissue (Forsythe et al., 1996; Hirota & Semenza, 2006; Van Hove & Benoit, 2015). Next steps are detachment of pericytes and sprouting of ECs, followed by EC migration towards the gradient, degradation of the local extracellular matrix (ECM), and proliferation to produce required cell amount for further vessel formation (Adams & Alitalo, 2007; Hirota & Semenza, 2006). ECs organize into tubular luminal structures, initiating the formation of a nascent vascular network. Subsequently, pericytes are recruited to this evolving vasculature, and their interaction with ECs is consolidated through factors such as platelet-derived growth factor (PDGF) and Angiopoietin 1. This intricate process, depicted in Figure 5, entails the involvement of various growth factors, with some emanating from the ischemic tissue itself and others being produced by ECs and pericytes in response to prior stimuli.

Figure 5

Schematic overview of the process of angiogenesis

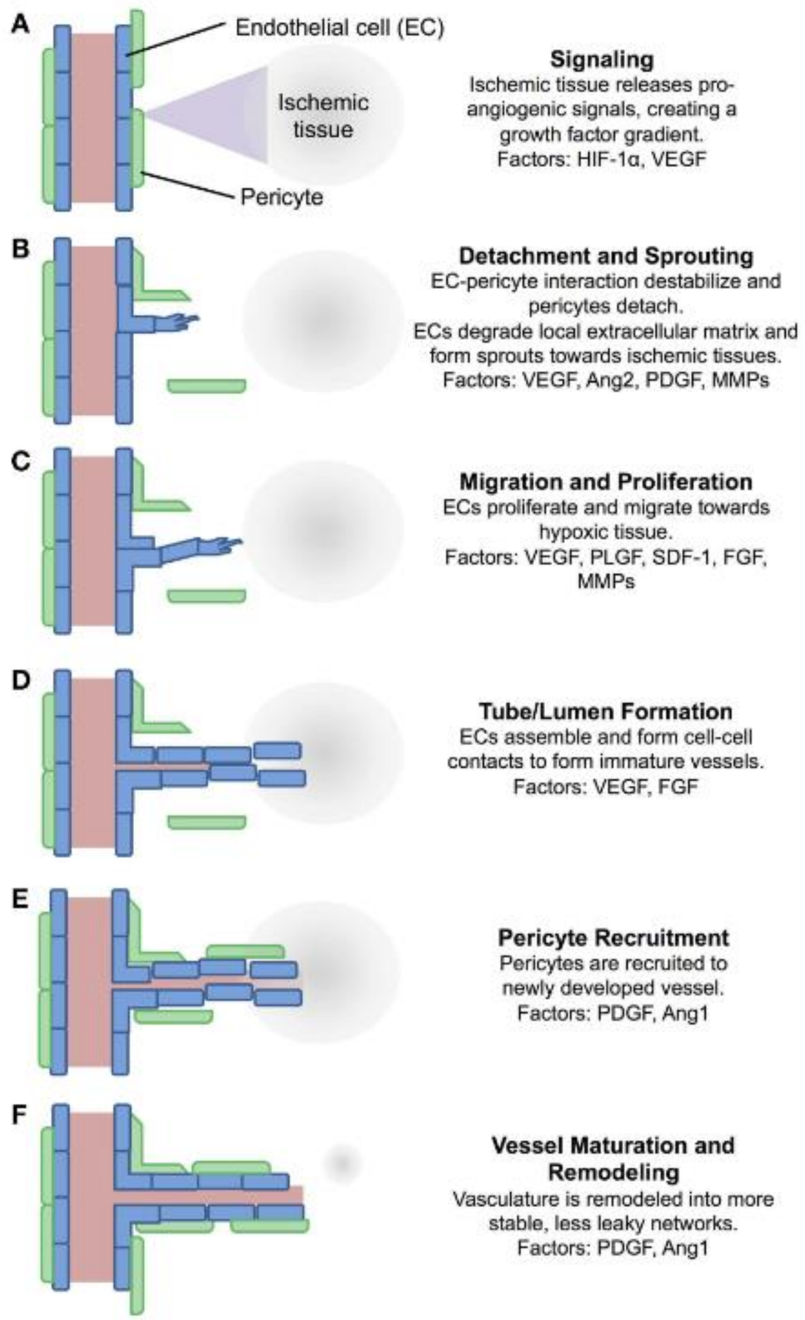

Note. Angiogenesis is a process tightly controlled by a number of factors. (A) Ischemic tissue release pro-angiogenic signals, which diffuse into nearby tissue. (B) Pericytes detach from nearby vessels, and ECs form sprouts. (C) ECs proliferate and migrate towards the signal gradient. (D) ECs align into immature vessels. (e) Pericytes are recruited to the new vessels. (F) Vasculature is remodeled and stabilized. Many of the factors involved in this process have been exploited for pharmacological intervention, either supplementing them for pro-angiogenic applications, or inhibiting them for anti-angiogenic applications. EC, endothelial cell; HIF-1α, hypoxia-inducible factor-1α; VEGF, vascular endothelial growth factor; Ang2, angiopoietin 2; PDGF, platelet-derived growth factor; MMPs, matrix metalloproteinases; PLGF, placenta growth factor; SDF-1, stromal cell-derived factor-1; FGF, fibroblast growth factor; Ang1, angiopoietin 1 (Source: Van Hove & Benoit (2015), p.2).

Two types of angiogenesis can be distinguished: 1) the non-sprouting or intussusceptive and 2) the sprouting type (Figure 6). The modification of pre-existing vessels by forming an intravascular pillar is called non-sprouting angiogenesis. This leads to the division of the vessel, which branches to become two independent capillaries. Sprouting angiogenesis, in comparison, leads to a tip cell phenotype of the existing capillaries, resulting in the formation of a sprout on the existing vessel (Burri & Djonov, 2002; Folkman & Klagsbrun, 1987; Risau, 1997).

Figure 6

Overview of sprouting and non-sprouting angiogenesis

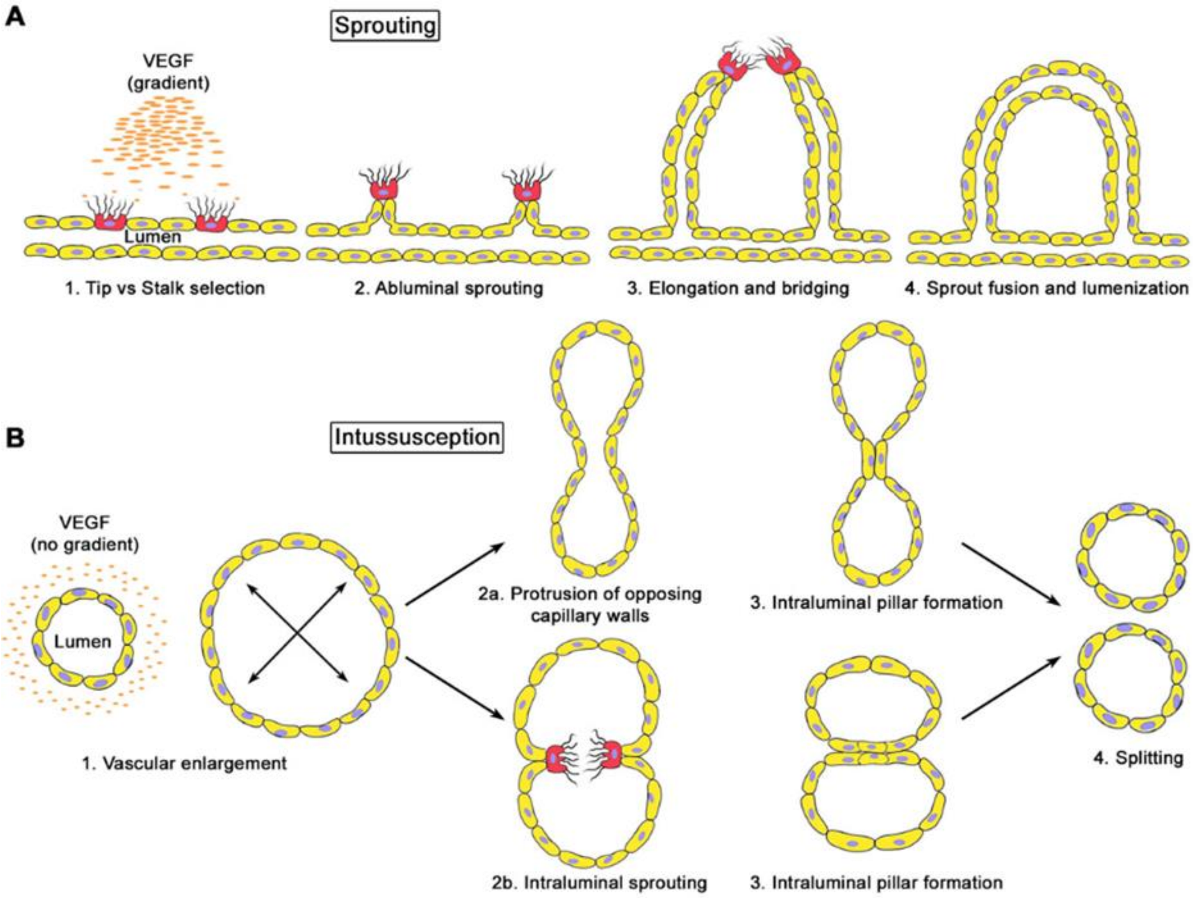

Note. A. Endothelial tip cells (in red) specification is induced by VEGF gradients in the extracellular matrix. Those tip cells migrate towards the gradient source. Stalk cells (in yellow) proliferate behind the tip cells, leading to formation of ab-luminal sprouts that fuse together and generate new vessels. B. Without a VEGF gradient, all cells remain in a stalk cell phenotype. Intraluminal pillars are formed, which fuse together and finally cause longitudinal splitting into two new vessels (adapted from Uccelli et al. (2019), p.4).

6.3.1 Molecular mechanism of angiogenesis in health and disease

As described above, the successful growth of blood and lymphatic vessels during angiogenesis needs coordination of cell proliferation, cell-cell communication, as well as guided migration (Adams & Alitalo, 2007). Additionally, the secretion of VEGF-A by monocyte-derived macrophages seems to be crucial for angiogenesis induction during tissue repair. But not only VEGF-A is secreted by macrophages, other pro- as well as antiangiogenic growth factors can be secreted (Corliss et al., 2016; Stockmann et al., 2011).

Angiogenesis is a highly regulated process that depends on specific mechanisms within various types of ECs (Potente et al., 2011). In summary, initially, tip cells guide the developing sprout, while stalk cells proliferate to extend the neovessel sprout in response to pro-angiogenic signals such as hypoxia and VEGF. Subsequently, tip cells merge through the process of anastomosis to create the lumen, facilitating functional blood flow. Ultimately, vascular remodeling, including the adoption of a quiescent endothelial phalanx phenotype and branch regression, transforms the vascular plexus into a network of stable vessels (Adams & Alitalo, 2007; Lamalice et al., 2007; Potente et al., 2011).

Since angiogenesis is a complex process, it is not surprising that many molecules have already been identified as regulators via studies in mice and zebrafish. First and foremost, the VEGF family, PDGF family, TGF-β signaling pathways, fibroblast growth factor (FGF) superfamily, the NOTCH and WNT signaling, GPCRs, junctional molecules, and Hippo signaling (Adams & Alitalo, 2007; Carmeliet & Jain, 2011; Potente et al., 2011; Risau, 1997).

In health as well as in disease, angiogenesis is modulated. A lack of exercise finally leads to capillary regression, whereas exercise itself stimulates angiogenesis in the heart and skeletal muscle. In adipose tissue, capillaries grow during weight gain and regress during weight loss, depending on the functional demands of the tissue (Adair & Montani, 2010). Besides being a normal development and a part of the healing process, angiogenesis is also key to tumor branching and arborization in cancer or other pathological conditions (Buschmann & Schaper, 1999; Quintero-Fabián et al., 2019).

Abnormalities in angiogenesis can precipitate severe pathological states. Thus, the imbalance between pro- and anti-angiogenic factors decreases the functional resources of the affected tissue (La Mendola et al., 2022). In diseases like cancer, rheumatoid arthritis, diabetic retinopathy or age-related macular degeneration, excessive angiogenesis is characteristic. Conversely, inadequate angiogenesis is linked to cerebal ischemia as well as cardiovascular diseases and impaired wound healing (Fallah et al., 2019; Potente et al., 2011; Yoo & Kwon, 2013; Ziche et al., 2005).

6.3.2 The role of macrophages in angiogenesis

Many studies have already shown, that macrophages are not “per se” angiogenic. They have to be in an activated state to promote angiogenesis (Sunderkötter et al., 1991). If macrophages are exposed to low oxygen tensions, for example, they get activated and start to promote angiogenesis (Knighton et al., 1983). These activated macrophages were historically divided into classically activated macrophages (M1), activated by pro-inflammatory stimuli, and alternatively activated macrophages (M2), stimulated by anti-inflammatory conditions. However, the current understanding is that macrophages are no longer considered to be distinctly categorized as M1 or M2 macrophages. There is evidence that macrophages exist in a continuum of phenotypes between M1 and M2 *in vivo* (Murray, 2017).

Macrophages are involved in angiogenesis by performing different tasks. First of all, they are able to secrete angiogenic factors, including VEGF-A, FGF-2, and PDGF. These factors then stimulate the proliferation and migration of ECs, which are important steps in forming new blood vessels (Glim et al., 2013; Jetten et al., 2014). Additionally, macrophages participate in the remodeling of the extracellular matrix by secretion of enzymes, like matrix metalloproteinases (MMPs). These enzymes help breaking down the existing matrix and creating a pathway for EC migration and vessel formation (Senger & Davis, 2011). The chemotactic signals, released by macrophages, additionally help to direct ECs to where new blood vessels are needed. But not only guidance and secretion are tasks that include macrophages. Also the clearance of apoptotic cells is assisted by macrophages to maintain a balanced and controlled process of vessel formation (Gordon & Plüddemann, 2018; Murray & Wynn, 2011). Not to forget the important of resolving angiogenesis once the new blood vessels have formed. Here, macrophages help to regulate vessel maturation and stabilize the vasculature. Overall, the interplay between macrophages and ECs is crucial for the successful progression of angiogenesis (Sunderkötter et al., 1991, 1994).

6.3.3 Mouse models to study angiogenesis *in vivo*

Over the last decades, mouse retinas have been extensively used to study physiological and pathophysiological angiogenesis. In opposition to human embryonic development, blood vessel formation in retinas of mice doesn’t occur *in utero* but immediately after birth. Within the first week after birth, the initial phase of angiogenesis, characterized by the growth of a single superficial vessel layer from the center to the retinal periphery, accompanied by EC proliferation and migration, is completed (Fruttiger, 2007; Stahl et al., 2010).

The progressing of angiogenesis directly after birth, the short observation time of only one week, as well as the convenient access to visualize the developing vasculature for further imaging, make the retinal angiogenesis model in mouse a very good readout for observation on differences caused by gene depletion (Stahl et al., 2010).

In physiological conditions like retinal vascularization, angiogenesis is necessary to complete the process and ceases upon reaching the endpoint. By contrast, angiogenesis in malignancy is non self-limiting and continues indefinitely until the whole tumor is eliminated or the host dies. There are different kinds of tumor angiogenesis models based on their application method. Subcutaneous injection of tumor cells is primarily used to study formation of primary tumors, whereas intravenous injections are used for tumor metastasis. However, there is also the possibility to inject orthotopically to the organ of malignant cells, in order to mimic the tumor growth within the most relevant tissue environment. In common with all kinds of models is the possibility to genetically modify either transplanted cells or recipient mice to specifically study genes of interests or label for cell tracing and *in vivo* imaging (Staton et al., 2004). A frequently used tumor cell line is the Lewis Lung Carcinoma 1 cell line (LLC1). As the name implies, it is derived from a Lewis lung carcinoma of a mouse with C57/BL6 background. The cells grow fast and homogeneous while having a weak immunogenicity. Additionally, they are highly tumorigenic with tumor incidences reaching 100% (Bertram & Janik, 1980; Janker et al., 2018; Lechner et al., 2013).

Another mouse model for studying angiogenesis is the femoral artery ligation (FAL) model. As aforementioned, adaptive responses in the context of angiogenesis are mainly due to ischemia-induced tissue damage. Therefore, ischemia models like

FAL or myocardial infarction have been commonly employed for investigating aberrant angiogenesis associated with pathology. Depending on the site of ligation, the observed phenotypes correlate more with either angiogenesis or arteriogenesis. The main trigger for angiogenesis is hypoxia in the tissue, but the expansion of the microvasculature only reaches limited number of cells in the surrounding tissue and observations are made mainly distal to the ligation site. In contrast, arteriogenesis is triggered by increased shear forces and pressures in the arterioles and can be observed mainly proximal of the ligation site (Aref et al., 2019; Kochi et al., 2013; Nowak-Sliwinska et al., 2018). Angiogenesis is thereby reflected through the capillary density and the reduction in hind limb blood flow can be measured using Laser Doppler Perfusion Imaging (LDPI) and immunostaining (Brenes et al., 2012; Couffinhal et al., 1998; Limbourg et al., 2009). Neovascularization induced by ischemic conditions is believed to preserve functionality of tissue and integrity during injury (Folkman, 1995).

Due to the large number of ligation sites and the variability of used readouts, Lee et al. (2020) started to define angiogenesis landmarks and validate published studies. Mapping of the full hind limb showed inconsistency and regional variability in skeletal muscle injury as well as angiogenesis. Following their approach, I chose to include also the *tibialis anterior* muscle to gain more specialized knowledge about ongoing processes within the animals.

7 Aim of the study

APP and APLP2 are type 1 single-pass transmembrane proteins and highly expressed in ECs. Besides playing a role within Alzheimer's disease progressing, their functional role is still poorly understood. Given their high expression levels in ECs, I hypothesize a critical yet unknown role in either development or functionality of the blood vessels.

The aim of this study was to …

1) … investigate the physiological and/or pathophysiological role of the APP family in endothelial cells and their roles in the endothelium *in vivo.*

2) … dissect the underlying molecular mechanism *in vivo* by using two different knock-in mouse lines of APP.

8 Materials

8.1 Chemicals/reagents/plates/instruments

8.1.1 Cell transfection reagents

Table 3
Cell transfection reagents

Name	Company
AllStars negative control siRNA	Qiagen
Lipofectamine RNAiMAX	Invitrogen
OPTI-MEM®	Gibco

8.1.2 Enyzmes

Table 4
Overview of enzymes

Name	Company
Collagenase II	Worthington
Dispase	Thermo Fisher Scientific
DNase I	New England Biolabs
Elastase I	Sigma-Aldrich
Protoscript II reverse transcriptase	New England Biolabs

8.1.3 Instruments/Equipments

Table 5
Instruments and equipments

Name	Company
Analytical balance	Sartorius
ChemiDoc MP Imaging System	Bio-Rad
Cryotome	Leica

FACSMelody cell sorter	BD Biosciences
Gel casting platform	Bio-Rad
Gel combs	Bio-Rad
gentleMACS™ Octo Dissociator with Heaters	Miltenyi Biotec
IX81 Live-cell imaging microscope	Olympus
Leica SP5 confocal microscope	Leica
Lightcycler 480 qPCR cycler	Roche
MoorFLPI-2	Moor instruments
NanoDrop ND1000 Spectrophotometer	PeqLab Biotechnologie GmbH
Neubauer counting chamber	Karl Hecht
Power Pack P25 T	Biometra
QuantStudio1	Applied biosystems
SP8 (MP)	Leica
Thermo cycler	Analytik Jena
Waterbath #1083	GFL

8.1.4 Plates/Consumables

Table 6
Plates and consumables

Name	Company
µ-Slides 15 Well 3D	Ibidi
1.5 ml Tube	Eppendorf
10 cm Cellstar® cell culture dishes	greiner bio-one
6-well Cellstar® cell culture dishes	greiner bio-one
96-well FrameStar® RealTime-PCR plates	4titude
Adhesion slides SuperFrostUltra	Fisher Scientific: J3800AMNZ

Cell Strainer 70 µm	Corning
Cryomolds intermediate squares	Weckert Labortechnik
Glass coverslips, thickness 1 mm, 24 x 60 mm	Marienfeld
High Precision Coverslips, thickness 1.5 mm, 24x60 mm	Marienfeld
MicroAmpOptical 96 Well Reaction plate	Applied biosystems by life technologies

8.1.5 Other reagents

Table 7
Other reagents

Name	Company
Collagen Type I solution	Corning
Debris removal solution	Miltenyi Biotec B.V. & Co.KG
Eosin Y-Lösung	Applichem
Fetal bovine serum (FBS)	Thermo Fisher Scientific
Fluoromont W	SERVA Electrophoresis
Halt™ Protease und Phosphatase Inhibitor Cocktail, EDTA-frei (100x)	Thermo Fisher Scientific
Hematoxylin	Sigma
Isoflurane	Abbott
Matrigel	Corning
Miglyol	Caelo
NaCl 0.9%	B.Braun
Nitrocellulose, 0.45 µm, Typ PROTRAN BA	VWR
Non-fat skimmed milk powder	Biomol
Optimal cutting temperature (O.C.T.) medium	Tissue-Tek
PageRuler Plus Prestained Protein Ladder	Thermo Fisher Scientific

Paraformaldehyde (PFA)	ROTH
Pertex	Medite GmbH
Pierce ECL western blotting substrate	Thermo Fisher Scientific
Power SYBR Green PCR master mix	Applied biosystems by Thermo Fisher Scientific
ProLong Gold Antifade Mountant	Thermo Fisher Scientific
Rimadyl (Carprofen)	Zoetis
RIPA Lysis and Extraction Buffer	Thermo Fisher Scientific
ROTI®Cell Gelatine-Lösung	ROTH
Sucrose	Sigma-Aldrich
Tamoxifen	Sigma: T5648
TEMED	VWR
Trypsin-EDTA	Thermo Fisher Scientific

8.2 Selfmade buffers

Distilled water, used to prepare all the solutions, was filtered with the "Milli-Q-Water System" (Millipore).

Table 8
Selfmade buffers

Phosphate- buffered saline (PBS)	For 1 L
NaCl (137 mM)	8 g
KCl (2.7 mM)	0.20 g
Na_2HPO_4 (10 mM)	1.44 g
KH_2PO_4 (2 nM)	0.24 g

Note: Distilled water was added to the final volume of 1000 ml. pH was adjusted to 7.4 using HCl.

TBST 10x	For 1 L
Tris	24.2 g

NaCl	204.4 g
Tween20	5 ml

Note: Distilled water was added to the final volume of 1 L. pH was adjusted to 7.5 using HCl.

Blocking buffer Retina	For 30 ml
BSA	0.06 g
Triton-X (10x)	0.9 ml
FBS	1.5 ml
PBS	27.6 ml

Blocking buffer muscle	For 30 ml
BSA	0.3 g
Triton X	0.075 ml
PBS	29.92 ml

MACS buffer	For 1 l
2 mM EDTA	4 ml
BSA	5 g

Note: Adjust pH to 8,8 with HCL, fill up with 1x PBS to 1l and filter before use.

8.3 Primers

Table 9
RealTime-PCR primers (mouse)

Primer	Sequence (5´-3´)
PDGFRα	CTCGTGCTTGGTCGGATTT TCTTCACAGCCACCTTCATTAC
GAPDH	GGAGAAACCTGCCAAGTATGA TCCTCAGTGTAGCCCAAGA
APP	AAGCGACAGCGTGGATTC TCCACCCCACCAGACATC
APLP2	CAGACAAGGAGATTGTTCACGA AGTACCAACGAGGCATCACA
CD45	CTGAATACCCGTGGAATGCT GATTGCTGATGACCCCAGAC
CDH5	GGTCTGTGGCCTCAATGTAGA TCATCAAACCCACGAAGTCC
Myh11	AGGCACTTGCATTGTAGTCC CCCAAGCAGCTAAAGGACAA
CD31	ACTCACGCTGGTGCTCTATG TGCTGTTGATGGTGAAGGAG
Myh6	CGCATCAAGGAGCTCACC CCTGCAGCCGCATTAAGT
Postn	CGGGAAGAACGAATCATTACA

	ACCTTGGAGACCTCTTTTTGC

Table 10
RealTime-PCR primers (human)

Primer	Sequence (5´-3´)
GAPDH	GCATCCTGGGCTACACTGA CCAGCGTCAAAGGTGGAG
APP #88	GTGACAATGTGGATTCTGCTG CTCCCATCTGCATAGTCTGTGT
APLP2 #9	CCACGGTCATCGTCATCA TGGCTGATGGTGCCATACT

8.3.1 Antibodies

Table 11
Primary antibodies

Name	Company: catalogue number	Dilution
Alexa Fluor® 647 goat anti-rabbit IgG	Lifetechnologies: A21244	1:300
Alexa Fluor® 488 anti-mouse CD68	BioLegend BV: 137011	1:100
APLP2	Ulrike Müller Heidelberg	1:1000
APP	Abcam: AB32136	1:1000
CD31	BD Biosciences: 550274	1:100
CD31	eBioscience: 25-0311-81	1:50
CD45	BD Pharmingen: 553079	
DAPI	Invitrogen: D3571	1:1000
ERG	Abcam: ab92513	1:300 for retinas 1:50 for muslces
GAPDH (14C10)	cell signaling: 2118S	1:1000
Isolectin GS-IB4 488	Invitrogen: 121411	1:200

Isolectin GS-IB4 647	I32450	Life Technologies GmbH	Life Technologies GmbH: I32450
PDGFRα			BioLegend: 135906

Table 12
Secondary antibodies

Name	Company: catalogue number	Dilution
Alexa Fluor 488 Goat anti-rat IgG	Life Technology: A11006	1:500
Alexa Fluor 647 Goat anti rabbit IgG	Life Technology: A21244	1:500
Anti-Mouse IgG, HRP-linked Antibody	Cell Signaling: 7076S	1:10.000
Anti-Rabbit IgG, HRP-linked Antibody	Cell Signaling: 7074S	1:10.000

8.4 siRNAs

Table 13
siRNA (human)

Gene name	Target sequence (5' → 3')
APP (#5)	GAAGAUGUGGGUUCAAACA
APP (#6)	GACUGAACAUGCACAUGAA
APLP2 (#7)	CAAGGAAAUUACUCAUGAU
APLP2 (#8)	CUGAGUAGCAGUGCUCUCA

8.5 Cell lines and cell culture media

Table 14
Cell lines

Name	Origin	Source
HUVEC	Human Umbilical Vein	Lonza
LLC1	Lewis Lung Carcinoma mouse	LGC Standards GmbH

Table 15
Cell culture media

Name	Source
Dulbecco's modified eagle medium (DMEM)	Gibco
EBM™-2 Endothelial Cell Growth Basal Medium-2	Lonza
EGM™-2 Endothelial SingleQuots™ Kit	Lonza

8.6 Kits

Table 16
Kits

Name	Source
cDNA synthesis kit	Roche
Click-iT™ Plus EdU Cell Proliferation Kit for Imaging, Alexa Fluor™ 488 dye	Thermo Fisher Scientific
RNA isolation- RNAeasy Mini kit	Qiagen
Quick RNA micro prep kit	Zymo
ProtoScript II Reverse transcription kit	New England BioLabs

8.7 Softwares

Table 17
Softwares

Name	Version
(Fiji Is Just) ImageJ	2.14.0/1.54f; Java 1.8.0_322 [64-bit]
Adobe illustrator 2022	Version 26.3.1 (64-bit)
Cellpose	v2.2.2
Ilastik	Version 1.4.0rc6
Image Lab	Version 6.1.0 Standard Edition
MoorFLPI-2	Review V 6.0
Prism 19 for Windows 64 bit	Version 10.1.1
QuantStudio™Design&Analysis Software	Version 1.5.2

8.8 Genetic mouse models

The group of Ulrike Müller from Heidelberg kindly provided double floxed animals for *APP* and *APLP2*. In the APP genomic locus and the APLP2 genomic locus, locus of X-over P1 (loxP) sites were introduced upstream of the promoter and downstream of exon 1, respectively (Mallm et al., 2010). This allows the genes to be deleted after mating with Cre recombinase-expressing animals. If no Cre recombinase is introduced into the mouse, the modified alleles behave like WT alleles. If not stated otherwise, experiments were performed 2 weeks after the last injection. To generate endothelium-specific *App/Aplp2* deficiency, double floxed animals were crossed with tamoxifen-inducible CDH5CreERT2 mice. The offspring were then intercrossed. All mice were backcrossed onto the C57BL/6 background for at least 8 generations. For experiments, male and female animals at an age of 8-12 weeks were used, if not stated otherwise. Littermates served as controls. Mice were housed under a 12-h light-dark cycle with free access to food and water and under specific pathogen-free conditions. Double KOs and control littermates were treated with tamoxifen at an age of 6 weeks, if not stated otherwise. Protocols were performed according to institutional and national guidelines.

9 Methods

9.1 Cell culture of LLC1 cells

LLC1 cells were cultured in DMEM growth medium supplemented with 10% FBS, LGlutamine (1:100), and Penicillin-Streptomycin (1:100) at 5% CO_2 and 37 °C. Confluent cells were washed with PBS and then treated with 0.25% Trypsin-Ethylenediaminetetraacetic (EDTA) solution until the cells were dissociated (1-3 min). Complete growth medium was added and the resuspended cells were centrifuged for 3 min at 900 rpm. After centrifugation, cell suspension was split 1:4 and grown until 75-80% confluence. To prepare the cells for further experiments, cells were washed again with PBS, dissociated with 0.25% Trypsin-EDTA, and centrifuged after resuspension in complete growth medium. Following the centrifugation, cells were counted with a Neubauer counting chamber and used for tumor angiogenesis model.

9.2 Cell culture of HUVECs

For the culture of ECs, Endothelial Cell Growth Basal Medium-2 was supplemented with Endothelial Single Quots^{TM} Kit, to achieve growth factor-supplemented endothelial growth medium (EGM)-2. Human umbilical vein endothelial cells (HUVECs) were obtained from Lonza. Cells were cultured in EGM-2 and passages <P6 were used for all experiments. For coating of cell culture plates, Collagen Type I solution was diluted 1:100 in sterile autoclaved 0.1% acetic acid in Millipore water. After coating for 30 min, plates were once washed with 10 ml Dulbecco’s phosphate buffer saline (DPBS). Afterwards, 10 ml EGM-2 medium was added and cells were

seeded on top. Cells were tested negative for mycoplasma contamination before experiments. All cells were incubated at 37 °C and 5% CO_2. Nearly confluent cells were washed with DPBS for one time and treated with 1.5 ml 0.25% Trypsin-EDTA solution for 1 to 3 min until the cells were dissociated. Next, 3 ml growth factor-supplemented EGM-2 medium was added, and resuspended cells were centrifuged for 4 min at 800 rpm, splitted according to the needs and seeded onto the new, coated cell culture dish.

9.3 siRNA-mediated knockdown

HUVECs at 50-70% confluency were transfected with different siRNA shown in the list (see 8.4) using lipofectamine RNAiMAX with the following preparation seen in Table 18.

Table 18
Transfection mix

	plate	
Tube 1	6 well	12 well
Opti-MEM	150.0 µl	25.0 µl
siRNA (20 µM)	1.9 µl	1.5 µl
Tube 2		
Opti-MEM	150.0 µl	10.0 µl
Lipofectamine RNAiMAX	2.0 µl	0.15 µl

First, single tubes were mixed well and then subsequently combined by gentle pipetting. After incubation for 20 min at room temperature (RT), mixtures were added to the cells. Media were changed 6 hours post-transfection and next day, a second transfection step was performed with the same procedure except the media change. Cells were lysed according to the needs on the morning of the 3rd day.

9.4 Quantitative RT-PCR analysis

Total RNA was isolated from EC monolayers using the Quick-RNA Micro prep kit according to the manufacturer’s protocol. A Nanodrop ND-100 Spectrophotometer was used for quality control of the samples. Complementary DNA synthesis was performed using the ProtoScript II Reverse Transcription kit. Afterwards, quantitative real-time PCR was performed using primers designed with the online tool provided by Roche and the Light-Cycler 480 Probe Master System (Roche). PCR was performed by initial denaturation at 95 °C for 5 min, followed by 40 cycles of 10 s at 95 °C, 30 s at 60 °C and 1 s at 72 °C. Duplicates or triplicates of each reaction were run and relative gene expression levels were normalized to Glycerinaldehyd-3-phosphat-dehydrogenase (GAPDH). The ΔΔCt method was used to calculate relative expression of the genes of interest. In 2023, the Light-Cycler 480 Probe Master System from Roche has been replaced by the QuantStudio1 from Applied Biosystems in our lab. Since then, quantitative RT-PCR mixes were prepared as shown in Table 19 New mix.

Table 19
Overview of PCR mixes

Old mix		New mix	
Volume	Component	Volume	Component
0,4 µl	Primer F (10 µM)	1 µl	Primer Forward (10 µM)
0,4 µl	Primer R (10 µM)	1 µl	Primer Reverse (10 µM)
0,2 µl	UPL-Probe according to Primer	10 µl	SYBR green
10 µl	Probes Master	3 µl	RNAse/DNAse free water
4 µl	RNAse/DNAse free water	5 µl	cDNA
5 µl	cDNA		

9.5 RNA sequencing

For RNA sequencing, I contacted Dr. Stefan Günther at our Bioinformatics core facility. I provided him with the RNA samples for whole transcriptome analysis sequencing and additionally a 1:10 dilution for quality control analysis. He performed the RNA sequencing according to our inhouse bioinformatics pipeline

(Figure 7). I received DeSeq2 normalized count matrix, quality control plots and a basic Gene Ontology analysis for further analysis.

Figure 7
Overview of in-house bioinformatics pipeline

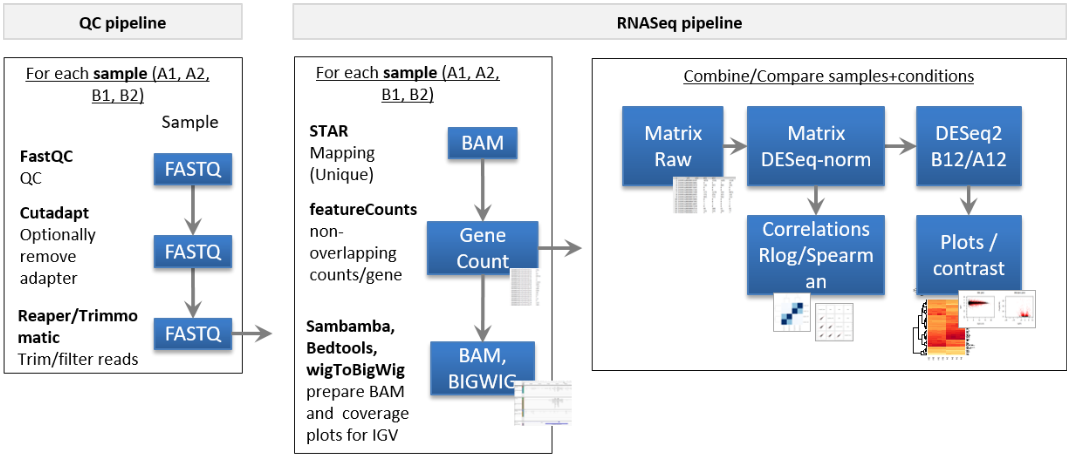

Note. Shown is an overview, starting with the quality control (QC) pipeline on the left, followed by the RNA sequencing pipeline of the right side.

9.6 Tube formation assay

A 15 well 3D µ-slide was used to study tube formation of HUVECs *in vitro*. First, 10 µl of matrigel was applied to each inner well. Plane filling levels were double checked using millimeter paper, to avoid gel meniscus. After solidification of matrigel at 37 °C for 1 h, secondly 10.000 transfected ECs in 50 µl EGM-2 medium per well were seeded on top. Live-cell images were taken with an Olympus IX81 microscope directly after seeding and 5 h later. During tube formation, the µ-slide was kept at 37 °C and 5% CO_2. Angiogenesis Analyzer plug-in was used in Fiji to automatically analyze images.

9.7 Genetic mouse models

APP$^{flox/flox/}$APLP2$^{flox/flox}$ mice were kindly provided by Ulrike Müller (Mallm et al., 2010). To generate tamoxifen-inducible endothelium-specific double KO mice, APP$^{flox/flox}$APLP2$^{flox/flox}$ mice were mated to CDH5CreERT2 mice. All mice were backcrossed onto the C57BL/6 background for at least 8 generations. Experiments were performed with littermates as controls. Male and female animals at an age of 8-12 weeks were used, if not stated otherwise. Mice were housed under a 12-h light-dark cycle with free access to food and water and under specific pathogen-free conditions. Cre-mediated recombination was induced by intraperitoneal injections of 1 mg tamoxifen per animal/day on 5 consecutive days. If not stated otherwise, experiments were performed 2 weeks after the last injection.

9.8 Knockout efficiency testing

Animals were sacrificed with CO_2 and perfused with 15 ml PBS via the left ventricle. Heart, upper and lower hind limb muscles were dissected out and stored on ice. For further processing, tissues were cut into pieces of about 1 mm^3 volume and were then enzymatically digested for 60 min on a gentleMACS™ Octo Dissociator with Heaters (Miltenyi Biotec). Digestion mixes differed between tissues and are represented below.

Table 20
Overview of enzyme mixes

Per 10 ml	Enzyme mix heart
20.0 mg	Collagenase II
50.0 Units	DNAse I
5.0 mg	Dispase
0.4 mg	Elastase
Fill to 10 ml	DMEM
Per 50 ml	Enzyme mix muscle
200.0 mg	Collagenase II
250.0 Units	DNAse I
Fill to 50 ml	DMEM

Digestion was stopped by adding 5 ml DMEM containing 10% FBS. Cell suspensions were filtered through 70 µm cell strainers followed by centrifugation at 500 g for 10 min at 4 °C. Supernatants were removed and 6.2 ml cold DPBS were added. Cell suspensions were transferred to 15 ml Falcons. Debris was removed by adding 1.8 ml Debris Removal Solution, followed by vortexing and gently overlaying with 4 ml cold DPBS. After centrifugation at 3.000 g for 10 min at 4 °C, the two top phases were aspirated. Then the tubes were filled up with 10 ml cold DPBS, gently inverted for three times and centrifuged again at 1.000 g for 10 min at 4 °C to remove remaining debris removal solution.

For testing KO efficiency on RNA levels, supernatant was removed completely and cells were suspended in 200 µl DMEM with 10% FBS for final staining. From now on samples were always kept on ice and sorting was proceeded at 4 °C. To

generate appropriate controls, totally 60 µl cell solution was randomly taken from the samples, further divided and labeled according to Table 21.
Remaining cell suspensions were also labeled with 2 µl of each antibody (AB). After 10 min incubation, 20 µl of unsorted cells were kept separately for quality check. Each sorting was started with detection of the fluorophores minus one (FMO) first, with adding 1 µl of Diamidino-2-phenylindole (DAPI) AB to the tubes directly prior sorting. After finishing the gating strategy, sorting of the samples was continued by Fluorescence-activated cell sorting (FACS). Thereby, cells were sorted into a 1.5 ml Eppendorf tube containing 300 µl of DMEM with 10% FBS. Already proceeded samples were stored on ice and finally all samples were centrifuged at 1.000 rpm for 10 min at 4 °C. Supernatant was removed and 100 µl of Zymo RNA lysis buffer was added, before storing the samples at -80 °C until further processing for quantitative polymerase chain reaction (qPCR) analysis.

Table 21
Labeling procedure of cells for FACS

	FMO all stainings	FMO CD45	FMO PDGFRα	FMO CD31
Cell suspension (µl)	22.5	12.5	12.5	12.5
CD31 AB (µl)	1	0.5	0.5	-
CD45 AB (µl)	1	-	0.5	0.5
PDGFRα (µl)	1	0.5	-	0.5

9.9 Retinal angiogenesis

Pups were injected with Tamoxifen from postnatal day 1 until 3 (P1-P3). At P6 pups were weighted and sacrificed by decapitation, eyes were cut out and incubated in 4% PFA on ice for two hours at RT. With the help of a dissection microscope, retinas were dissected out and four radial incisions were made. Then, retinas were washed with PBS for 5 min while rocking at 450 rpm. After incubation in blocking buffer for 1.5 h at 450 rpm, retinas were stained with ERG-AB (1:50 in blocking buffer) overnight. Retinas were then washed five times in PBS supplemented with 0.3% Triton for 10 min and AB binding was detected using goat anti-rabbit IgG 647 secondary AB diluted 1:300 in PBS for 2 h at RT. Additionally, Isolectin-B4 (IB4) AB conjugated with Alexa Fluor 488 was incubated at the same time. Finally, retinas were washed again five times in PBS supplemented with 0.3% Triton for 10 min and then mounted on glass slides using ProLong Gold Antifade Mountant and normal coverslips.

Overview images were taken with an SP8 from Leica at 10x magnification and 20x magnification images were taken with an SP5 from Leica.

9.10 Tumor angiogenesis model

For the study of primary tumor formation and the investigation of APP/APLP2 involvement in tumor angiogenesis, 50 µl of PBS containing 10^6 LLC1 cells were injected subcutaneously into the right flank of the animals. Tumor size was measured using a caliper at least twice a week, starting one week after tumor cell injection. If the tumor began to ulcerate or reached a maximum size of 1.7 cm^3, the animals were excluded and immediately euthanized for tissue removal. The calculation of tumor volume was performed according to the following formula:

$$V = 0.5 \times d^2 \times D$$

Hereby d represents the minor and D the major tumor axis. Only female mice at an age between 10-12 weeks were used for experiments.

9.11 Femoral artery ligation

Two weeks after tamoxifen injections, mice at the age of 8-12 weeks underwent FAL surgery. To study the ongoing angiogenesis, ligation of the femoral artery was performed proximal to *A. iliaca interna*, following the protocol of Limbourg et al. (2009). Under isoflurane anesthesia, blood flow was visiualized by laserspeckle imaging using a laser speckle imaging device (MoorFLPI-2, Moor Instruments, UK) mounted on an adjustable tripod before and directly after ligation of the *A. femoralis*. A real-time data acquisition software (MoorFLPI measurement software) was used for laserspeckle imaging and anesthetized mice were placed on a 37 °C heating pad for 3 min prior the measurement. 1 image/sec was recorded for 60 secs. Hind limb perfusion was additionally assessed on day 3, day 7, day 14, day 21 and day 28. An area of 2 cm x 3 cm from both limbs was scanned at a 10 cm distance, with a pixel resolution of 256 x 256 and a region of interest of approx. 80 mm^2 containing each foot was defined. Evaluation of data was done by MoorFLPI review software (moorFLPI Full-Field Laser Perfusion Imager Review Version 5.0). Further evalutions were done after euthanization.

In the second run of experiments, in 2023, mice received 5-Ethynyl-2'-desoxyuridine (EdU) (500 µg/ ml) via the drinking water directly after surgery for the time of the experiment or for the maximum duration of 2 weeks. 30 min prior ending the experiment, mice were injected primary fluorophore-labeled AB against IB4 via tail vein to stain the perfused vasculature.

In addition to the duration of 28 days, the morphology of the vasculature was assessed in another group of mice at seven days after ligation of the *A. femoralis*. This was intended to give further insights into the primary phase angiogenesis events in contrast to the late phase events at day 28.

9.12 Histological and immunohistochemical analysis of murine muscles

For histological and immunohistochemical analysis of murine muscles, animals were perfused via the left ventricle with 10 ml PBS, followed by 15 ml of 4% PFA in PBS. Tibialis anterior muscles as well as gastrocnemius and soleus muscles were dissected out and soaked into 10% sucrose in PBS overnight. Percentage of sucrose was increased further to 20% and 30% on the following 2 days. Tissues were then embedded in Tissue-Tek® O.C.T.™ using Tissue-Tek® Cryomold® Cryomolds intermediate squares on dry ice. Immediately after curing of Tissue-Tek® O.C.T.™, samples were stored in -80 °C until further process. Frozen samples were cryosectioned (10 µm) and fixed again with 4% PFA for 5 min on ice.

For immunohistochemical analysis, samples were first washed with PBS three times for 5 min at RT. If EdU was applied into the drinking water, EdU click-it kit from Thermo Fisher Scientific was first used to detect EdU according to the manufacturer's protocol. Otherwise, sections were directly immunostained with AB against Cluster of differentiation 31 (CD31), CD68, IB4 or a combination of them overnight at 4 °C. After washing three times with PBS, bound primary AB were detected using Alexa Fluor 594-conjugated secondary donkey anti rat AB DAPI (1:1000) was used to label cell nuclei. Mounting was performed with either Fluoromount or Dako. The latter was used for farRed imaging due to less background noise. Images were acquired using a Ni-E ECLIPSE widefield microscope (Nikon) equipped with a SlideExpress 2 slideloader (Märzhäuser), a SOLA light engine (Lumencor) and a DS-Qi2 Mono Digital Microscope camera (Nikon) controlled by the NIS-AR software v.5.3 (Nikon). All acquisition parameters (light sources, illumination time, camera gain etc.) were kept constant for the entire

imaging experiment. Image acquisition was automated using the NIS-AR JOBS module: Overview images in the DAPI channel were acquired using a CFI Plan Achromat UW 2x objective (Nikon) and regions of interest selected for all slides. A 500 µm autofocus in the DAPI channel was performed in the middle of each region, followed by the acquisition of a large image for all fluorescent channels (filters: DAPI-5060C (Nikon), FITC-3540C (Nikon), mCherry-B (Nikon) and Cy5-4040C(Nikon)) using a CFI Plan Apochromat 10x Lambda objective (Nikon). The resulting images were automatically processed in the NIS-AR software by a fluorescence-based stitching using the parameters "Image Registration" and "Optimal Path".
The muscle samples from seven days after FAL were processed with the Axioscan 7 from Zeiss during a testing period of the machine within our institute. The advantage of the Axioscan 7 compared to the Nikon Slideloader, we have in house, is the ability to image five different colors at once instead of four. Therefore, ERG AB could be included for these samples. The 5th color was intended to be used to clearly separate ECs from other cells. However, probably to insufficient perfusion of the hindlimbs, ERG AB was not equally working in all slides and therefore the planned analysis could not be performed.

For quantification of all slides, the EC area was defined by CD31 staining using ImageJ software, and the fluorescent signal indicating IB4 was then divided by the total EC area to display the microvascular perfusion. To depict ongoing proliferation, EdU positive labeled cells within the CD31 positive area were counted as EdU positive EC with Fiji.

For histological analysis, slides were stained with hematoxylin for 10 min, followed by soaking in warm running tap water for 3 min. Afterwards they were stained with eosin for 5 min. Next steps were rinsing with distillated water and subsequently dehydrating through a series of alcohol solutions in ascending concentration (70%, 85%, 95%, and 100%, 2 min each). Then samples were cleared in two changes of xylene for 5 min, mounted with Pertex Mounting medium, covered with glass coverslips (1mm) and dried overnight.

Images were acquired using a Ni-E ECLIPSE widefield microscope (Nikon) equipped with a SlideExpress 2 slideloader (Märzhäuser), a LED 100 coolwhite diascopic lightsource (Märzhäuser) and a DS-Ri2 Digital Microscope camera

(Nikon) controlled by the NIS-AR software v.5.3 (Nikon). All acquisition parameters (light sources, illumination time, camera gain etc.) were kept constant for the entire imaging experiment.

Image acquisition was automated using the NIS-AR JOBS module: Overview images were acquired using a CFI Plan Achromat UW 2x objective (Nikon) and regions of interest selected for all slides. A 500 µm autofocus in the DAPI channel was performed in the middle of each region, followed by the acquisition of a large image using a CFI Plan Apochromat 10x Lambda objective (Nikon).

The resulting images were automatically processed in the NIS-AR software by a widefield stitching using the parameters “Image Registration” and “Blending”.

9.13 Statistical analysis

Statistical data analysis utilized are included in each figure and described in detail on the respective figure legends. Trial experiments or experiments done previously were used to determine sample size with adequate statistical power. Samples were excluded in cases where RNA/cDNA quality or tissue quality after processing was poor (below commonly accepted standards). Data are presented as means ± Standard Deviation (SD). All statistical analyses were performed using Prism 10 software (GraphPad). Normality testing was always done prior analysis using Shapiro Wilk test.

9.14 Study approval

All procedures of animal care and use in this study were approved by the local animal welfare authority and committee (Regierungspräsidium Darmstadt).

10 Results

10.1 APP and ALPL2 but not APLP1 are highly expressed in endothelial cells

To validate the previous findings of our group and to justify the study of the APP family members in ECs, I checked the transcriptional expression of APP, APLP1 and APLP2 in HUVECS by whole transcriptome RNA sequencing (Figure 8).

Figure 8
App and Aplp2, but not Aplp1 are highly expressed in endothelial cells

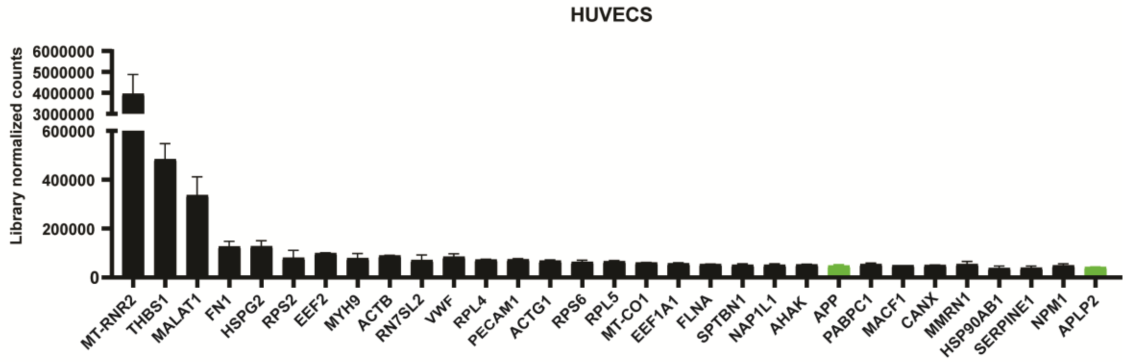

Note: Whole transcriptome RNA sequencing of HUVECs was performed to determine highly expressed genes in endothelium under basal conditions. Shown is a histogram of the library normalized counts.

I found that APP and APLP2, but not APLP1 are among the TOP 31 genes and highly expressed in ECs under basal conditions. As shown in the introduction part, this is in accordance with gene expression profiles of the APP family members.

10.2 Confirmation of successful depletion of *APP* and *APLP2* after siRNA-mediated knockdown

To assess the efficacy of the designed siRNA targeting *APP* and *APLP2*, I cultured HUVECs upon 70% of confluence before I transfected them with siRNA on two consecutive days. On the third day, I isolated RNA, prepared cDNA and checked KD efficiency with qPCR. As depicted in Figure 9 relative expression levels of both APP and APLP2 were highly reduced, indicating a high efficiency of siRNA.

Figure 9

Confirmation of successful depletion of APP and APLP2 after siRNA-mediated knockdown in HUVECs

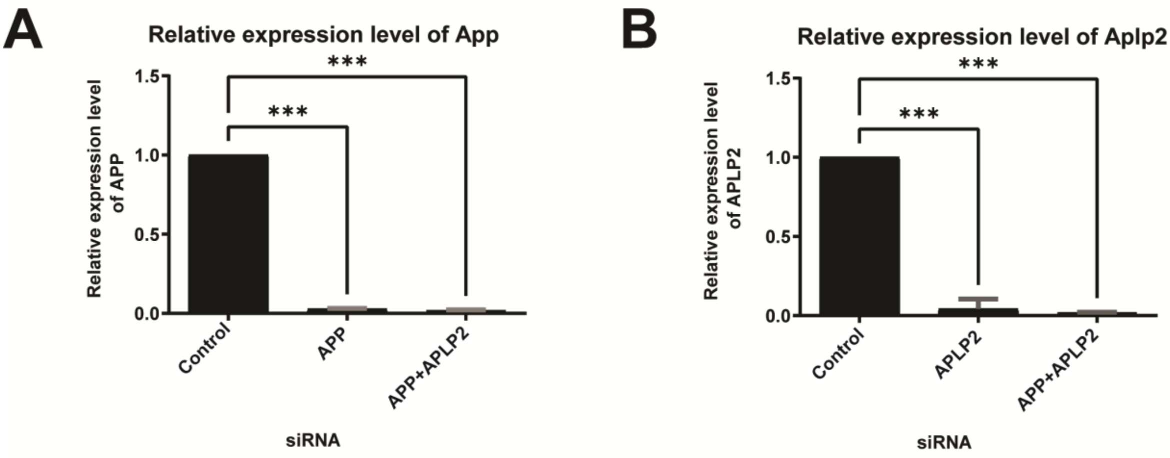

Note: (A-B) Expression of APP and APLP2 in HUVECs after transfection with control siRNA or siRNA against APP(n=3), APLP(n=3) or both (n=2) in independent experiments; all data normalized to GAPDH and controls were set as 1.Data are presented as mean ± SD. p> 0.12 (ns); p < 0.033 (*), p ≤0.002 (**), p ≤0.001 (***)
Comparisons were performed using Kruskal-Wallis Test.

Additionally, I found a significant increase of APP expression after KD of APLP2 (Figure 1Figure 10A). Elevation of APLP2 gene expression after KD of APP couldn't be detected (Figure 10B). As consequence of these findings, I decided to always knockdown (KD) both genes in further experiments to avoid compensatory effects.

Figure 10

Compensatory effects of APP after siRNA-mediated knockdown of APLP2 in HUVECs

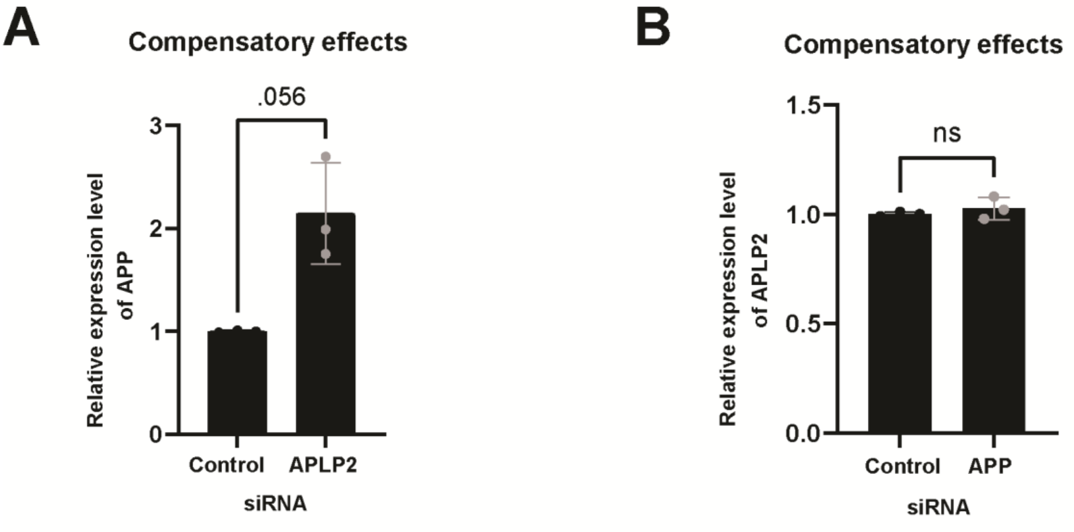

Note: (A) Relative expression levels of APP in HUVECs after transfection with control siRNA or siRNA against APLP2 (n=3 independent experiments); all data normalized to GAPDH and controls were set as 1.(B) Relative expression levels of APLP2 in HUVECs after transfection with control siRNA or siRNA against APP (n=3 independent experiments); all data normalized to GAPDH and controls were set as 1. Data are presented as mean ± SD. p> 0.12 (ns); p < 0.033 (*), p ≤0.002 (**), p ≤0.001 (***)
Comparisons were performed using Welch’s t-test.

10.3 Compromised tube formation after knockdown of *APP* and *APLP2* in HUVECs

To analyze a role of APP/APLP2 in vascular development, I used an *in vitro* model and tested in HUVECs whether the KD by siRNA of *APP*, *APLP2* or of both had an effect on angiogenesis in a tube formation assay. I observed a reduced tube formation in single *APP* KD cells and an almost complete disability to form tubes in cells with double KD as shown in Figure 11, while KD of *APLP2* alone had no effect. These observations could be replicated with three different, independent siRNAs leading to the same results (data not shown). However, the physiological relevance and the mechanism behind this observation still needs to be unraveled.

Figure 11
Loss of endothelial APP and APLP2 highly affects tube formation ability

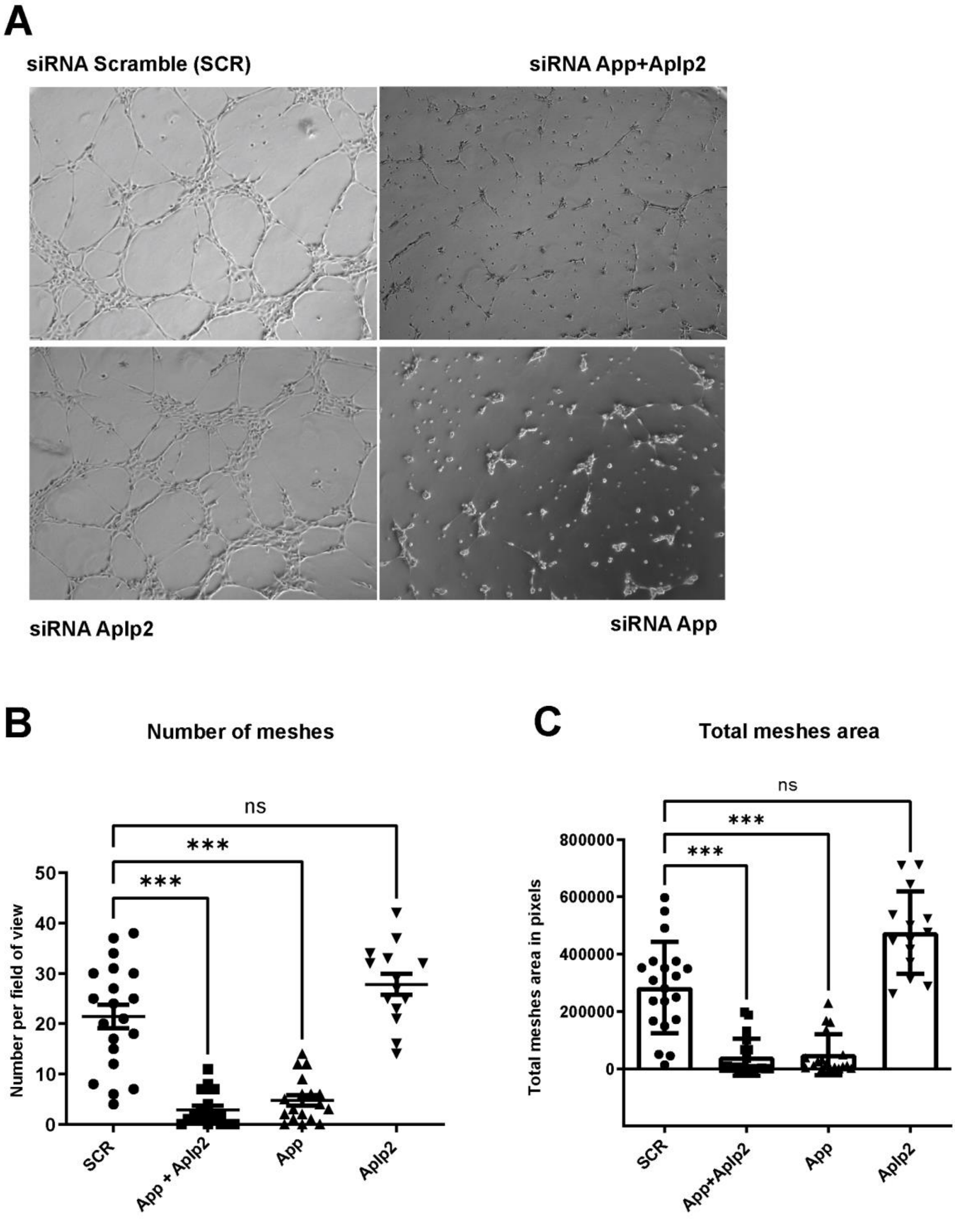

Note: (A) Representative images of HUVECs after KD, 5 hours after seeding on matrigel. (B-C) Statistical analysis of number of meshes per field view and total meshes area in pixels (n=20 for SCR /App+Aplp2, n=18 for App and n=14 for Aplp2). Data are presented as mean ± SD. p> 0.12 (ns); p <0.033 (*), p ≤0.002 (**), p ≤0.001 (***).
Comparisons were performed using Kruskal-Wallis Test.

10.4 Successful deletion of APP and APLP2 in the endothelium

To confirm the KO of *App* and *Aplp2* in the endothelium, I isolated hearts and upper as well as lower limb muscles from control and double KO mice 10 days after tamoxifen injection. Further, I sorted for ECs cells with FACS, lysed the sorted ECs, isolated mRNA, performed cDNA synthesis and quantified relative expression levels of both genes in relation to GAPDH as housekeeping gene using qPCR. As shown in Figure 12, KO of *App* as well as *Aplp2* strongly decreased mRNA levels in all organs, leading to a successfully generated double KO mouse line.

Figure 12

Knockout efficiency of App and Aplp2 at mRNA levels in endothelial cells from different organs

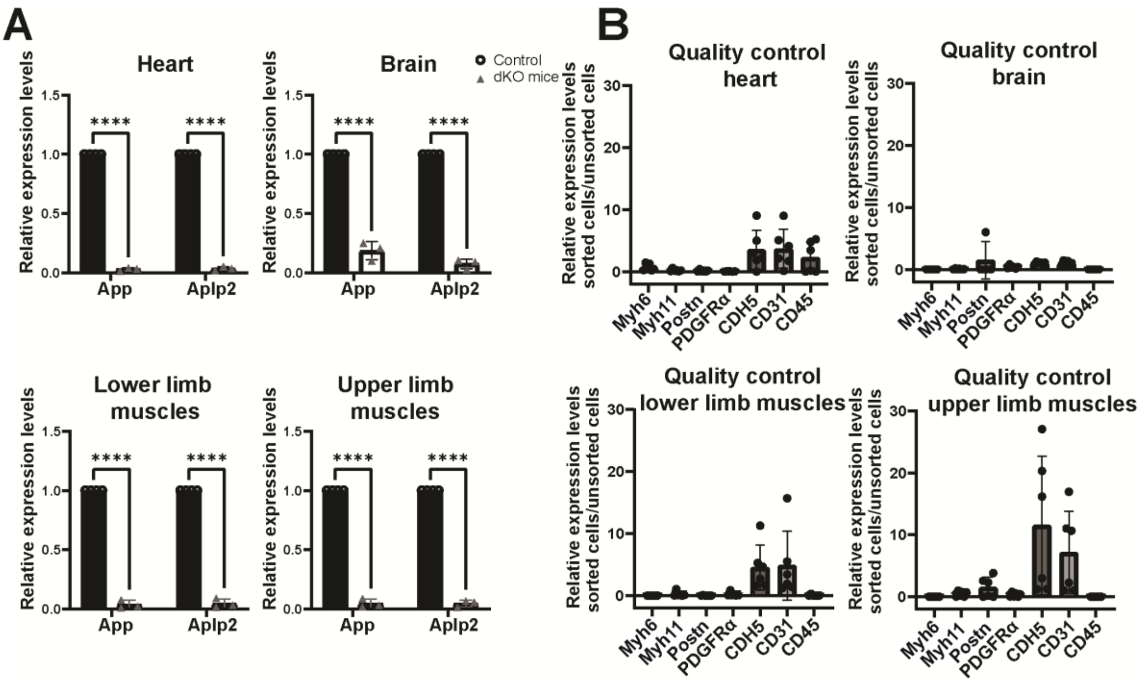

Note. Knockout efficiency of *App* and *Aplp2* was tested in FACS sorted endothelial cells. (A)Expression levels of *App* and *Aplp2* relative to GAPDH in different organs are shown.
(B) Quality control for effective cell sorting is displayed as the ratio of relative expression levels of sorted cells divided by the relative expression levels of unsorted cells.
Data are presented as mean ± SD. p> 0.12 (ns); p < 0.033 (*), p ≤0.002 (**), p ≤0.001 (***), p ≤0.0001 (****)
Comparisons were performed using ordinary 2way ANOVA with Šidák's multiple comparisons test with a single pooled variance.
Myh6: Myosin heavy chain 6; Myh11: Myosin heavy chain 11; Postn: Periostin;

I assessed the efficiency of cell sorting by comparing the gene expression profiles between sorted and unsorted cells using qPCR. Additionally, I validated the successful sorting by examining the enrichment of EC markers such as CDH5 and CD31. Importantly, I ensured there was no significant upregulation of markers associated with other tissue or cell types, including Myh6 for cardiomyocytes, Myh11 for smooth muscle cells, Postn for connective tissues, PDGFRα for mesenchymal stem cells, pericytes, fibroblasts, and smooth muscle cells, as well as CD45 for leukocytes such as lymphocytes, monocytes, macrophages, and granulocytes (Figure 12B).

10.5 Endothelium-specific double knockout mice show no differences in body weight

To further study APP and APLP2 function *in vivo*, floxed mice for *App* and *Aplp2* (App $^{fl/fl}$; Aplp2 $^{fl;fl}$) were crossed with CDH5CreERT2 mice to generate endothelium-specific double KO mice (CDH5CreERT2;App $^{fl/fl}$; Aplp2 $^{fl;fl}$). All mice were injected with tamoxifen for five consecutive days, followed by weekly inspections. As shown in Figure 13, endothelium-specific double KO mice developed normally without any alterations in body weight.

Figure 13
Endothelium-specific double KO mice show no differences in body weight

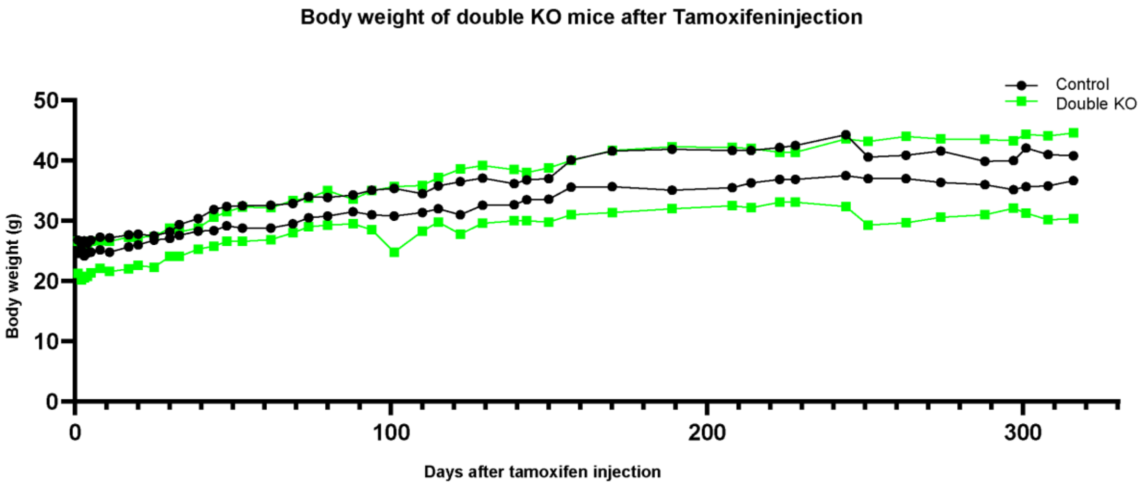

Note: Endothelium-specific App/Aplp2 knockout mice and control littermates were injected with 50 µl of tamoxifen (10 mg/ml) for five consecutive days, followed up by weekly body weight scoring. Shown are body weights in grams over 316 days post injections. n= 2 mice per group.

10.6 Reduction in vascularization at postnatal day 6 in double KO group but no differences in single *App* KO group

To study angiogenesis *in vivo* and to see whether APP or APLP2 play a role in blood vascular development, I chose the retinal angiogenesis model. Mice were treated with tamoxifen at P1-P4 and retina were analyzed at P6. Endothelium-specific double KO pups showed a reduction in vascularization at postnatal day six compared to control littermates (Figure 14A and B).

Figure 14

Loss of endothelial APP and APLP2 results in decreased postnatal angiogenesis in vivo

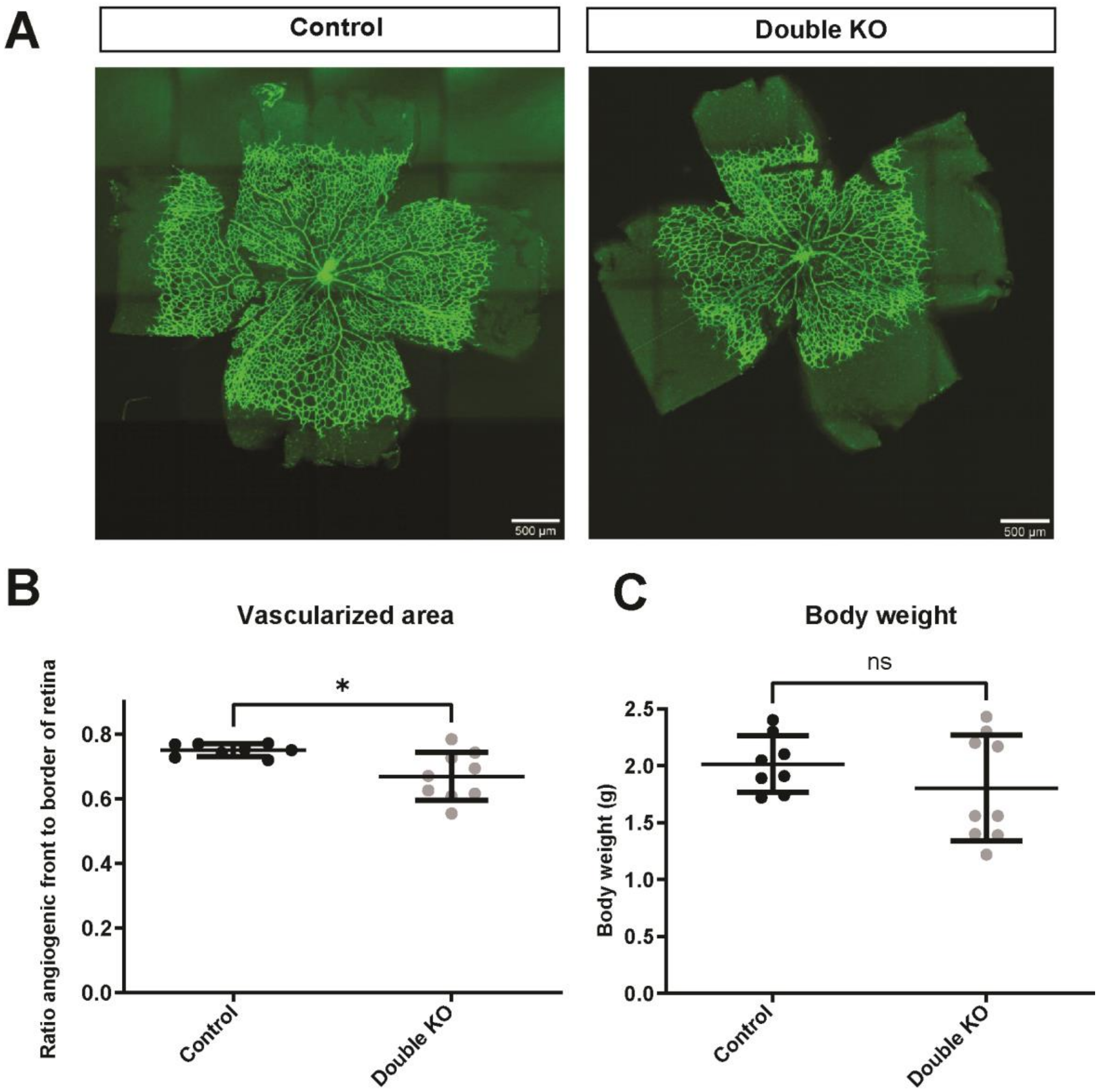

Note. (A-C) Wild-type (WT) and EC-APP-APLP2-dKO newborns were treated at P1-4 with tamoxifen, and retinae were prepared at P6. Shown are the representative photomicrographs of retinae stained for isolectin B4 (IB4) Scale bar: 500µm (A) and the statistical evaluation of staining for IB4 (n=8, WT; n=9, EC-App/Aplp2-KO (B) and the body weights (C). Data are presented as mean ± SD. p> 0.12 (ns); p < 0.033 (*), p ≤0.002 (**), p ≤0.001 (***)
Comparisons were performed using two-tailed unpaired t-test with Welch's correction.

To test, whether this was due to growth retardation, I also compared the body weight of both groups, but there was no significant difference (Figure 14C).

Since the vascularization in double KO mice was affected, I aimed to closely examine the arteries and veins in both groups. Therefore, I measured the diameter of veins and arteries, as well as counted the number of branching points present in each group (Figure 15). Statistical analysis did not reveal significant differences in either the diameters or numbers of branching points.

Figure 15
Loss of endothelial APP and APLP2 does not affect vessel diameter nor the number of branching points in vivo

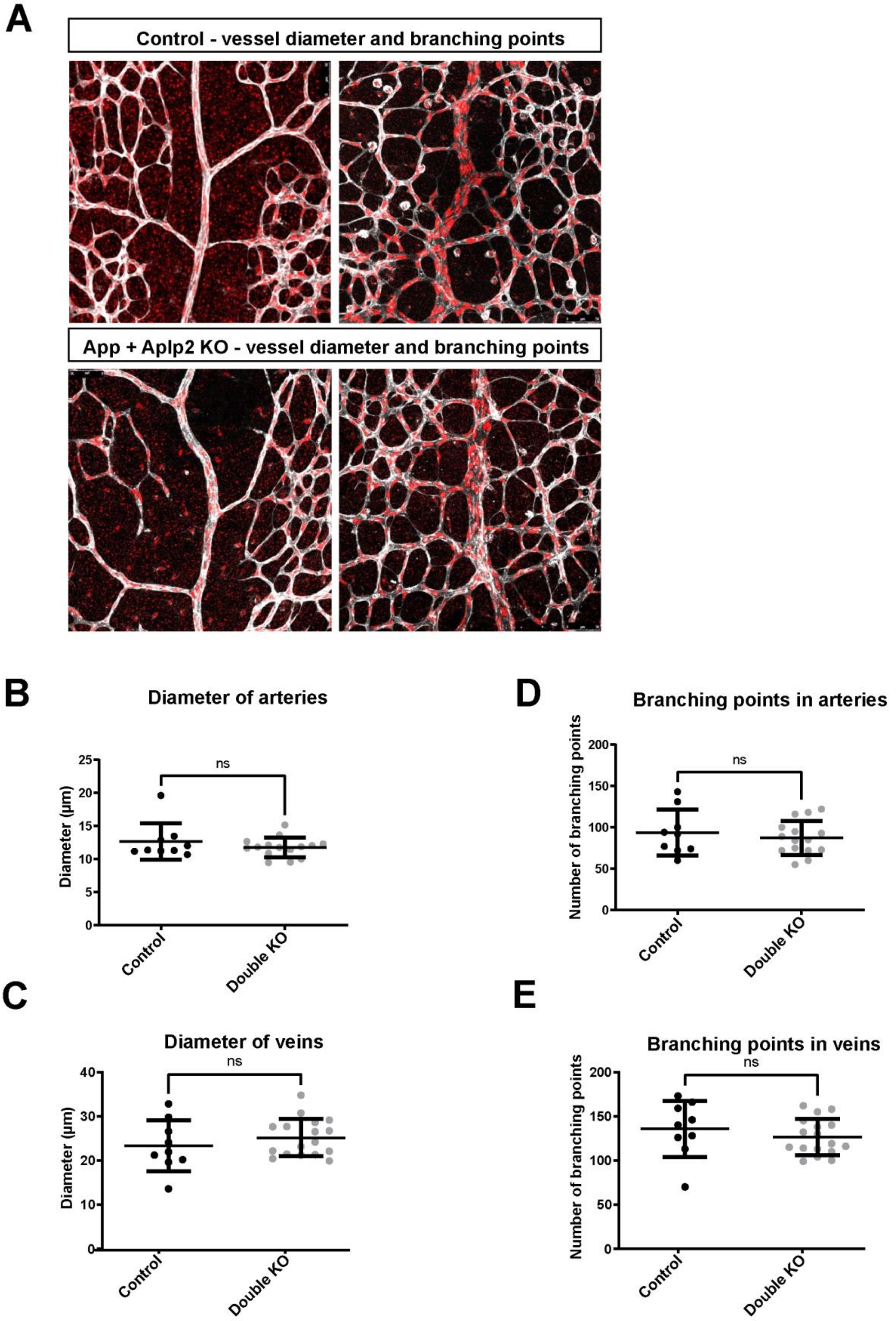

Note. (A-C) Wild-type (WT) and EC-APP-APLP2-dKO newborns were treated at P1-4 with tamoxifen, and retinae were prepared at P6. Shown are the representative photomicrographs of retinae stained for isolectin B4 (IB4)(gray) and ERG (red) (A) and the statistical evaluation of diameters of arteries (n=12, WT; n=9, EC-Fat1-KO (B) and veins (C) as well as of number of branching points in arteries (D) and veins (E). Data are presented as mean ± SD. $p > 0.12$ (ns); $p < 0.033$ (*), $p \leq 0.002$ (**), $p \leq 0.001$ (***) Comparisons were performed using two-tailed unpaired t-test with Welch's correction for Branching points and diameters in arteries.

To investigate whether the reduction in vascularization could be related to either APP or APLP2 alone, I generated endothelium-specific single KO (CDH5CreERT2;App $^{fl/fl}$) mice by crossing floxed mice for *App* (App $^{fl/fl}$) with CDH5CreERT2 mice and afterwards performed retinal angiogenesis.

As seen in Figure 16, the vascularized area in the single *Aplp2* KO group was slightly reduced while the body weight in KO and control group was equal.

Figure 16

Loss of endothelial APLP2 alone slightly affects angiogenesis in vivo

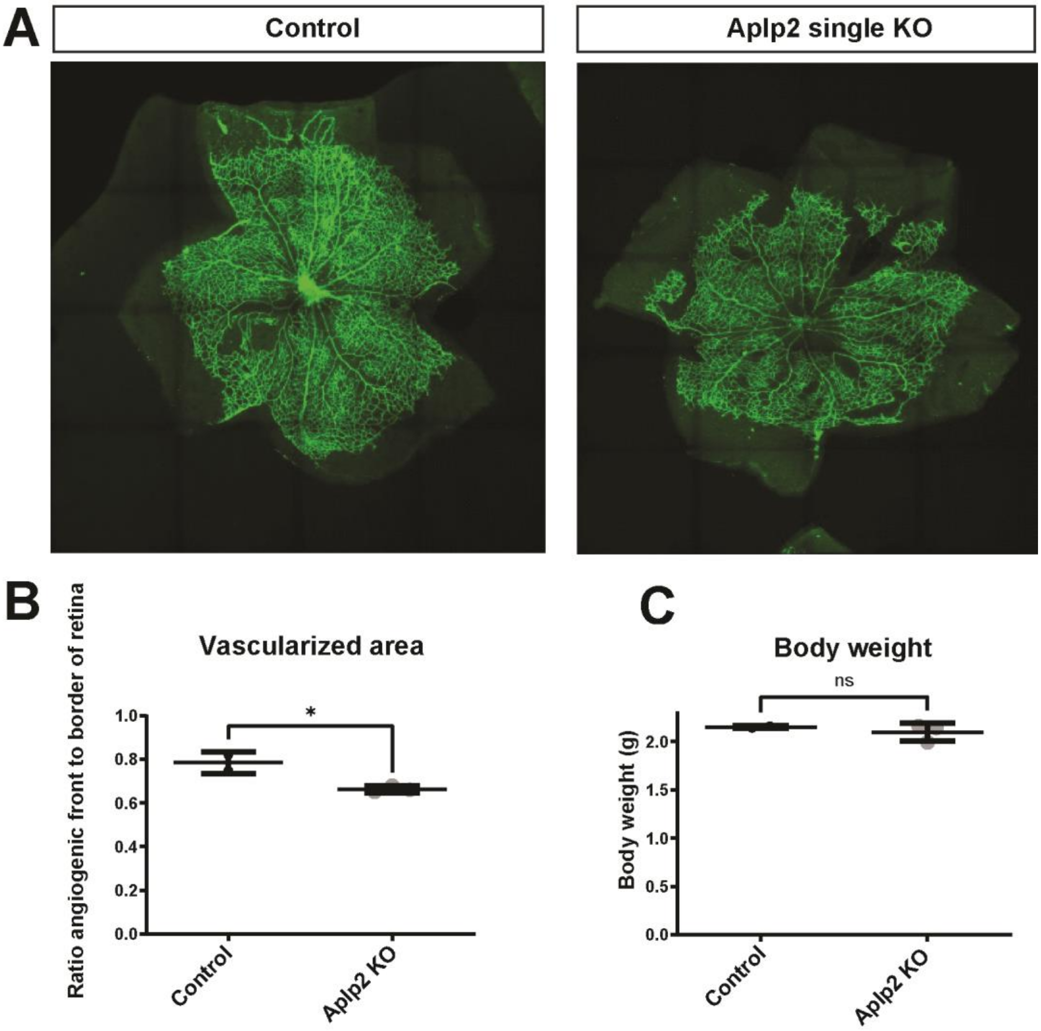

1*Note.* A-C) Wild-type (WT) and EC-APP-sKO newborns were treated at P1-3 with tamoxifen, and retinas were prepared at P6. Shown are the representative photomicrographs of retinas stained for isolectin B4 (IB4) (A) and the statistical evaluation of vascularized areas (n=2, WT; n=3, EC-Aplp2-KO)(B) and body weight (C).Data are presented as mean ± SD. p> 0.12 (ns); p < 0.033 (*), p ≤0.002 (**), p ≤0.001 (***)
Comparisons were performed using two-tailed unpaired t-test

The single KO of APP did not demonstrate differences in body weight nor in vascularization (Figure 17). This contradicts the results of the tube formation assay conducted *in vitro*, where *App* single KD had a huge impact on tube formation, whereas *Aplp2* single KD resulted in unchanged tube formation.

Figure 17

Loss of endothelial APP alone does not affect angiogenesis in vivo

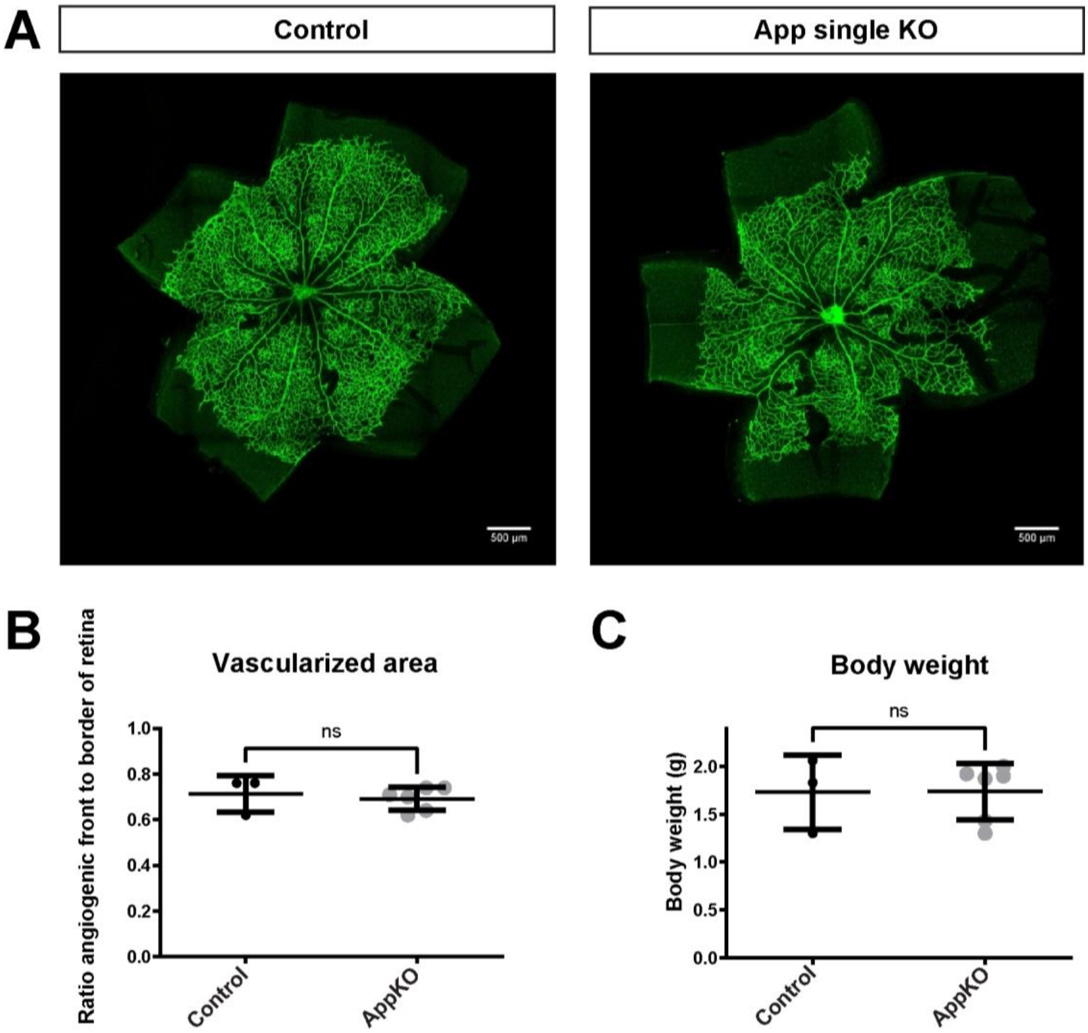

Note. (A-C) Wild-type (WT) and EC-APP-sKO newborns were treated at P1-3 with tamoxifen, and retinas were prepared at P6. Shown are the representative photomicrographs of retinas stained for isolectin B4 (IB4) (A) and the statistical evaluation of vascularized areas (n=2, WT; n=3, EC-App-KO)(B) and body weight (C). Data are presented as mean ± SD. $p > 0.12$ (ns); $p < 0.033$ (*), $p \leq 0.002$ (**), $p \leq 0.001$ (***)
Comparisons were performed using two-tailed unpaired t-test.

Meanwhile Brash et al. (2020) could show that Cre-ER^{T2}, activated by tamoxifen as well as 4-hydroxytamoxifen, compromises angiogenesis in perinatal retinas. Vascular network extension as well as branch density but not body weight were affected (Brash et al., 2020). Since I didn't include a control for CreER toxicity in my studies, I can't automatically refer the findings only to effects of CreER toxicity, but the likelihood is quite high that it influenced the results (Brash et al., 2020; Rashbrook et al., 2022). Hence, I decided to choose another *in vivo* model to study angiogenesis in the endothelium-specific double KO mouse line.

10.7 Tumor angiogenesis as another model for *in vivo* angiogenesis

In the next step, I investigated whether KO of *App* and *Aplp2* affect tumor angiogenesis in adult mice. Therefore, LLC1 cells were subcutaneously injected into the right flank of mice and body weight, tumor volume as well as tumor weight were assessed. There were no significant differences on the body weights between both groups. Due to ulcerations in tumors, two control and one double KO mice needed to be euthanized before reaching the endpoint. Out of the remaining eight control mice, four didn't develop any tumor after 28 days (Figure 18).

Figure 18

Tumor angiogenesis in endothelial-specific double KO mice

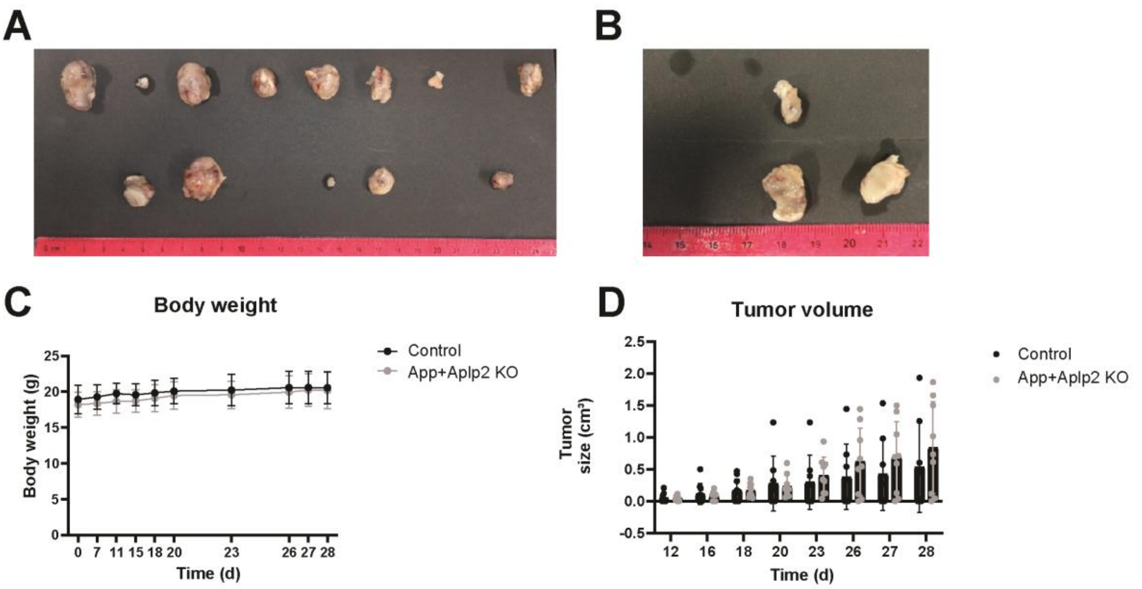

Note. (A) tumors of double KO mice (upper line) and control littermates (lower line) after overnight incubation in 4% PFA. (B) tumors of drop-out mice after overnight incubation in 4% PFA. (C) Body weights and (D) tumor volumes are shown. Data are presented as mean ± SD. $p > 0.12$ (ns); $p < 0.033$ (*), $p \leq 0.002$ (**), $p \leq 0.001$ (***)
Multiple Mann-Whitney tests with False Discovery Rate (FDR) as multiple comparisons have been performed.

Since the control group did not show a homologous distribution of tumors as expected, no meaningful assessment could be made regarding the involvement of APP and APLP2 in tumor angiogenesis. Consequently, I decided to study the role of APP and APLP2 in angiogenesis in another *in vivo* model.

10.8 Sporadic observation of necrosis after femoral artery ligation in double KO mice

Manavski et al. (2018) demonstrated that proliferation of ECs contributes to the generation of mature and perfused microvessels after hind limb ischemia. To examine whether ischemia-induced angiogenesis is also controlled by APP and/or APLP2, Kerstin Troidl and I performed FAL in control and double KO mice 10 days after tamoxifen treatment. In the first batch of FAL in double KO mice in 2019, two out of seven mice developed severe necrosis in the ligated legs within the first week after surgery. One was found dead in the cage, while the other one was immediately euthanized after observation of necrosis on day 7. A third mouse developed necrotic digits by day 14, whereas no ischemic symptoms have been observed within control littermates. These three necrotic events led to the premature termination of the animal experiment. Analysis of perfusion ratio did not reveal a significant difference between both groups (Figure 19).

Figure 19
Femoral artery ligation leads to sporadic observation of necrosis in double KO mice

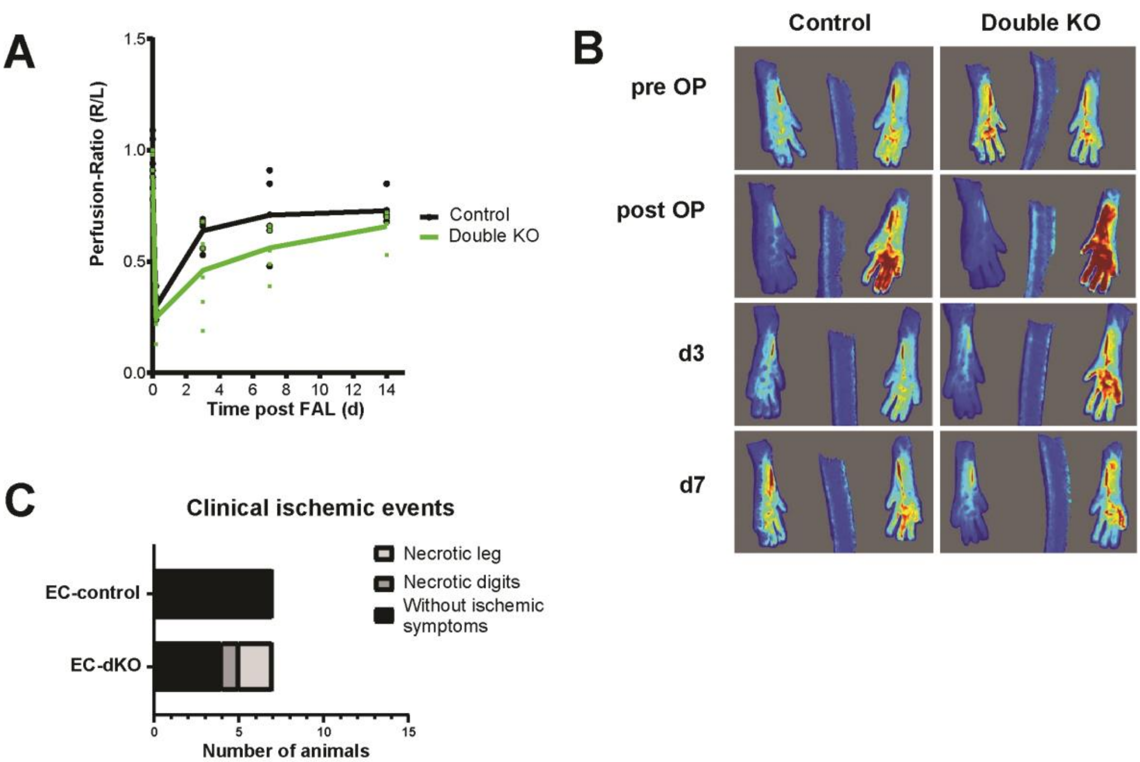

Note. (A) Perfusion-Ratios of ligated to non-ligated legs are shown. (B) Representative images of laser speckle imaging are presented. (C) Overview of clinical ischemic events are illustrated.
Data are presented as mean ± SD. $p > 0.12$ (ns); $p < 0.033$ (*), $p \leq 0.002$ (**), $p \leq 0.001$ (***)

Multiple Mann-Whitney tests with False Discovery Rate (FDR) as multiple comparisons have been performed.

However, the values are not fully representative due to the early drop out of mice with necrosis. Further examination of the gastrocnemius muscles revealed that the structure of the vasculature in the remaining double KO mice appeared to be affected as shown in Figure 20.

Figure 20
CD31 looks affected in endothelium-specific double KO mice

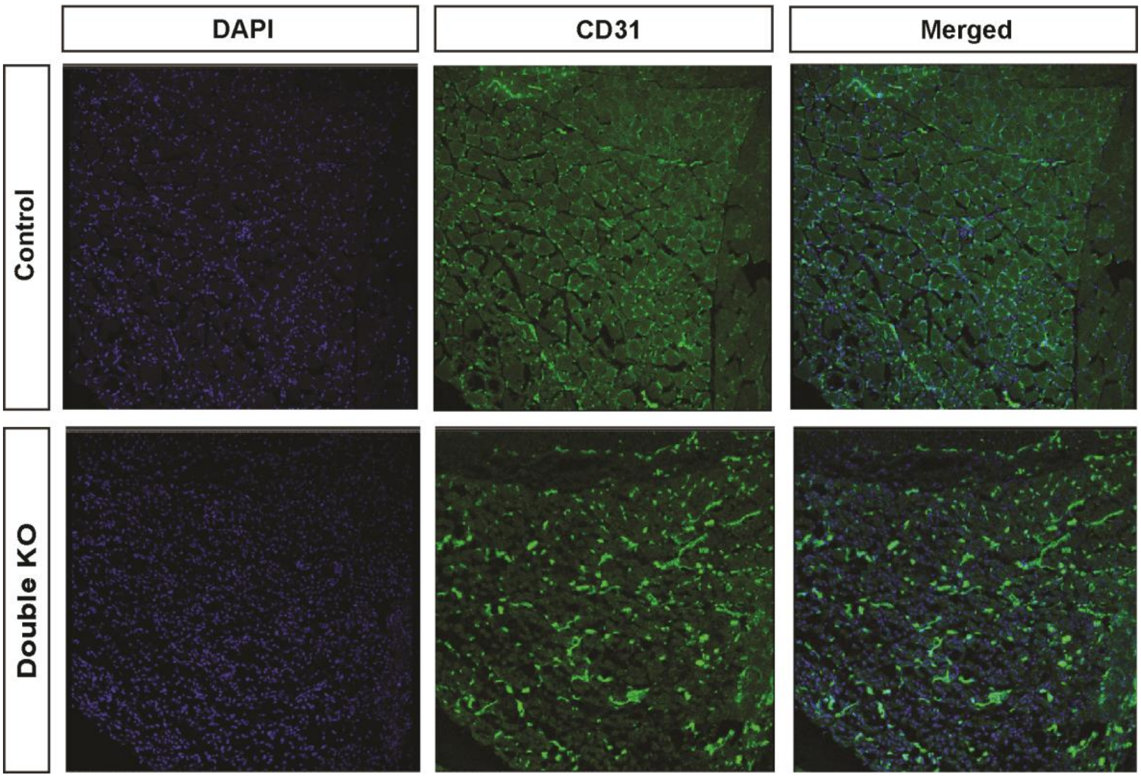

Note. Hind-limb ischemia was induced by femoral artery ligation in EC-App/Aplp2-KO mice and control littermates. Shown are representative photomicrographs of sections of the soleus muscle of the ligated hind limbs 14 days after the surgery stained with DAPI (blue) and CD31 (green).

10.9 Endothelium-specific knockout of *APP/APLP2* leads to less proliferation but no significant change in perfusion 28 days after femoral artery ligation

For the repetition of FAL in 2023, I made several changes. As the mouse paws are quite far away from the ischemic region in the hind limb, where angiogenesis is ongoing, laser speckle imaging of the mouse paws might not be the most appropriate method for this analysis. That is why I decided to still use it for confirmation of successful ligation, but not for further evaluation of reperfusion. Since the gastrocnemius muscles in the double KO group in 2019 showed affected

CD31 staining of the vasculature, I additionally decided to inject fluorescently labeled IB4 AB via the tail vein before killing the animals to detect which vessels are physiological in use. By administration of EdU via the drinking water after surgery, I examined the ongoing proliferation. Additionally, a new surgeon, Shangmin Liu, helped me with the ligation experiments.

Following ligation of the femoral artery, mice were given EdU via the drinking water for the first 2 weeks. After a total of 28 days, mice were anesthetized and received IB4 AB conjugated to Alexa fluor 647 via the tail vein 30 min before euthanasia. Immunohistochemistry analysis of the tibialis anterior and soleus muscles showed reduced proliferation of ECs in the tibialis anterior muscles of double KO mice (Figure 21). However, not such reduction could be observed within the soleus muscles (Figure 21C). The endothelium-specific KO of App and Aplp2 did not affect the microvascular perfusion, which was reflected by the ratio of IB4+ area divided by the CD31+ area (Figure 21E and F).

Figure 21

Less proliferation but no significant change in perfusion 28 days after femoral artery ligation

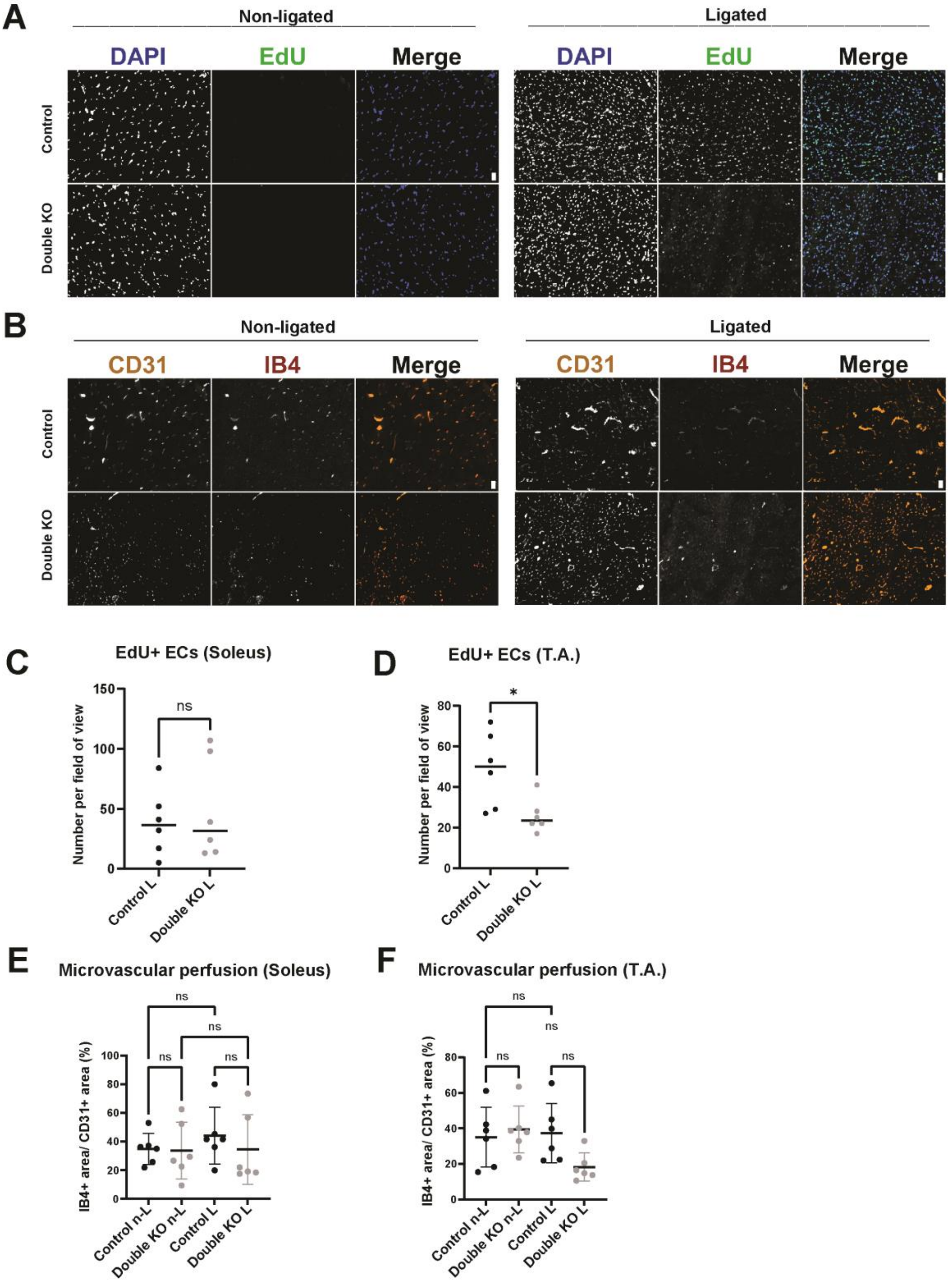

Note. Hind-limb ischemia was induced by femoral artery ligation in EC-App/Aplp2-KO mice and control littermates. Representative photomicrographs of sections of the tibialis anterior muscle of the ligated hind limb (L) and of the non-ligated side (n-L) 28 days after the surgery (n= 6 mice in both groups) are shown. Representative sections stained with DAPI and EdU are presented (A). Representative photomicrographs of sections of the tibialis anterior muscle of the ligated hind limb (L) and of the non-ligated side (n-L) 28 days after the surgery, stained with CD31 and IB4 are shown (B). Bar length 20 µm (A+B). Quantitative analysis of EdU labeled endothelial cells in soleus (C) and tibialis anterior (D) muscles from mice 28 days after femoral artery ligation. Statistical evaluation of

the IB4+/CD31+ area in soleus (E) and tibialis anterior (F),reflecting the perfusion in the muscles, are shown. Values have been excluded if tissue quality after processing was below commonly accepted standards. Data are presented as mean ± SD. $p > 0.12$ (ns); $p < 0.033$ (*), $p \leq 0.002$ (**), $p \leq 0.001$ (***).
Comparisons have been performed using unpaired t-test (C+D), Kruskal-Wallis with Dunn's post-hoc test(E) and ordinary ANOVA with Holm Sidak's post-hoc test(F).

10.10 Less muscle fibers in endothelium-specific double KO mice 28 days after femoral artery ligation

In order to examine morphological changes in the hind limb muscles after FAL, I stained 10 µm thick sections with H&E and quantified the number of muscle fibers present in the field of view. In tibialis anterior muscles, higher numbers of muscle fibers of ligated legs in both control und double KO group have been present, compared to muscle fiber numbers of non-ligated legs (Figure 22B.1). However, significantly less muscle fibers could be observed in the ligated legs after double KO of *App* and *Aplp2*. This observation was not present in the soleus muscles (Figure 22D.1).

Additionally, I quantified the number of centralized nuclei and related them to the total number of muscle fibers to describe the ongoing regeneration after surgical induced ischemia in the tissue. However, there were no significant changes between double KO mice and control littermates in both muscle types (Figure 22B.2 and D.2). These data suggest, that ischemia-induced angiogenesis accompanied by muscle regeneration is somehow affected, however either 28 days after ligation might be too late or the number of animals involved might be too low for statistical relevance.

Figure 22

Fewer muscle fibers in endothelium-specific double KO mice 28 days after femoral artery ligation

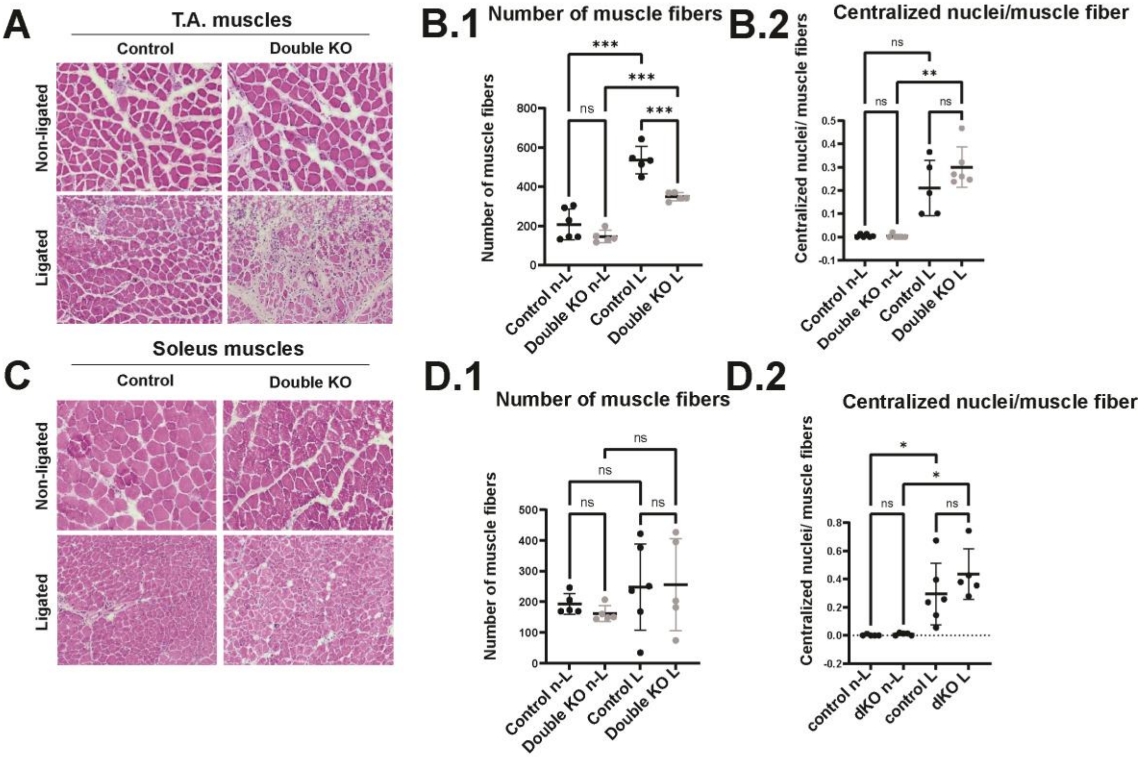

Note. Hind-limb ischemia was induced by femoral artery ligation in EC-App/Aplp2-KO mice and control littermates. Shown are representative photomicrographs of sections of the tibialis anterior (A) and soleus (C) muscle of the ligated hind limb (L) and of the non-ligated side (n-L) 28 days after the surgery (n= 6 mice in both groups).Representative sections stained H&E are presented.
Statistical evaluations of the number of muscle fibers for tibialis anterior muscles (B.1) and soleus muscles (D.1) as well as the ratio of centralized nuclei to number of muscle fiber in tibilias anterior (B.2) and in soleus muscles (D.2) are shown. Values have been excluded if tissue quality after processing was below commonly accepted standards. Data are presented as mean ± SD. $p > 0.12$ (ns); $p < 0.033$ (*), $p \leq 0.002$ (**), $p \leq 0.001$ (***)
Comparisons have been performed using ordinary one-way ANOVA with Holm-Šídák test (B.1) and Kruskal-Wallis test with Dunn’s post-hoc test (B.2, D.1, D.2).

10.11 Vascular changes are displayed through changes in perimeter size

To analyze the structural differences of vasculature seen in the immunofluorescence (IF) stainings, I decided to evaluate the perimeter of each vessel within the sections of soleus and tibialis anterior muscles from both double KO and control group. As seen in Figure 23A, perimeter size of control mice group are slightly higher compared to double KO group in the soleus muscles.

Figure 23
Vascular changes in double KO mice are displayed through larger perimeter size in tibialis anterior muscles

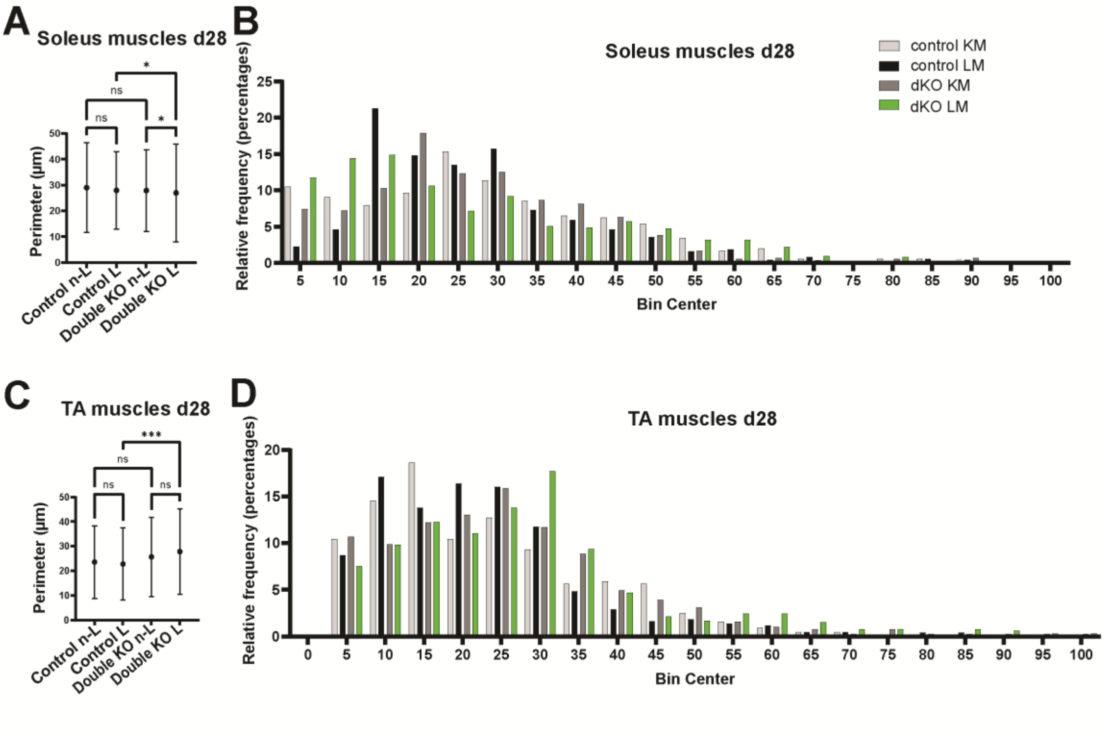

Note. Sections of soleus and tibialis anterior muscles from dKO mice (n=6) and control litter mates (n=6) were stained with CD31 and perimeter size was measured with Fiji. Statistical evaluation is shown for soleus muscles (A) as well as tibialis anterior (C) muscles. Relative frequencies are displayed in the associated histograms (B and D). Values have been excluded if tissue quality after processing was below commonly accepted standards. Data are presented as mean ± SD. $p > 0.12$ (ns); $p < 0.033$ (*), $p \leq 0.002$ (**), $p \leq 0.001$ (***)
Kruskal-Wallis test followed by Dunn's multiple comparisons tests have been performed.

However, looking at the perimeter size of the tibialis anterior muscles, I observed an even stronger adverse effect (Figure 23C). 28 days after FAL, the perimeter of vessels in the double KO group was significantly higher in the tibialis anterior muscles. To better visualize the observation, I built up categories with 5 µm width and created histograms showing the relative frequency in percentage of perimeter size present in each category (Figure 23B and D).

10.12 Angiogenesis events induced differences between control and dKO appear later than 7 days femoral artery ligation

To figure out whether the differences present at d28 post-surgery could be even more prominent at earlier time points, I decided to investigate the involvement of APP and/or APLP2 in ischemia-induced angiogenesis at day 7 after FAL.

10.12.1 7 days after femoral artery ligation is too early to observe differences in number of muscle fibers

As described for the samples at 28 days after FAL, I stained 10 µm thick sections with H&E and quantified the number of muscle fibers present in the field of view. In both tibialis anterior and soleus muscles, no significant differences in the number of muscles fibers neither between control and ligated legs nor between control and double KO group after ligation could be observed at day 7 after FAL. There have been significantly more centralized nuclei per muscle fibers in both mice group after ligation, showing ongoing regeneration processes in the muscles. However, no significant differences between ligated legs of control or double KO mice groups have been identified (Figure 24).

Figure 24

7 days after femoral artery ligation is too early to observe differences in number of muscle fibers

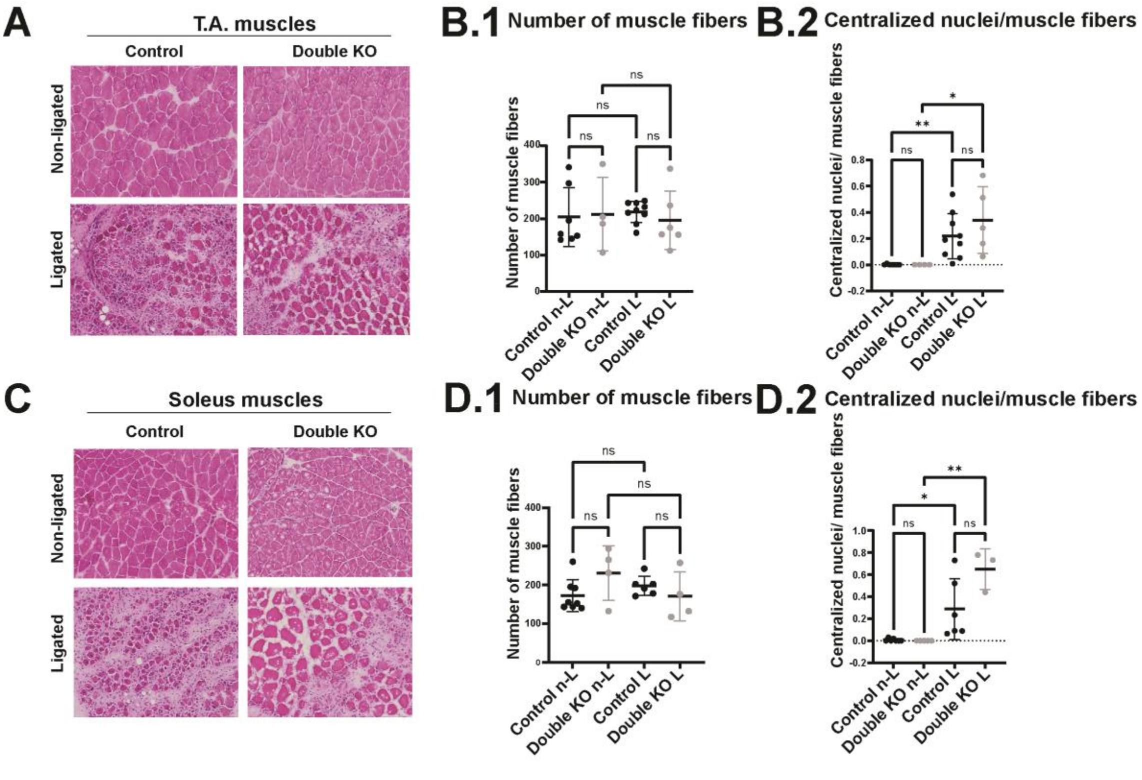

Note. Hind-limb ischemia was induced by femoral artery ligation in EC-App/Aplp2-KO mice and control littermates. Shown are representative photomicrographs of sections of the tibialis anterior (A) and soleus (C) muscle of the ligated hind limb (ligated) and of the non-ligated side (non-ligated) 7 days after the surgery (n= 9 control and n=7 dKO mice). Representative sections stained H&E are presented. Statistical evaluations of the number of muscle fibers for the tibialis anterior muscles (B.1) and soleus muscles (D.1) as well as the ratio of centralized nuclei to number of muscle fiber in the tibilias anterior (B.2) and in the soleus muscles (D.2) are shown. Values have been excluded if tissue quality after processing was below commonly accepted standards. Data are presented as mean ± SD. p> 0.12 (ns); p < 0.033 (*), p ≤0.002 (**), p ≤0.001 (***)
Comparisons have been performed using ordinary Kruskal-Wallis test with Dunn’s post-hoc test.

10.12.2 No significant differences in proliferation or microvascular perfusion seven days after femoral artery ligation

Double KO mice and control littermates underwent FAL and received EdU via drinking water for 7 days. At day 7, mice were injected with IB4 AB into the tail vein and further proceeded as described above. In Figure 25, representative images of DAPI and EdU staining, as well as CD31 and IB4 stainings are shown. In contrast to the results after 28 days post-surgery, no significant reduction of proliferation after double KO could be observed. The microvascular perfusion, displayed as the ratio of $IB4^+$ area divided by $CD31^+$ area, was unchanged between both groups, like at day 28.

Figure 25

Day 7 after femoral artery ligation is too early to detect differences in proliferation or microvascular perfusion

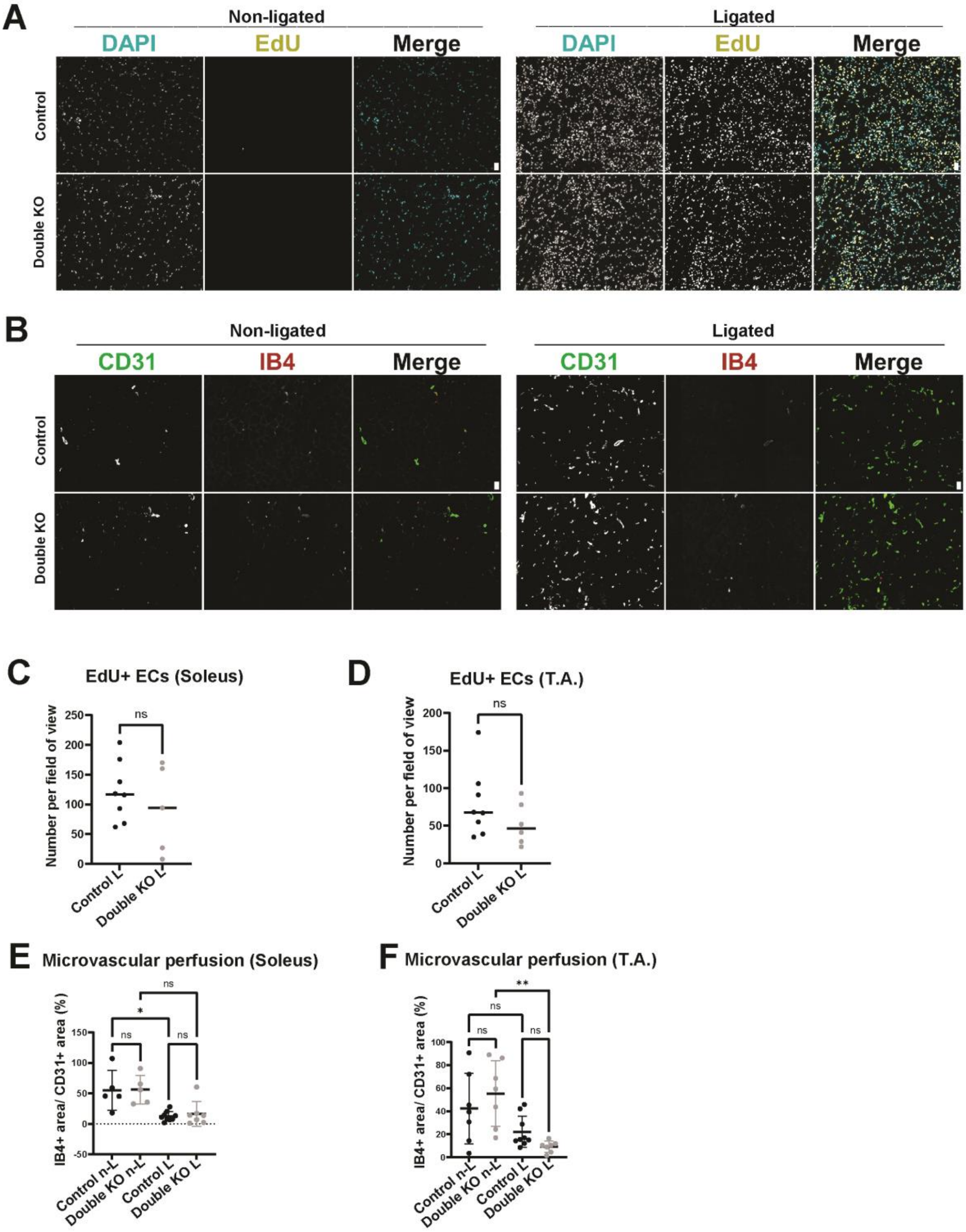

Note. Hind-limb ischemia was induced by femoral artery ligation in EC-App/Aplp2-KO mice and control littermates. (A) Shown are representative photomicrographs of sections of the tibialis anterior muscle of the ligated hind limb (L) and of the non-ligated side (n-L) 7 days after the surgery (n= 9 control and n=7 dKO mice). Representative sections stained with DAPI and EdU are presented. (B) Representative photomicrographs of sections of the tibialis anterior muscle of the ligated hind limb (L) and of the non-ligated side (n-L) 7 days after the surgery, stained with CD31 and IB4, are shown. Quantitative analysis of EdU labeled total cells in the soleus (C) and tibialis anterior (D) muscles from mice 7 days after femoral artery ligation. Statistical evaluation of the IB4+/CD31+ area in the soleus (E) and tibialis anterior (F), reflecting the perfusion in the muscles, are shown. Bar length 20

µm (A and B). Values have been excluded if tissue quality after processing was below commonly accepted standards. Data are presented as mean ± SD. p> 0.12 (ns); p < 0.033 (*), p ≤0.002 (**), p ≤0.001 (***)
Comparisons have been performed using unpaired t-test (C and D), Kruskal-Wallis with Dunn's post-hoc test (E and F)

10.12.3 Soleus and tibialis muscles perimeters are unaffected by endothelium-specific APP/APLP2 deletion

As seen in Figure 26 perimeter sizes increased after ligation in both control and double KO group in the tibialis anterior muscles. In contrast, in control group in the soleus muscles perimeter is decreased after ligation and perimeter in control legs from control group and double KO group were significantly different already. Beside, no significant difference was found between control and double KO mice in ligated legs, neither in the soleus nor in the tibialis anterior muscles.

Taken together, an inconsistency between soleus and tibialis anterior muscles could be observed again.

Figure 26
Day 7 after femoral artery ligation is too early to detect significant differences in perimeter size

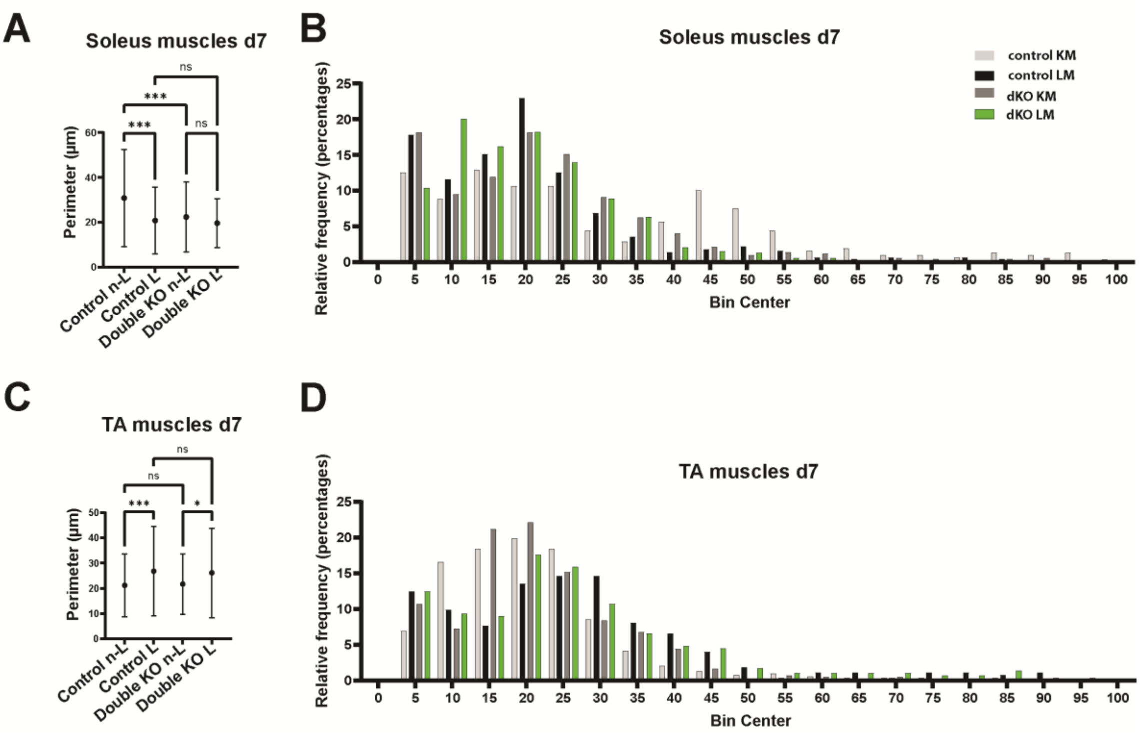

Note. Sections of soleus and tibialis anterior muscles from dKO mice (n=7) and control litter mates (n=9) were stained with CD31 and perimeter size was measured with Fiji. Statistical evaluation is shown for soleus muscles (A) as well as tibialis anterior (C) muscles. Relative frequencies are displayed in the associated histograms (B and D). Values have been excluded if tissue quality after processing was below commonly accepted standards. Data are presented as mean ± SD. p> 0.12

(ns); $p < 0.033$ (*), $p \leq 0.002$ (**), $p \leq 0.001$ (***)
Kruskal-Wallis test and Dunn's multiple comparisons tests have been performed.

10.13 No differences in macrophages recruitment post surgery

As previously described, the interplay between ECs and macrophages is very important for the success in angiogenesis. Since I observed a reduction of proliferative ECs 28 days after surgery, as well as significantly enlarged perimeters in the tibialis anterior muscles, I hypothesized that recruitment of macrophages could be affected after endothelium-specific KO of *App* and *Aplp2*. To prove this hypothesis, I stained slices of tibialis anterior muscles and soleus muscles with ABs against DAPI and CD68 and analyzed the CD68 positive area for non-ligated and ligated legs of double KO mice and their control littermates. As seen in Figure 27, at day 7 a significant difference in recruitment of macrophages between non-ligated and ligated side in both soleus and tibialis anterior muscles was detected. Meaning that after ligation, macrophages have been recruited near the side of ligation independent of the genotype. However, no significant differences after ligation between double KO mice and control littermates could be observed neither at day 7 nor at day 28 post-surgery.

Figure 27

No significant difference in macrophage recruitment at day 7 and day 28 post-surgery

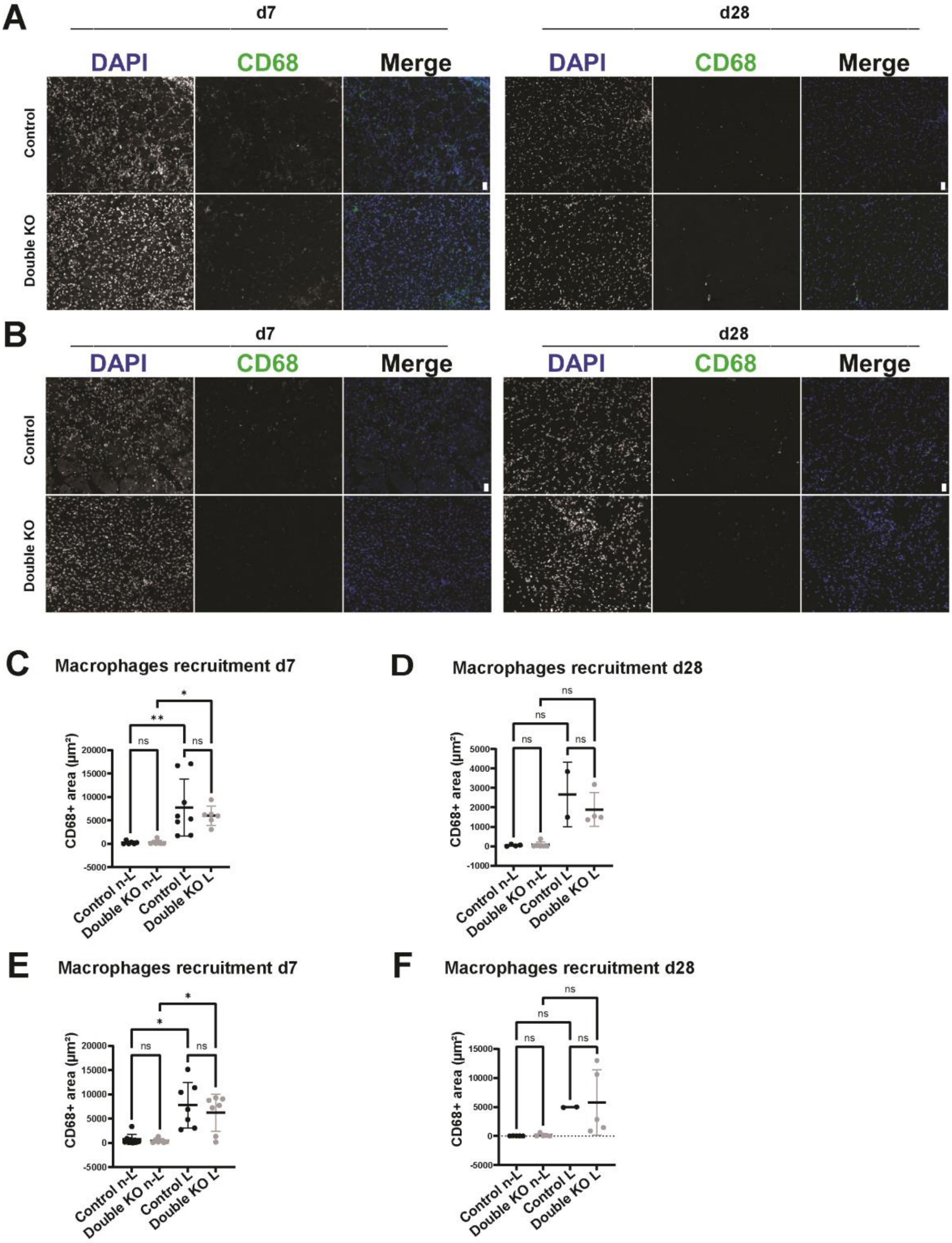

Note. Hind-limb ischemia was induced by femoral artery ligation in EC-App/Aplp2-KO mice and control littermates. (A) Shown are representative photomicrographs of sections of the tibialis anterior muscle stained with DAPI and D68 at 7 and 28 days after the surgery. (B) Representative photomicrographs of sections of the soleus muscle of the ligated hind limb 28 days after the surgery are shown. Quantitative analysis of CD68-positive stained area in tibialis anterior (C+D) and soleus (E and F) muscles after femoral artery ligation. N=9 (control) vs n=7 double KO mice at day 7, n=6 (both animal groups) at day 28. Values have been excluded if tissue quality after processing was below commonly accepted standards. Bar length 20 µm (A and B). Data are presented as mean ± SD. $p > 0.12$ (ns); $p < 0.033$ (*), $p \leq 0.002$ (**), $p \leq 0.001$ (***)

Comparisons have been performed using Kruskal-Wallis with Dunn’s post-hoc test.

In the late stages of angiogenesis, particularly at day 28 post-ischemia induction, I observed a convergence in the CD68+ area between ligated and non-ligated muscles. This indicates a notable decline in the inflammatory and reparative signals typically associated with induced ischemia. It suggests that the macrophages are nearing the completion of their role in tissue clearance, repair, and regeneration.

11 Discussion

Despite being identified 40 years ago, the functional roles of APP and its family members, APLP1 and APLP2, remain incompletely understood. While their critical involvement in Alzheimer’s disease development is known, their broader functional significance is still being elucidated. Moreover, the distribution between functions of full-length APP and its multiple fragments, such as sAPPα and sAPPβ, as well as AICD and p3, has not been consistently and fully determined (Delport & Hewer, 2022; Dunot et al., 2023). Notably, our whole transcriptome RNA sequencing data from HUVECs identified APP and APLP2 as among the highest expressed genes in the endothelium and we therefore postulate a yet unknown, critical role in either the development or functionality of the blood vessels.

Therefore, I first investigated the tube formation of HUVECs after siRNA-mediated KD of *App* and/or *Aplp2* compared to scramble (SCR) treated HUVECs. Here, I demonstrated that the loss of APP and APLP2 together significantly reduces ability to form tubes and mesh like structures, indicative of their involvement in angiogenesis *in vitro*. Further analysis of the KD of individual *App* and *Aplp2* revealed that the observed phenotype in double KD cells predominantly stems from the loss of *App*. This conclusion is supported by the finding that *Aplp2* KD alone did not yield any significant alteration in tube formation. Additionally, Ristori et al. (2020), demonstrated that maintaining an appropriate expression level of APP could be crucial for ensuring proper function of ECs. They also performed an tube formation assay after siRNA-mediated knockdown of APP in HUVECS with additional treatment of VEGFa, resulting in a reduced angiogenic response of siAPP cells.

To further explore the role APP and APLP2 in blood vascular development *in vivo*, I utilized inducible, endothelium-specific double KO mice and demonstrated a reduction in vascularization in the retinal angiogenesis mouse model. In the absence of both APP and APLP2, a reduction in vascularization without growth retardation in general at postnatal day six was observed. However, the reduction in vascularization was not accompanied by changes in the number of branching points or diameter size of arteries or veins. Interestingly, the investigation of endothelium-specific single KO mice revealed mild reduction in vascularization only in *Aplp2* single KO mice, contrary to the *in vitro* findings where only APP deficiency affected tube formation. These inconsistencies may be influenced by the effects of tamoxifen activated Cre-ER^{T2} found by Brash et al. (2020). They identified compromised angiogenesis in perinatal retinas of only Cre-ER^{T2} inserted mice, where branch density and vascular network extension were affected. Omitting a control for CreER^{T2} toxicity in my studies would render it inappropriate to solely attribute the results to this factor. However, the likelihood of it influencing the outcomes remains considerable.

Another extensively studied angiogenesis model involves primary tumor formation in adult mice, which I subsequently investigated. Given that angiogenesis occurs in both male and female subjects, first depicting a fundamental role in the body and second having a cohort of female mice readily available for experimentation, I made the deliberate choice to exclusively utilize female mice for primary tumor formation. 28 days after injection of LLC1 cells, two control mice were prematurely excluded due to ulcer development, while four out of the remaining eight control mice did not exhibit tumor growth. Consequently, meaningful assessment regarding the involvement of APP and APLP2 in angiogenesis *in vivo* was precluded.

As the tube formation assay is a model to mimic the initial steps of angiogenesis like EC migration and alignment, as well as proliferation and formation of elongated structures, I was interested whether those steps are also affected *in vivo* by finally studying ischemia-induced angiogenesis after ligation of the *A. femoralis*. In the first cohort of double KO mice and their control littermates, I observed necrosis in 3 out of 7 mice lacking APP and APLP2, whereas no clinical ischemic events have been present in control mice. Perfusion ratios of ligated to non-ligated legs didn't reveal significant differences, however, the values of double KO mice have not been fully representative due to the early drop out of the mice showing necrosis. Moreover, processing of the gastrocnemius muscles exposed abnormalities in the vascular structure in double KO mice compared to control littermates. Four years later, another cohort of mice was used to study ischemia-induced angiogenesis after FAL. However, no clinical ischemic events have been observed. The inability to replicate the necrotic phenotype observed in 3 out of 7 double KO mice after femoral artery ligation in 2019 presents a perplexing inconsistency. Notably, within our laboratory, this phenomenon marked the first occurrence of animals suffering from necrotic limb complications after FAL. Despite meticulous efforts to replicate the experimental conditions and procedures, the anticipated necrotic manifestation failed to manifest in subsequent experimental trials in 2023. While the change of surgeon could potentially have influenced the different outcome, it is worth noting that Shangmin Liu, who took over, was trained by Kerstin Troidl, both of whom possess extensive expertise in FAL. Potentially, variations in genetic backgrounds, environmental conditions or unforeseen experimental variables could contribute to the observed discrepancy between the experimental groups of 2019 and 2023.

For example, there is more and more evidence that the microbiome has a huge impact on our bodies in health and disease. By-products, like some short-chain fatty acids, resulting from metabolic processes in bacteria, are suggested to play roles in inhibiting inflammatory processes. Therefore, one possible explanation could be that the microbiome within the animal facility, as well as the mouse colony, has changed within the last four years (Franklin & Ericsson, 2017). Another reason could be an accumulation of genetic mutations. Over multiple generations, mutations may occur randomly and could affect the expression of genes related to the phenotype observed in the FAL experiment (Yoshiki et al., 2022). In addition, epigenetic changes such as histone modifications and DNA methylations can influence gene expression without altering the underlying DNA sequence. These modifications might change over generations and might contribute to variations in phenotype(Jaenisch & Bird, 2003; Kouzarides, 2007). The only possibility to eliminate these causes would have been to reconstruct the mouse colony using the frozen sperms, performing FAL again and comparing results to the results from 2019. Unfortunately, this was not possible due to time constraints.

In 2023, 28 days after FAL, I could observe a mild reduction in EC proliferation after endothelium-specific KO of *App* and *Aplp2*, but only in tibialis anterior muscles and not in soleus muscle. The differences in both muscle types can be explained by the systematic interrogation by Lee et al. (2020). They figured out, that the distal anterior hindlimb muscles, including the tibialis anterior muscle, are the most reliable injured muscles after FAL. The consistency of injury as well as the sites of angiogenesis seem to be time independent for tibialis anterior muscles. Soleus muscles in contrast, are not included in the pictured angiogenesis sites at day 28 anymore. Also on day 10, a difference between C57BL/6J and C57BL/6N, with the latter not showing sites of angiogenesis within soleus muscles have been found. Surprisingly, the reduction in EC proliferation, expected to be an early step in angiogenesis, was not observed at the earlier time point, seven days after FAL, in either muscle type. Furthermore, I investigated the functionality of the vessel by injection of IB4 AB via tail vein 30 min before the end of the experiment. No differences between both groups could be observed regarding the microvascular perfusion, displayed by the ratio of $IB4^+$ area to $CD31^+$ area. This suggests that all existing vessels are functional and used for blood supply of the tissue. In contrast, I observed a strong decrease in the number of muscle fibers in the double KO group 28 days post-surgery, suggesting that hypertrophy events, to compensate decreased supply of oxygen and nutrients after FAL, of muscle fibers could be somehow affected by endothelium-specific KO of *App* and *Aplp2*. At day 7, no significant change in the number of muscle fibers was present yet. Moreover, the ratio of centralized nuclei to the number of muscle fibers was not significantly altered at both timepoints (Scheidegger et al., 1997).

The adaptability and responsiveness of blood vessels are heavily dependent on EC. Alterations in blood flow dynamics, like observed after FAL, trigger responses in EC, initiating signaling pathways, which lead to changes in cell behavior. Consequently, under normal conditions, ECs can reorganize themselves to restore normal blood circulation within the vessel. However, when these processes are dysregulated, it can result in severe pathological conditions (Gifre-Renom & Jones, 2021). In the tibialis anterior muscles, I found a significant increase in perimeter size after double KO of *App* and *Aplp2* at 28 days after ligation. The changes in the vasculature morphology is not fully represented by the perimeter size, however, it is a first indicator of the abnormal vasculature. I therefore postulate that the remodelling and maturation of vessels after ligation in the double KO mice seemed to be affected. Contritely, in soleus muscles I observed a mild reduction in perimeter size. These findings are somehow similar to the observations at day 7 after ligation.

Here, a significant dilation was found in both groups after ligation compared to the non-ligated legs in tibialis anterior muscles, but no significant differences between double KO and control mice were observed. Moreover, in soleus muscles the opposite was detected again. After ligation, perimeter size significantly dropped in thecontrol group, while the reduction in double KO group was not significant. However, non-ligated legs of double KO mice already showed a significant reduction in perimeter size compared to control littermates. The reason for this observation remains unclear. One has to take into account that after ligation of a big vessel like the *A. femoralis*, not only angiogenesis but also arteriogenesis is happening. Thereby, NO is released leading to vasodilation and therefore a rise in perimeter size appears (Schaper, 2009; Troidl et al., 2010). So the increase in perimeter size at d28 in tibialis anterior muscles of the double KO group could be either related to inability of vessel remodeling after double KO leading to bigger, unorganized vessels or simply the effect of NO present in the tissue or a combination of both. Ligation of the femoral artery like we did it, proximal of *A. iliaca interna*, is somehow a compromise to study both arteriogenesis and angiogenesis at the same time. In conclusion, total excision of the femoral artery, as described by Aref et al. (2019) would have been more accurate to assign angiogenesis.

Also, Lee et al 2020 mentioned that in regard of angiogenesis studies *in vivo*, a lot of things are remaining to be more precisely monitored. Out of more than 5000 studies included in their study, only less than 10% used the correct region for analysis. Therefore, translation from mouse ligation experiment to human clinical care or therapeutically guidance becomes challenging. Additionally, Müller et al. (2017) mentioned already that there are many conflicting findings in the field regarding the functions of APP and it's homologues due to non verified *in vitro* data. The complexity of the functions *in vivo* appears challenging to depict solely through *in vitro* experimentation.

Johnstone et al. (1991) revealed conservation of amino acid sequence of APP in dog, polar bear and other mammals, whereas mouse and rat seemed to be evolutionary a distinct group. This suggests that the possible involvement of APP and/ or APLP2 in angiogenesis may be concealed in mouse and rat models, indicating that other animal models could be more suitable. Additionally, the redundancy/compensation between the three different family members makes it very difficult to clearly assign a function to only one of them (Dunot et al., 2023).

This might be the main reason, why the massive reduction in tube formation after double KD of *APP* and *APLP2*, could not be detected *in vivo.* Moreover, there is a lack of available data on tissue specific cleavage under certain conditions, such as ischemia. Processing of APP and its family members is a very rapid process, which makes it extremely difficult to rebuild the environment *ex vivo*. To be more specific, *in vitro* experiments are so far not able to fully depict the whole complexity of the ongoing processes *in vivo* (Dunot et al., 2023).

As APP and its family members can act as receptors and ligands, even over long distances, it could be possible that under ischemic conditions, the body is able to use APP fragments from other sources than the endothelium. Evin & Li (2012) mentioned that platelets are the primary source of APP in the periphery. Approximately 90% of circulating sAPPα/sAPPβ arises from APP cleavage following platelet activation (Bush et al., 1990; Kitazume et al., 2012; Li et al., 1994). Since platelets and the endothelium are in close contact with each other, it would not be surprising, if compensatory effects occur after endothelium-specific knockout of *App* and *Aplp2* in mice.

Addressing those open questions in future studies may require the development of a knockout mouse line specific for endothelium and platelet KO of *App* and *Aplp2*, which could serve as a helpful tool.

In general, the functional study of the APP family is challenging because of the high similarity between APP and the two other members, and the multiple fragments of APP after processing. Although if I could not definitively unravel the physiological role of APP in the endothelium and the underlying mechanism, there is strong evidence that APP plays an important role *in vivo* besides the involvement in Alzheimer's disease. To date, no reports of human homozygous nonsense or frameshift mutations in the APP gene have been reported (Klein et al., 2016). This is very interesting and could support the hypothesis that APP performs a very important function the human body. However, it is still premature to discuss the therapeutic potential of APP and APLP2. Dunot et al. (2023) argue that basic understanding of APP's function, in spatial and temporal considerations, must first be expanded before a safe therapeutic solution can be found. Additionally, future approaches are needed to distinguish between full-length APP functions and functions related to intra- or extracellular fragments of APP. Drawing from research

in the Alzheimer's disease domain, it's evident that prioritizing the targeting of individual protein fragments and their removal or prevention, without comprehensively grasping the underlying mechanisms and sources of processing, can prove detrimental. (Delport & Hewer, 2022). Unforeseen toxic side effects, lack of efficacy or no physiological relevance of fragment removal could be consequences (Moussa-Pacha et al., 2020; Pulina et al., 2020; van Dyck, 2018). To investigate the functional roles of different APP fragments, Dunot et al. (2023) highlighted two strategies to gain more insights. One approach would be using cell-specific KDs combined with rescue strategies like applying fragments of APP as synthetic peptides. Another suggestion would be to prevent the production of specific fragments via secretase inhibition. However, the latter would not be as specific since secretases are able to cleave several other proteins, too.
Taken together, my study highlights the complex and multifaceted roles of APP and APLP2 in EC function, particularly in angiogenesis. The observed mild reduction of EC proliferation in tibialis anterior muscles, along with the increased perimeter size at day 28, represent the most promising findings *in vivo*. Although the reduction of muscle fiber number in tibialis anterior muscles at day 28, was also notable, it is likely not directly attributable to the KO in endothelium. Considering the implications of my findings, it is important to acknowledge the potential limitations stemming from the relatively small sample size utilized in this study. While a larger sample size might have increased the likelihood of detecting statistically significant results, it is crucial to adhere to the principles of the 3Rs (Replacement, Reduction, and Refinement) for animal experimentation. The decision to limit the number of experimental animals was made in accordance with ethical considerations and efforts to minimize harm to animals. While this approach may have impacted the statistical power of my analyses, it aligns with ethical guidelines aimed at reducing unnecessary animal use and suffering.

However, due to inconsistencies across different muscles types and the absence of changes in proliferation and macrophages recruitment at day 7, we decided to not continue with the second aim, dissection of possible underlying mechanisms in mutant mouse lines for APP. While my findings provide valuable insights, further investigation is warranted to elucidate the specific pathways through which the APP family influences angiogenesis *in vivo* and to develop therapeutically relevant strategies for targeting these pathways. Alternative ischemic models, such as myocardial infarction resulting in heart ischemia, or stroke models leading to brain ischemia, may provide more suitable platforms for pursuing these objectives.

12 References

Adair, T., & Montani, J. (2010). Overview of Angiogenesis. In *Angiogenesis*. https://www.ncbi.nlm.nih.gov/books/NBK53238/

Adams, R. H., & Alitalo, K. (2007). Molecular regulation of angiogenesis and lymphangiogenesis. *Nature Reviews Molecular Cell Biology*, *8*(6), 464–478. https://doi.org/10.1038/nrm2183

Aird, W. C. (2007). Phenotypic heterogeneity of the endothelium: I. Structure, function, and mechanisms. *Circulation Research*, *100*(2), 158–173. https://doi.org/10.1161/01.RES.0000255691.76142.4A

Akaaboune, M., Allinquant, B., Farza, H., Roy, K., Magoul, R., Fiszman, M., Festoff, B. W., & Hantaï, D. (2000). Developmental regulation of amyloid precursor protein at the neuromuscular junction in mouse skeletal. *Molecular and Cellular Neurosciences*, *15*(4), 355–367. https://doi.org/10.1006/mcne.2000.0834

Andrew, R. J., Kellett, K. A. B., Thinakaran, G., & Hooper, N. M. (2016). A Greek Tragedy: The Growing Complexity of Alzheimer Amyloid Precursor Protein Proteolysis. *Journal of Biological Chemistry*, *291*(37), 19235–19244. https://doi.org/10.1074/JBC.R116.746032

Anliker, B., & Müller, U. (2006). The functions of mammalian amyloid precursor protein and related amyloid precursor-like proteins. *Neurodegenerative Diseases*, *3*(4–5), 239–246. https://doi.org/10.1159/000095262

Aref, Z., de Vries, M. R., & Quax, P. H. A. (2019). Variations in surgical procedures for inducing hind limb ischemia in mice and the impact of these variations on neovascularization assessment. In *International Journal of Molecular Sciences* (Vol. 20, Issue 15). Int J Mol Sci. https://doi.org/10.3390/ijms20153704

Belyaev, N. D., Kellett, K. A. B., Beckett, C., Makova, N. Z., Revett, T. J., Nalivaeva, N. N., Hooper, N. M., & Turner, A. J. (2010). The transcriptionally active amyloid precursor protein (APP) intracellular domain is preferentially produced from the 695 isoform of APP in a β-secretase-dependent pathway. *Journal of Biological Chemistry*, *285*(53), 41443–41454. https://doi.org/10.1074/jbc.M110.141390

Bertram, J. S., & Janik, P. (1980). Establishment of a cloned line of Lewis Lung Carcinoma cells adapted to cell culture. *Cancer Letters*, *11*(1), 63–73. https://doi.org/10.1016/0304-3835(80)90130-5

Black, R. A., Rauch, C. T., Kozlosky, C. J., Peschon, J. J., Slack, J. L., Wolfson, M. F., Castner, B. J., Stocking, K. L., Reddy, P., Srinivasan, S., Nelson, N., Boiani, N., Schooley, K. A., Gerhart, M., Davis, R., Fitzner, J. N., Johnson, R. S., Paxton, R. J., March, C. J., & Cerretti, D. P. (1997). A metalloproteinase disintegrin that releases tumour-necrosis factor-alpha from cells. *Nature*, *385*(6618), 729–733. https://doi.org/10.1038/385729A0

Brash, J. T., Bolton, R. L., Rashbrook, V. S., Denti, L., Kubota, Y., & Ruhrberg, C. (2020). Tamoxifen-Activated CreERT Impairs Retinal Angiogenesis

Independently of Gene Deletion. *Circulation Research*, *127*(6), 849–850. https://doi.org/10.1161/CIRCRESAHA.120.317025

Brenes, R. A., Jadlowiec, C. C., Bear, M., Hashim, P., Protack, C. D., Li, X., Lv, W., Collins, M. J., & Dardik, A. (2012). Toward A Mouse Model of Hind Limb Ischemia to Test Therapeutic Angiogenesis. *Journal of Vascular Surgery*, *56*(6), 1669–1679. https://doi.org/10.1016/j.jvs.2012.04.067

Burri, P. H., & Djonov, V. (2002). Intussusceptive angiogenesis - The alternative to capillary sprouting. *Molecular Aspects of Medicine*, *23*(6 SUPPL.), 1–27. https://doi.org/10.1016/s0098-2997(02)00096-1

Buschmann, I., & Schaper, W. (1999). Arteriogenesis versus angiogenesis: Two mechanisms of vessel growth. *News in Physiological Sciences*, *14*(3), 121–125. https://doi.org/10.1152/physiologyonline.1999.14.3.121

Bush, A. I., Martins, R. N., Rumble, B., Moir, R., Fuller, S., Milward, E., Currie, J., Ames, D., Weidemann, A., Fischer, P., Multhaup, G., Beyreuther, K., & Masters, C. L. (1990). The amyloid precursor protein of Alzheimer's disease is released by human platelets. *Journal of Biological Chemistry*, *265*(26), 15977–15983. https://doi.org/10.1016/S0021-9258(18)55493-4

Buxbaum, J. D., Liu, K. N., Luo, Y., Slack, J. L., Stocking, K. L., Peschon, J. J., Johnson, R. S., Castner, B. J., Cerretti, D. P., & Black, R. A. (1998). Evidence that tumor necrosis factor alpha converting enzyme is involved in regulated alpha-secretase cleavage of the Alzheimer amyloid protein precursor. *The Journal of Biological Chemistry*, *273*(43), 27765–27767. https://doi.org/10.1074/JBC.273.43.27765

Carmeliet, P. (2003). Angiogenesis in health and disease. *Nature Medicine*, *9*(6), 653–660. https://doi.org/10.1038/NM0603-653

Carmeliet, P., & Jain, R. K. (2011). Molecular mechanisms and clinical applications of angiogenesis. *Nature*, *473*(7347), 298–307. https://doi.org/10.1038/nature10144

Cole, S. L., & Vassar, R. (2007). The Alzheimer's disease β-secretase enzyme, BACE1. *Molecular Neurodegeneration*, *2*(1). https://doi.org/10.1186/1750-1326-2-22

Corliss, B. A., Azimi, M. S., Munson, J. M., Peirce, S. M., & Murfee, W. L. (2016). Macrophages: An Inflammatory Link Between Angiogenesis and Lymphangiogenesis. *Microcirculation*, *23*(2), 95–121. https://doi.org/10.1111/micc.12259

Couffinhal, T., Silver, M., Zheng, L. P., Kearney, M., Witzenbichler, B., & Isner, J. M. (1998). Mouse model of angiogenesis. *American Journal of Pathology*, *152*(6), 1667–1679. /pmc/articles/PMC1858441/?report=abstract

Delport, A., & Hewer, R. (2022). The amyloid precursor protein: a converging point in Alzheimer's disease. *Molecular Neurobiology*, *59*(7), 4501–4516. https://doi.org/10.1007/s12035-022-02863-x

Deyts, C., Thinakaran, G., & Parent, A. T. (2016). APP Receptor? To Be or Not to Be. *Trends in Pharmacological Sciences*, *37*(5), 390–411. https://doi.org/10.1016/j.tips.2016.01.005

Dunot, J., Ribera, A., Pousinha, P. A., & Marie, H. (2023). Spatiotemporal insights of APP function. *Current Opinion in Neurobiology*, *82*, 102754. https://doi.org/10.1016/J.CONB.2023.102754

d'Uscio, L. V., He, T., Santhanam, A. V., & Katusic, Z. S. (2018). Endothelium-specific amyloid precursor protein deficiency causes endothelial dysfunction in cerebral arteries. *Journal of Cerebral Blood Flow and Metabolism*, *38*(10), 1715–1726. https://doi.org/10.1177/0271678X17735418

D'Uscio, L. V., & Katusic, Z. S. (2019). Vascular phenotype of amyloid precursor protein-deficient mice. *American Journal of Physiology - Heart and Circulatory Physiology*, *316*(6), H1297–H1308. https://doi.org/10.1152/AJPHEART.00539.2018/ASSET/IMAGES/LARGE/ZH40051928080013.JPEG

d'Uscio, L. V., & Katusic, Z. S. (2021). Endothelium-specific deletion of amyloid-β precursor protein exacerbates endothelial dysfunction induced by aging. *Aging*, *13*(15), 19165–19185. https://doi.org/10.18632/AGING.203401

Esch, F. S., Keim, P. S., Beattie, E. C., Blacher, R. W., Culwell, A. R., Oltersdorf, T., McClure, D., & Ward, P. J. (1990). Cleavage of Amyloid β Peptide During Constitutive Processing of Its Precursor. *Science*, *248*(4959), 1122–1124. https://doi.org/10.1126/science.2111583

Evin, G., & Li, Q.-X. (2012). Platelets and Alzheimer's disease: Potential of APP as a biomarker. *World Journal of Psychiatry*, *2*(6), 102. https://doi.org/10.5498/WJP.V2.I6.102

Fallah, A., Sadeghinia, A., Kahroba, H., Samadi, A., Heidari, H. R., Bradaran, B., Zeinali, S., & Molavi, O. (2019). Therapeutic targeting of angiogenesis molecular pathways in angiogenesis-dependent diseases. *Biomedicine & Pharmacotherapy* , *110*, 775–785. https://doi.org/10.1016/J.BIOPHA.2018.12.022

Félétou, M. (2011). The Endothelium. *The Endothelium: Part 1: Multiple Functions of the Endothelial Cells—Focus on Endothelium-Derived Vasoactive Mediators*, *24*(1), 10–12. https://www.ncbi.nlm.nih.gov/books/NBK57149/

Folkman, J. (1995). Clinical applications of research on angiogenesis. *Seminars in Medicine of the Beth Israel Hospital Boston*, *333*(26), 1757–1763.

Folkman, J., & Klagsbrun, M. (1987). Angiogenic factors. *Science*, *235*(4787), 442–447. https://doi.org/10.1126/SCIENCE.2432664

Forsythe, J. A., Jiang, B.-H., Iyer, N. V., Agani, F., Leung, S. W., Koos, R. D., & Semenza, G. L. (1996). Activation of vascular endothelial growth factor gene transcription by hypoxia-inducible factor 1. *Molecular and Cellular Biology*, *16*(9), 4604–4613. https://doi.org/10.1128/MCB.16.9.4604

Franklin, C. L., & Ericsson, A. C. (2017). Microbiota and reproducibility of rodent models. *Lab Animal*, *46*(4), 114–122. https://doi.org/10.1038/laban.1222

Fruttiger, M. (2007). Development of the retinal vasculature. *Angiogenesis*, *10*(2), 77–88. https://doi.org/10.1007/S10456-007-9065-1

Galloway, S., Jian, L., Johnsen, R., Chew, S., & Mamo, J. C. L. (2007). β-Amyloid or its precursor protein is found in epithelial cells of the small intestine and is stimulated by high-fat feeding. *Journal of Nutritional Biochemistry*, *18*(4), 279–284. https://doi.org/10.1016/j.jnutbio.2006.07.003

Gifre-Renom, L., & Jones, E. A. V. (2021). Vessel Enlargement in Development and Pathophysiology. *Frontiers in Physiology*, *12*, 1–13. https://doi.org/10.3389/FPHYS.2021.639645

Glim, J. E., Niessen, F. B., Everts, V., van Egmond, M., & Beelen, R. H. J. (2013). Platelet derived growth factor-CC secreted by M2 macrophages induces alpha-smooth muscle actin expression by dermal and gingival fibroblasts. *Immunobiology*, *218*(6), 924–929. https://doi.org/10.1016/J.IMBIO.2012.10.004

Goldgaber, D., Lerman, M. I., McBride, O. W., Saffiotti, U., & Gajdusek, D. C. (1987). Characterization and chromosomal localization of a cDNA encoding brain amyloid of Alzheimer's disease. *Science*, *235*(4791), 877–880. https://doi.org/10.1126/SCIENCE.3810169

Gordon, S., & Plüddemann, A. (2018). Macrophage clearance of apoptotic cells: A critical assessment. *Frontiers in Immunology*, *9*(JAN), 315565. https://doi.org/10.3389/FIMMU.2018.00127/BIBTEX

Gralle, M., Oliveira, C. L. P., Guerreiro, L. H., McKinstry, W. J., Galatis, D., Masters, C. L., Cappai, R., Parker, M. W., Ramos, C. H. I., Torriani, I., & Ferreira, S. T. (2006). Solution conformation and heparin-induced dimerization of the full-length extracellular domain of the human amyloid precursor protein. *Journal of Molecular Biology*, *357*(2), 493–508. https://doi.org/10.1016/J.JMB.2005.12.053

Hartmann, D., De Strooper, B., Serneels, L., Craessaerts, K., Herreman, A., Annaert, W., Umans, L., Lübke, T., Illert, A. L., Von Figura, K., & Saftig, P. (2002). The disintegrin/metalloprotease ADAM 10 is essential for Notch signalling but not for alpha-secretase activity in fibroblasts. *Human Molecular Genetics*, *11*(21), 2615–2624. https://doi.org/10.1093/HMG/11.21.2615

Heber, S., Herms, J., Gajic, V., Hainfellner, J., Aguzzi, A., Rulicke, T., Kretzschmar, H., Von Koch, C., Sisodia, S., Tremml, P., Lipp, H. P., Wolfer, D. P., & Muller, U. (2000). Mice with Combined Gene Knock-Outs Reveal Essential and Partially Redundant Functions of Amyloid Precursor Protein Family Members. *The Journal of Neuroscience*, *20*(21), 7951. https://doi.org/10.1523/JNEUROSCI.20-21-07951.2000

Hirota, K., & Semenza, G. L. (2006). Regulation of angiogenesis by hypoxia-inducible factor 1. *Critical Reviews in Oncology/Hematology*, *59*(1), 15–26. https://doi.org/10.1016/J.CRITREVONC.2005.12.003

Hoefgen, S., Coburger, I., Roeser, D., Schaub, Y., Dahms, S. O., & Than, M. E. (2014). Heparin induced dimerization of APP is primarily mediated by E1 and regulated by its acidic domain. *Journal of Structural Biology*, *187*(1), 30–37. https://doi.org/10.1016/J.JSB.2014.05.006

Jacobsen, K. T., & Iverfeldt, K. (2009). Amyloid precursor protein and its homologues: A family of proteolysis-dependent receptors. *Cellular and Molecular Life Sciences*, *66*(14), 2299–2318. https://doi.org/10.1007/s00018-009-0020-8

Jaenisch, R., & Bird, A. (2003). Epigenetic regulation of gene expression: how the genome integrates intrinsic and environmental signals. *Nature Genetics 2003 33:3*, *33*(3), 245–254. https://doi.org/10.1038/ng1089

Janker, F., Weder, W., Jang, J. H., & Jungraithmayr, W. (2018). Preclinical, non-genetic models of lung adenocarcinoma: a comparative survey. *Oncotarget*, *9*(55), 30527–30538. https://doi.org/10.18632/ONCOTARGET.25668

Jetten, N., Verbruggen, S., Gijbels, M. J., Post, M. J., De Winther, M. P. J., & Donners, M. M. P. C. (2014). Anti-inflammatory M2, but not pro-inflammatory M1 macrophages promote angiogenesis in vivo. *Angiogenesis*, *17*(1), 109–118. https://doi.org/10.1007/S10456-013-9381-6/FIGURES/5

Johnstone, E. M., Chaney, M. O., Norris, F. H., Pascual, R., & Little, S. P. (1991). Conservation of the sequence of the Alzheimer's disease amyloid peptide in dog, polar bear and five other mammals by cross-species polymerase chain reaction analysis. *Molecular Brain Research*, *10*(4), 299–305. https://doi.org/10.1016/0169-328X(91)90088-F

Kimura, N., & Yanagisawa, K. (2018). Traffic jam hypothesis: Relationship between endocytic dysfunction and Alzheimer's disease. In *Neurochemistry International* (Vol. 119, pp. 35–41). https://doi.org/10.1016/j.neuint.2017.07.002

Kitazume, S., Yoshihisa, A., Yamaki, T., Oikawa, M., Tachida, Y., Ogawa, K., Imamaki, R., Hagiwara, Y., Kinoshita, N., Takeishi, Y., Furukawa, K., Tomita, N., Arai, H., Iwata, N., Saido, T., Yamamoto, N., & Taniguchi, N. (2012). Soluble amyloid precursor protein 770 is released from inflamed endothelial cells and activated platelets: a novel biomarker for acute coronary syndrome. *The Journal of Biological Chemistry*, *287*(48), 40817–40825. https://doi.org/10.1074/JBC.M112.398578

Klein, S., Goldman, A., Lee, H., Ghahremani, S., Bhakta, V., Nelson, S. F., & Martinez-Agosto, J. A. (2016). Truncating mutations in APP cause a distinct neurological phenotype. *Annals of Neurology*, *80*(3), 456–460. https://doi.org/10.1002/ANA.24727

Knighton, D. R., Hunt, T. K., Scheuenstuhl, H., Halliday, B. J., Werb, Z., & Banda, M. J. (1983). Oxygen tension regulates the expression of angiogenesis factor by macrophages. *Science*, *221*(4617), 1283–1285. https://doi.org/10.1126/SCIENCE.6612342

Kochi, T., Imai, Y., Takeda, A., Watanabe, Y., Mori, S., Tachi, M., & Kodama, T. (2013). Characterization of the arterial anatomy of the murine hindlimb: Functional role in the design and understanding of ischemia models. *PLoS ONE*, *8*(12). https://doi.org/10.1371/journal.pone.0084047

Koike, H., Tomioka, S., Sorimachi, H., Saido, T. C., Maruyama, K., Okuyama, A., Fujisawa-Sehara, A., Ohno, S., Suzuki, K., & Ishiura, S. (1999). Membrane-anchored metalloprotease MDC9 has an alpha-secretase activity responsible for processing the amyloid precursor protein. *Biochemical Journal*, *343*(Pt 2), 371. https://doi.org/10.1042/0264-6021:3430371

Kouzarides, T. (2007). Chromatin modifications and their function. *Cell*, *128*(4), 693–705. https://doi.org/10.1016/J.CELL.2007.02.005

Krause, K., Karger, S., Sheu, S. Y., Aigner, T., Kursawe, R., Gimm, O., Schmid, K. W., Dralle, H., & Fuhrer, D. (2008). Evidence for a role of the amyloid precursor protein in thyroid carcinogenesis. *The Journal of Endocrinology*, *198*(2), 291–299. https://doi.org/10.1677/JOE-08-0005

Lamalice, L., Le Boeuf, F., & Huot, J. (2007). Endothelial cell migration during angiogenesis. *Circulation Research*, *100*(6), 782–794. https://doi.org/10.1161/01.RES.0000259593.07661.1E

La Mendola, D., Trincavelli, M. L., & Martini, C. (2022). Angiogenesis in Disease. *International Journal of Molecular Sciences*, *23*(18). https://doi.org/10.3390/IJMS231810962

Lammich, S., Kojro, E., Postina, R., Gilbert, S., Pfeiffer, R., Jasionowski, M., Haass, C., & Fahrenholz, F. (1999). Constitutive and regulated alpha-secretase cleavage of Alzheimer's amyloid precursor protein by a disintegrin metalloprotease. *Proceedings of the National Academy of Sciences of the United States of America*, *96*(7), 3922–3927. https://doi.org/10.1073/PNAS.96.7.3922

Lechner, M. G., Karimi, S. S., Barry-Holson, K., Angell, T. E., Murphy, K. A., Church, C. H., Ohlfest, J. R., Hu, P., & Epstein, A. L. (2013). Immunogenicity of murine solid tumor models as a defining feature of in vivo behavior and response to immunotherapy. *Journal of Immunotherapy*, *36*(9), 477–489. https://doi.org/10.1097/01.CJI.0000436722.46675.4A

Lee, J. J., Arpino, J. M., Yin, H., Nong, Z., Szpakowski, A., Hashi, A. A., Chevalier, J., O'Neil, C., & Pickering, J. G. (2020). Systematic Interrogation of Angiogenesis in the Ischemic Mouse Hind Limb: Vulnerabilities and Quality Assurance. *Arteriosclerosis, Thrombosis, and Vascular Biology*, *40*(10), 2454–2467. https://doi.org/10.1161/ATVBAHA.120.315028

Lee, Y. H., Tharp, W. G., Maple, R. L., Nair, S., Permana, P. A., & Pratley, R. E. (2008). Amyloid precursor protein expression is upregulated in adipocytes in obesity. *Obesity*, *16*(7), 1493–1500. https://doi.org/10.1038/oby.2008.267

Limbourg, A., Korff, T., Napp, L. C., Schaper, W., Drexler, H., & Limbourg, F. P. (2009). Evaluation of postnatal arteriogenesis and angiogenesis in a mouse model of hind-limb ischemia. *Nature Protocols*, *4*(12), 1737–1748. https://doi.org/10.1038/nprot.2009.185

Li, Q., Berndt, M., Bush, A., Rumble, B., Mackenzie, I., Friedhuber, A., Beyreuther, K., & Masters, C. (1994). Membrane-Associated Forms of the βA4 Amyloid Protein Precursor of Alzheimer's Disease in Human Platelet and Brain: Surface Expression on the Activated Human Platelet. *Blood*, *84*(1), 133–142. https://doi.org/10.1182/BLOOD.V84.1.133.133

Liu, Q., Zhang, J., Tran, H., Verbeek, M. M., Reiss, K., Estus, S., & Bu, G. (2009). LRP1 shedding in human brain: roles of ADAM10 and ADAM17. *Molecular Neurodegeneration*, *4*(1). https://doi.org/10.1186/1750-1326-4-17

Mallm, J. P., Tschäpe, J. A., Hick, M., Filippov, M. A., & Müller, U. C. (2010). Generation of conditional null alleles for APP and APLP2. *Genesis*, *48*(3), 200–206. https://doi.org/10.1002/dvg.20601

Manavski, Y., Lucas, T., Glaser, S. F., Dorsheimer, L., Günther, S., Braun, T., Rieger, M. A., Zeiher, A. M., Boon, R. A., & Dimmeler, S. (2018). Clonal expansion of endothelial cells contributes to ischemia-induced neovascularization. *Circulation Research*, *122*(5), 670–677. https://doi.org/10.1161/CIRCRESAHA.117.312310

Manning, R. W., Reid, C. M., Lampe, R. A., & Davis, L. G. (1988). Identification in rodents and other species of an mRNA homologous to the human beta-amyloid precursor. *Brain Research*, *427*(3), 293–297. https://doi.org/10.1016/0169-328X(88)90052-6

Moussa-Pacha, N. M., Abdin, S. M., Omar, H. A., Alniss, H., & Al-Tel, T. H. (2020). BACE1 inhibitors: Current status and future directions in treating Alzheimer's disease. *Medicinal Research Reviews*, *40*(1), 339–384. https://doi.org/10.1002/med.21622

Müller, U. (1999). Ten years of gene targeting: targeted mouse mutants, from vector design to phenotype analysis. *Mechanisms of Development*, *82*(1–2), 3–21. https://doi.org/10.1016/S0925-4773(99)00021-0

Müller, U. C., Deller, T., & Korte, M. (2017). Not just amyloid: Physiological functions of the amyloid precursor protein family. *Nature Reviews Neuroscience*, *18*(5), 281–298. https://doi.org/10.1038/nrn.2017.29

Müller, U. C., Pietrzik, C. U., & Deller, T. (2012). The physiological functions of the β-amyloid precursor protein APP. *Experimental Brain Research*, *217*(3–4), 325–329. https://doi.org/10.1007/s00221-012-3039-2

Murray, P. J. (2017). Macrophage Polarization. *Annual Review of Physiology*, *79*, 541–566. https://doi.org/10.1146/annurev-physiol-022516-034339

Murray, P. J., & Wynn, T. A. (2011). Protective and pathogenic functions of macrophage subsets. *Nature Reviews Immunology 2011 11:11*, *11*(11), 723–737. https://doi.org/10.1038/nri3073

Norstrom, E. (2017). Metabolic Processing of the Amyloid Precursor Protein — New Pieces of the Alzheimer's Puzzle. *Discovery Medicine*, *23*(127), 269–276.

Nowak-Sliwinska, P., Alitalo, K., Allen, E., Anisimov, A., Aplin, A. C., Auerbach, R., Augustin, H. G., Bates, D. O., van Beijnum, J. R., Bender, R. H. F., Bergers, G., Bikfalvi, A., Bischoff, J., Böck, B. C., Brooks, P. C., Bussolino, F., Cakir, B., Carmeliet, P., Castranova, D., … Griffioen, A. W. (2018). Consensus guidelines for the use and interpretation of angiogenesis assays. *Angiogenesis*, *21*(3), 425–532. https://doi.org/10.1007/s10456-018-9613-x

Peschon, J. J., Slack, J. L., Reddy, P., Stocking, K. L., Sunnarborg, S. W., Lee, D. C., Russell, W. E., Castner, B. J., Johnson, R. S., Fitzner, J. N., Boyce, R. W., Nelson, N., Kozlosky, C. J., Wolfson, M. F., Rauch, C. T., Cerretti, D. P., Paxton, R. J., March, C. J., & Black, R. A. (1998). An essential role for ectodomain shedding in mammalian development. *Science*, *282*(5392), 1281–1284. https://doi.org/10.1126/SCIENCE.282.5392.1281

Peters-Libeu, C., Campagna, J., Mitsumori, M., Poksay, K. S., Spilman, P., Sabogal, A., Bredesen, D. E., & John, V. (2015). sAβPPα is a Potent Endogenous Inhibitor of BACE1. *Journal of Alzheimer's Disease*, *47*(3), 545–555. https://doi.org/10.3233/JAD-150282

Potente, M., Gerhardt, H., & Carmeliet, P. (2011). Basic and therapeutic aspects of angiogenesis. *Cell*, *146*(6), 873–887. https://doi.org/10.1016/J.CELL.2011.08.039

Puig, K. L., & Combs, C. K. (2013). Expression and Function of APP and its Metabolites Outside of the Central Nervous System. *Experimental Gerontology*, *48*(7), 608–611. https://doi.org/10.1016/j.exger.2012.07.009.Expression

Pulina, M. V., Hopkins, M., Haroutunian, V., Greengard, P., & Bustos, V. (2020). C99 selectively accumulates in vulnerable neurons in Alzheimer's disease. *Alzheimer's and Dementia*, *16*(2), 273–282. https://doi.org/10.1016/j.jalz.2019.09.002

Quintero-Fabián, S., Arreola, R., Becerril-Villanueva, E., Torres-Romero, J. C., Arana-Argáez, V., Lara-Riegos, J., Ramírez-Camacho, M. A., & Alvarez-Sánchez, M. E. (2019). Role of Matrix Metalloproteinases in Angiogenesis and Cancer. *Frontiers in Oncology*, *9*, 1–21. https://doi.org/10.3389/FONC.2019.01370

Rashbrook, V. S., Brash, J. T., & Ruhrberg, C. (2022). Cre toxicity in mouse models of cardiovascular physiology and disease. *Nature Cardiovascular Research*, *1*(9), 806–816. https://doi.org/10.1038/s44161-022-00125-6

Reinhard, C., Hébert, S. S., & De Strooper, B. (2005). The amyloid-β precursor protein: Integrating structure with biological function. *EMBO Journal*, *24*(23), 3996–4006. https://doi.org/10.1038/SJ.EMBOJ.7600860/ASSET/858108E0-9B4E-4DAD-A3E4-99A4470C32EB/ASSETS/GRAPHIC/EMBJ7600860-FIG-0005-M.JPG

Rice, H. C., Townsend, M., Bai, J., Suth, S., Cavanaugh, W., Selkoe, D. J., & Young-Pearse, T. L. (2012). Pancortins interact with amyloid precursor protein and modulate cortical cell migration. *Development*, *139*(21), 3986–3996. https://doi.org/10.1242/DEV.082909

Ring, S., Weyer, S. W., Kilian, S. B., Waldron, E., Pietrzik, C. U., Filippov, M. A., Herms, J., Buchholz, C., Eckman, C. B., Korte, M., Wolfer, D. P., & Müller, U. C. (2007). The Secreted-Amyloid Precursor Protein Ectodomain APPs Is Sufficient to Rescue the Anatomical, Behavioral, and Electrophysiological Abnormalities of APP-Deficient Mice. *Journal of Neuroscience*, *27*(29), 7817–7826. https://doi.org/10.1523/JNEUROSCI.1026-07.2007

Risau, W. (1997). Mechanisms of angiogenesis. *Nature*, *386*(6626), 671–674. https://doi.org/10.1038/386671A0

Ristori, E., Cicaloni, V., Salvini, L., Tinti, L., Tinti, C., Simons, M., Corti, F., Donnini, S., & Ziche, M. (2020). Amyloid-β precursor protein APP down-regulation alters actin cytoskeleton-interacting proteins in endothelial cells. *Cells*, *9*(11), 1–22. https://doi.org/10.3390/cells9112506

Sandbrink, R., Masters, C. L., & Beyreuther, K. (1994). βA4-Amyloid protein precursor mRNA isoforms without exon 15 are ubiquitously expressed in rat tissues including brain, but not in neurons. *Journal of Biological Chemistry*, *269*(2), 1510–1517. https://doi.org/10.1016/s0021-9258(17)42286-1

Schaper, W. (2009). Collateral circulation: past and present. *Basic Research in Cardiology*, *104*(1), 5–21. https://doi.org/10.1007/S00395-008-0760-X

Scheidegger, K. J., Nelissen-Vrancken, M. H. J. G., Leenders, P. J. A., Daemen, M. J. A. P., Smits, J. F. M., & Wood, J. M. (1997). Structural adaptation to ischemia in skeletal muscle: Effects of blockers of the renin-angiotensin system. *Journal of Hypertension*, *15*(12), 1455–1461. https://doi.org/10.1097/00004872-199715120-00013

Selkoe, D. J., Berman Podlisny, M., Joachim, C. L., Vickers, E. A., Lee, G., Fritzt, L. C., & Oltersdorft, T. (1988). β-Amyloid precursor protein of Alzheimer disease occurs as 110- to 135-kilodalton membrane-associated proteins in neural and nonneural tissues. *Proc. Nail. Acad. Sci. USA*, *85*, 7341–7345.

Senechal, Y., Larmet, Y., & Dev, K. K. (2006). Unraveling in vivo functions of amyloid precursor protein: Insights from knockout and knockdown studies. *Neurodegenerative Diseases*, *3*, 134–147. https://doi.org/10.1159/000094772

Senger, D. R., & Davis, G. E. (2011). Angiogenesis. *Cold Spring Harbor Perspectives in Biology*, *3*(8), 1–19. https://doi.org/10.1101/CSHPERSPECT.A005090

Shariati, S. A. M., & De Strooper, B. (2013). Redundancy and divergence in the amyloid precursor protein family. *FEBS Letters*, *587*(13), 2036–2045. https://doi.org/10.1016/J.FEBSLET.2013.05.026

Shivers, B. D., Hilbich, C., Multhaup, G., Salbaum, M., Beyreuther, K., & Seeburg, P. H. (1988). Alzheimer's disease amyloidogenic glycoprotein: expression pattern in rat brain suggests a role in cell contact. *The EMBO Journal*, *7*(5), 1365–1370. https://doi.org/10.1002/J.1460-2075.1988.TB02952.X

Stahl, A., Connor, K. M., Sapieha, P., Chen, J., Dennison, R. J., Krah, N. M., Seaward, M. R., Willett, K. L., Aderman, C. M., Guerin, K. I., Hua, J., Löfqvist, C., Hellström, A., & Smith, L. E. H. (2010). The Mouse Retina as an Angiogenesis Model. *Investigative Ophthalmology & Visual Science*, *51*(6), 2813–2826. https://doi.org/10.1167/iovs.10-5176

Staton, C. A., Stribbling, S. M., Tazzyman, S., Hughes, R., Brown, N. J., & Lewis, C. E. (2004). Current methods for assaying angiogenesis in vitro and in vivo. *International Journal of Experimental Pathology*, *85*, 233–248.

Stockmann, C., Kirmse, S., Helfrich, I., Weidemann, A., Takeda, N., Doedens, A., & Johnson, R. S. (2011). A Wound Size–Dependent Effect of Myeloid Cell–Derived Vascular Endothelial Growth Factor on Wound Healing. *Journal of Investigative Dermatology*, *131*(3), 797–801. https://doi.org/10.1038/JID.2010.345

Sunderkötter, C., Goebeler, M., Schulze-Osthoff, K., Bhardwaj, R., & Sorg, C. (1991). Macrophage-derived angiogenesis factors. *Pharmacology & Therapeutics*, *51*(2), 195–216. https://doi.org/10.1016/0163-7258(91)90077-Y

Sunderkötter, C., Steinbrink, K., Goebeler, M., Bhardwaj, R., & Sorg, C. (1994). Macrophages and angiogenesis. *Journal of Leukocyte Biology*, *55*(3), 410–422. https://doi.org/10.1002/jlb.55.3.410

Takayama, K. I., Tsutsumi, S., Suzuki, T., Horie-Inoue, K., Ikeda, K., Kaneshiro, K., Fujimura, T., Kumagai, J., Urano, T., Sakaki, Y., Shirahige, K., Sasano, H., Takahashi, S., Kitamura, T., Ouchi, Y., Aburatani, H., & Inoue, S. (2009). Amyloid Precursor Protein Is a Primary Androgen Target Gene That Promotes Prostate Cancer Growth. *Cancer Research*, *69*(1), 137–142. https://doi.org/10.1158/0008-5472.CAN-08-3633

Triggle, C. R., Samuel, S. M., Ravishankar, S., Marei, I., Arunachalam, G., & Ding, H. (2012). The endothelium: Influencing vascular smooth muscle in many ways. *Canadian Journal of Physiology and Pharmacology*, *90*(6), 713–718. https://doi.org/10.1139/Y2012-073

Troidl, C., Nef, H., Voss, S., Schilp, A., Kostin, S., Troidl, K., Szardien, S., Rolf, A., Schmitz-Rixen, T., Schaper, W., Hamm, C. W., Elsässer, A., & Möllmann, H. (2010). Calcium-dependent signalling is essential during collateral growth in the pig hind limb-ischemia model. *Journal of Molecular and Cellular Cardiology*, *49*(1), 142–151. https://doi.org/10.1016/J.YJMCC.2010.03.021

Uccelli, A., Wolff, T., Valente, P., Di Maggio, N., Pellegrino, M., Gürke, L., Banfi, A., & Gianni-Barrera, R. (2019). Vascular endothelial growth factor biology for regenerative angiogenesis. *Swiss Medical Weekly*, *149*, 1–8. https://doi.org/10.4414/smw.2019.20011

van der Kant, R., & Goldstein, L. S. B. (2015). Cellular Functions of the Amyloid Precursor Protein from Development to Dementia. *Developmental Cell*, *32*(4), 502–515. https://doi.org/10.1016/j.devcel.2015.01.022

van Dyck, C. H. (2018). Anti-Amyloid-β Monoclonal Antibodies for Alzheimer's Disease: Pitfalls and Promise. *Biological Psychiatry*, *83*(4), 311–319. https://doi.org/10.1016/j.biopsych.2017.08.010

Van Hove, A. H., & Benoit, D. S. W. (2015). Depot-based delivery systems for pro-angiogenic peptides: A review. *Frontiers in Bioengineering and Biotechnology*, *3*. https://doi.org/10.3389/fbioe.2015.00102

von der Kammer, H., Löffler, C., Hanes, J., Klaudiny, J., Scheit, K. H., & Hansmann, I. (1994). The Gene for the Amyloid Precursor-like Protein APLP2 Is Assigned to Human Chromosome 11q23-q25. *Genomics*, *20*(2), 308–311. https://doi.org/10.1006/GENO.1994.1174

Von Koch, C. S., Zheng, H., Chen, H., Trumbauer, M., Thinakaran, G., Van Der Ploeg, L. H. T., Price, D. L., & Sisodia, S. S. (1997). Generation of APLP2 KO mice and early postnatal lethality in APLP2/APP double KO mice. *Neurobiology of Aging*, *18*(6), 661–669. https://doi.org/10.1016/S0197-4580(97)00151-6

Wasco, W., Gurubhagavatula, S., Paradis, M., Romano, D. M., Sisodia, S. S., Hyman, B. T., Neve, R. L., & Tanzi, R. E. (1993). Isolation and characterization of APLP2 encoding a homologue of the Alzheimer's associated amyloid beta protein precursor. *Nature Genetics*, *5*, 95–100.

Weidemann, A., König, G., Bunke, D., Fischer, P., Salbaum, J. M., Masters, C. L., & Beyreuther, K. (1989). Identification, biogenesis, and localization of precursors of Alzheimer's disease A4 amyloid protein. *Cell*, *57*(1), 115–126. https://doi.org/10.1016/0092-8674(89)90177-3

Willem, M., Tahirovic, S., Busche, M. A., Ovsepian, S. V, Chafai, M., Kootar, S., Hornburg, D., Evans, L. D. B., Moore, S., Daria, A., Hampel, H., Müller, V., Giudici, C., Nuscher, B., Wenninger-Weinzierl, A., Kremmer, E., Heneka, M. T., Thal, D. R., Giedraitis, V., … Haass, C. (2015). η-Secretase processing of APP inhibits neuronal activity in the hippocampus. *Nature*, *526*(7573), 443–447. https://doi.org/10.1038/nature14864

Yamada, T., Sasaki, H., Furuya, H., Miyata, T., Goto, I., & Sakaki, Y. (1987). Complementary DNA for the mouse homolog of the human amyloid beta protein precursor. *Biochemical and Biophysical Research Communications*, *149*(2), 665–671. https://doi.org/10.1016/0006-291X(87)90419-0

Yamada, T., Sasakil, H., Dohura, K., Goto, I., & Sakaki, Y. (1989). Structure and expression of the alternatively-spliced forms of mRNA for the mouse homolog of Alzheimer's disease amyloid beta protein precursor. *Biochemical and Biophysical Research Communications*, *158*(3), 906–912.

Yoo, S. Y., & Kwon, S. M. (2013). Angiogenesis and its therapeutic opportunities. *Mediators of Inflammation*, *2013*. https://doi.org/10.1155/2013/127170

Yoshiki, A., Ballard, G., & Perez, A. V. (2022). Genetic quality: a complex issue for experimental study reproducibility. *Transgenic Research*, *31*(4–5), 413. https://doi.org/10.1007/S11248-022-00314-W

Zhang, H., Ma, Q., Zhang, Y., & Xu, H. (2012). Proteolytic processing of APP. *J Neurochem.*, *120*(Suppl 1), 9–21. https://doi.org/10.1111/j.1471-4159.2011.07519.x.Proteolytic

Zhao, Y. ;, Gu, Y. ;, Zhang, Q. ;, Liu, H. ;, Liu, Y., Marchi, D., Tondo, G., Rizzo, G., Zhao, Y., Gu, Y., Zhang, Q., Liu, H., & Liu, Y. (2023). The Potential Roles of Exosomes Carrying APP and Tau Cleavage Products in Alzheimer's Disease. *Journal of Clinical Medicine 2023, Vol. 12, Page 1883*, *12*(5), 1883. https://doi.org/10.3390/JCM12051883

Zheng, H., Jiang, M., Trumbauer, M. E., S Sirinathsinghji, D. J., Hopkins, R., Smith, D. W., Heavens, R. P., Ft Dawson, G., Boyce, S., Conner, M. W., Stevens, K. A., Slunt, H. H., Sangram Sisodia, ll S., Howard Chen, ll Y., & T Van der Ploeg, L. H. (1995). ß-Amyloid Precursor Protein-Deficient Mice Show Reactive Gliosis and Decreased Locomotor Activity. *Cell*, *81*, 525–531.

Zheng, H., & Koo, E. H. (2011). Biology and pathophysiology of the amyloid precursor protein. *Molecular Neurodegeneration*, *6*(1), 1–16. https://doi.org/10.1186/1750-1326-6-27/FIGURES/2

Ziche, M., Donnini, S., & Morbidelli, L. (2005). Development of New Drugs in Angiogenesis. *Current Drug Targets*, *5*(5), 485–493. https://doi.org/10.2174/1389450043345371

13 Eidesstattliche Erklärung

Ich erkläre:

Ich habe die vorgelegte Dissertation selbstständig und ohne unerlaubte fremde Hilfe und nur mit den Hilfen angefertigt, die ich in der Dissertation angegeben habe. Alle Textstellen, die wörtlich oder sinngemäß aus veröffentlichten Schriften entnommen sind, und alle Angaben, die auf mündlichen Auskünften beruhen, sind als solche kenntlich gemacht. Ich stimme einer evtl. Überprüfung meiner Dissertation durch eine Antiplagiat-Software zu. Bei den von mir durchgeführten und in der Dissertation erwähnten Untersuchungen habe ich die Grundsätze guter wissenschaftlicher Praxis, wie sie in der „Satzung der Justus-Liebig-Universität Gießen zur Sicherung guter wissenschaftlicher Praxis“ niedergelegt sind, eingehalten.

Linden, den ___________________

Sabrina Kurz

14 Acknowledgements

First, I would like to thank Prof. Dr. Stefan Offermanns for giving me the opportunity to carry out my research at the Max-Planck-Institute for Heart and Lung Research. Without his continuous scientific and methodical support, it would not have been possible to conduct this research. I sincerely appreciate his invaluable guidance.

I wish to also show my gratitude to Prof. Dr. Ivan Manzini and Prof. Dr. Nina Wettschureck, for being part of my Thesis Advisory Committee and their advice and support through all the years.

Thanks a lot also to ShengPeng Wang, who introduced me to the Offermanns lab and showed many techniques to me. It was a great time working with you and being one of your office mates. Special thanks also to Rui Li, for being the best office mate I could have imagined. You always had an open ear for me, no matter if there were science related questions or private ones.

A special thanks also to Haruya, who was willing to keep the mouse breeding ongoing during my two maternity breaks. Thanks a lot also for continuing the whole APP project in the heart.

I also want to thank Kerstin Troidl and Shangmin Liu for their help with the femoral artery ligation experiments.

Thanks to Adriana, Elena, Guozheng, Kenneth, Remy, Shenglan for all the great talks, discussion and help in the lab. It would have been much less fun without you guys!

Thanks to Veronika for doing my genotyping over all these years, to Ulli and Claudia for always being around when I needed help. As well for Martina who often helped me to finish mounting of my slides when I was already late.

I would like to thank again the entire lab and all former colleagues as well. It was a pleasure working with all of you. You are all great, inspiriting people.

Last but not least, a special thanks goes to my family, especially to Johannes, for always being there for me and keeping my back free.